ADVANCED MATERIALS
www.advmat.de

Computational Modeling of Reticular Materials: The Past, the Present, and the Future

*Wim Temmerman, Ruben Goeminne, Kuber Singh Rawat, and Veronique Van Speybroeck**

Dedicated to Prof. Omar Yaghi on the occasion of his 60th birthday, who is one of the pioneers in the field of reticular chemistry

Reticular materials rely on a unique building concept where inorganic and organic building units are stitched together giving access to an almost limitless number of structured ordered porous materials. Given the versatility of chemical elements, underlying nets, and topologies, reticular materials provide a unique platform to design materials for timely technological applications. Reticular materials have now found their way in important societal applications, like carbon capture to address climate change, water harvesting to extract atmospheric moisture in arid environments, and clean energy applications. Combining predictions from computational materials chemistry with advanced experimental characterization and synthesis procedures unlocks a design strategy to synthesize new materials with the desired properties and functions. Within this review, the current status of modeling reticular materials is addressed and supplemented with topical examples highlighting the necessity of advanced molecular modeling to design materials for technological applications. This review is structured as a templated molecular modeling study starting from the molecular structure of a realistic material towards the prediction of properties and functions of the materials. At the end, the authors provide their perspective on the past, present of future in modeling reticular materials and formulate open challenges to inspire future model and method developments.

1. Introduction

Reticular chemistry provides an exceptional platform for materials design thanks to the unique building concept of assembling molecular units to form framework materials in a controlled way. The building units may be organic or inorganic in nature, therefore reticular chemistry is situated at the interface of organic and inorganic chemistry. Furthermore, as one starts from molecular building units to make materials, reticular chemistry combines elements of molecular chemistry and solid-state physics. In this review, we will discuss the current status and future perspectives of modeling reticular materials, where one starts from the atomistic scale and aims to evaluate the properties and functions of the material at operating conditions. Given the unique positioning of reticular chemistry at the interface of various disciplines, its modeling also requires an open vision combining modeling concepts typically used in organic and inorganic chemistry, and molecular and solid-state physics. Furthermore, as in principle, the whole periodic table of elements becomes a playground to make materials, advanced quantum mechanical methods are necessary to describe with high accuracy all elements going from light elements to materials prone to strong electron correlation. In this sense—as will become clear—modeling reticular materials as realistic as possible, i.e., having imperfections, disorder and having dynamic behavior, will require elements from statistical physics, quantum mechanics but also artificial intelligence. Recently a major leap forward has been witnessed thanks to machine learning approaches which help to model reticular materials in a more realistic way.

Reticular chemistry is defined as the study of linking discrete molecules or metal clusters by strong covalent or coordinate bonds to make extended structures and the chief aim of reticular chemistry is the study and synthesis of materials with a well-defined porosity and functionality.[1,2] Reticular materials can be subdivided in several subclasses of materials, based on the identity and connectivity of the atomic constituents, such as metal–organic frameworks (MOFs), covalent organic frameworks (COFs), zeolitic imidazolate frameworks (ZIFs) as well as other crystalline porous materials such as porous organic frameworks (POFs), porous aromatic frameworks (PAFs), supramolecular organic frameworks (SOFs) and hydrogen-bonded organic frameworks (HOFs). **Figure 1** shows a rudimentary timeline of

W. Temmerman, R. Goeminne, K. S. Rawat, V. Van Speybroeck
Center for Molecular Modeling (CMM)
Ghent University
Technologiepark 46, Zwijnaarde 9052, Belgium
E-mail: Veronique.VanSpeybroeck@UGent.be

The ORCID identification number(s) for the author(s) of this article can be found under https://doi.org/10.1002/adma.202412005

DOI: 10.1002/adma.202412005

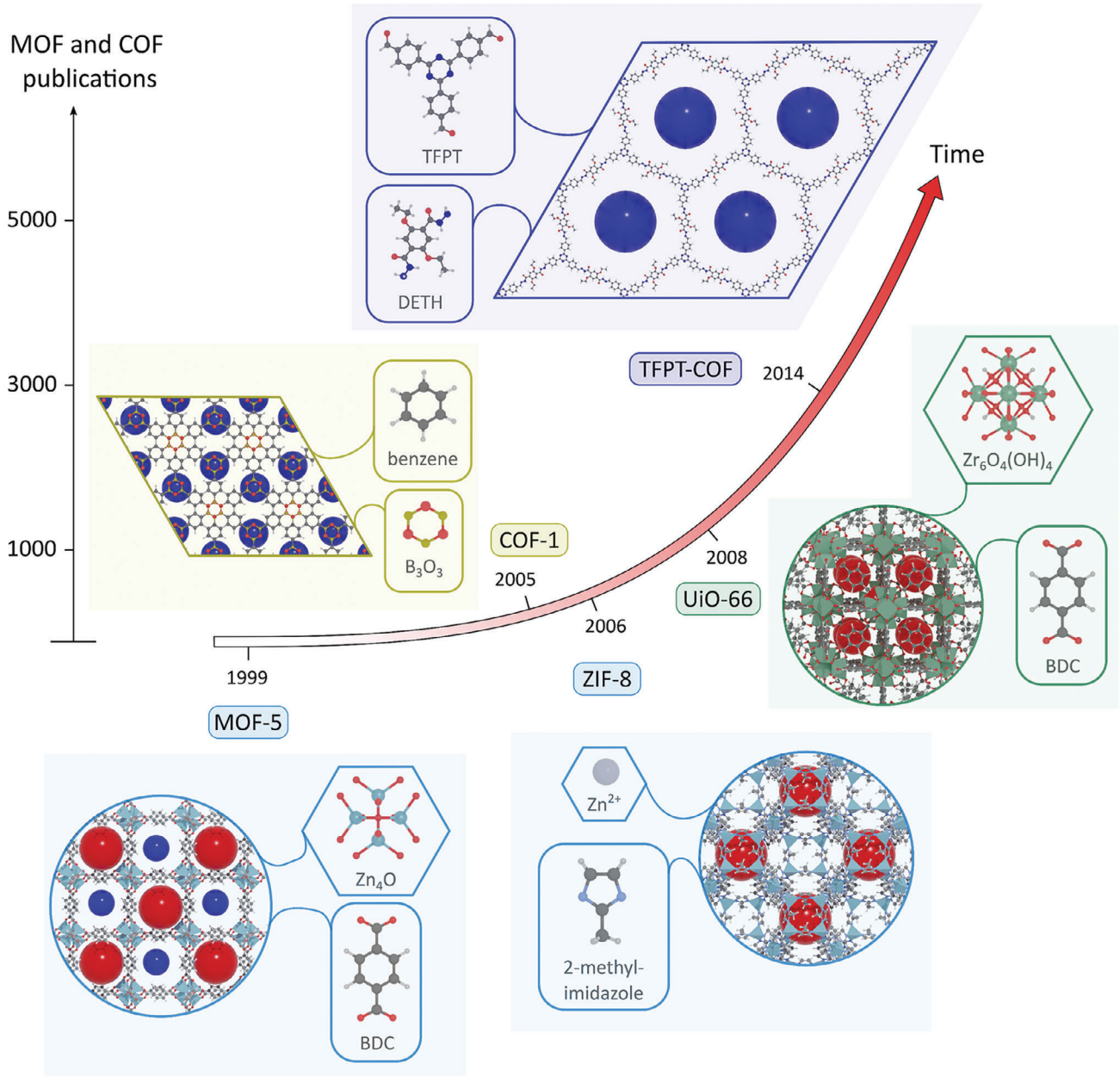

Figure 1. A view of the three-dimensional (pore)structure of some key MOFs (below the arrow) and COFs (above the arrow), together with their constituting building blocks. MOF-5, composed of Zn4O clusters tetrahedrally connected by 1,4-benzenedicarboxylate (BDC) linkers was synthesized in 1999, maintaining porosity during solvent removal.[3] ZIF-8 consists of zinc ions tetrahedrally connected by imidazolate linkers, being topologically isomorphic to zeolites.[4] UiO-66 is a highly studied MOF with high thermal stability due to its cuboctahedral zirconiumoxide node providing 12 connection points to BDC linkers.[5] COF-1 was the first discovered COF, consisting of two-dimensional layers of benzene and B_3O_3 rings.[6] TFPT-COF was the first reported COF capable of visible-light driven hydrogen generation and is constituted by 1,3,5-tris-(4-formyl-phenyl)triazine (TFPT) and 2,5-diethoxy-terephthalohydrazide (DETH).[7]

the development of the three largest classes of reticular materials, along with the different constituent building blocks and the three-dimensional pore structure of the most important examples of reticular materials.

The field of reticular chemistry was initiated by the discovery of metal–organic frameworks which are by far the largest subclass of reticular materials. The task group Coordination Polymers and Metal Organic Frameworks: Terminology and Nomenclature Guidelines of the International Union of Pure and Applied Chemistry (IUPAC) published a recommendation on the precise definition of a MOF: "A metal–organic framework ... is a coordination network with organic ligands containing potential voids."[8] Note that, according to the IUPAC definition, crystallinity or porosity

is not a requirement for a material to be classified as a MOF.

Although the concept of coordination polymers was already explored in the 1960s,[9,10] the development of MOFs as a distinct and separate class of materials was accelerated by the seminal work of Yaghi, Kitagawa, Férey, and others in the 1990s. The true innovation was the discovery of stable porous frameworks that do not collapse in the absence of solvents and in 1999, Yaghi and co-workers succeeded in synthesizing a crystalline MOF, named MOF-5, having a high chemical and architectural stability and a permanent high porosity (61% void fraction).[1,3] Since then the field expanded substantially and currently more than 100 000 MOF structures have been reported.[11,12] In 2008, Férey proposed to classify MOFs according to the dimensionality of the inorganic sublattice, leading to zero-, one-, two-, or three-dimensional structures, comprised of polynuclear inorganic nodes connected by chelating organic linkers.[13] MOFs have astonished the scientific community with their exceptional properties especially when being exposed to external triggers. Striking examples of such atypical behavior are negative linear compressibility where the material expands along one or more directions instead of contracting upon exertion of pressure or negative gas adsorption where the material releases gas from its pores when the gas pressure of the surroundings is increased.[14,15] Another intriguing aspect of some MOFs is their extraordinary flexible behavior under external stimuli, where the material can transform between various phases, often accompanied by huge volume changes upon exposure to external stimuli. Kitagawa and co-workers launched the terminology "soft porous crystals" for materials with a bistable or multistable behavior with long-range structural order.[16] Tremendous efforts have been undertaken to understand the conditions and material's characteristics that give rise to such flexible behavior. For a dedicated overview of flexible MOFs we refer to a recent book edited by Susumu Kitagawa on the topic.[17] MOFs can also exhibit more subtle flexible behavior, for example, associated with linker rotations. As will be shown further in this review, a slight swelling of the adsorption pocket between linkers induced by the adsorption of water may drastically affect the computed adsorption properties. As will be shown in the case study on water harvesting in Section 3, accurately modeling water adsorption isotherms is a highly challenging topic.

In 2005, the field of reticular chemistry was expanded thanks to a prominent discovery by Omar Yaghi who showed that it is possible to assemble organic building units towards crystalline porous materials, since then referred to as covalent organic frameworks (COFs). Linking organic monomers into polymers is obviously widely known, but the creation of crystalline nanoporous frameworks based merely on organic (metal-free) monomers was a new concept. COFs may be fabricated from planar 2D sheets or from non-planar building units, yielding 2D or 3D COFs respectively. Many COFs possess a relatively high chemical and thermal stability.[18–21] The absence of metals in COFs makes them much lighter than most other porous materials, while still possessing very high surface areas. Since their discovery, the synthesis of new COFs has increased rapidly and the new materials can be made with a large tunability in terms of functionality and porosity. The first 2D (2005) and 3D COFs (2007) were synthesized utilizing boroxine and boronic esters to build the extended structure with covalently bonded organic building blocks.[2]

The high architectural, structural, and thermal stability of MOFs is, in part, due to the chelating organic linkers in which a single organic linker forms two or more separate coordinate bonds to the inorganic nodes to build the framework, e.g., polydentate carboxylate ligands (organic linkers) in MOF-5, UiO-66, and other MOFs. Alternatively, monodentate imidazolate ligands induce the formation of tetrahedrally coordinated single transition metal nodes and the M-imidazolate-M angle is typically 145°, similar or identical to the Si-O-Si angle found in zeolites.[1,22] For these preceding reasons, ZIFs are considered a distinct subclass of MOFs and were first reported by Yaghi and coworkers in 2006,[4] who successfully synthesized twelve zeolitic imidazolate frameworks (termed ZIF-1 to ZIF-12) using Zn(II) or Co(II) to bridge imidazolate-type organic linkers.

Inspired by the successes of MOFs, COFs, and ZIFs, a recent complementary addition to the field are porous frameworks constructed from weak intermolecular hydrogen bonding, π–π stacking, or dispersion interactions between discrete organic molecules.[23,24,25] The weak intermolecular bonding complicates the synthesis of these porous networks with a desired structure and functionality.[23–27] The classification of these materials depends on the dominant intermolecular interaction and a distinction is made between supramolecular organic frameworks (SOFs) and hydrogen-bonded organic frameworks (HOFs). The first example of this newest class of reticular materials came in 2010, when Yang et al.[28] reported the synthesis of a stable porous 3D organic network held together by hydrogen bonds and π–π stacking, which the authors called SOF-1. In the following year, in 2011, He et al.[29] reported the synthesis of a microporous hydrogen-bonded organic framework (HOF-1) for the selective separation of acetylene and ethene. In the remainder of this review, the discussion will focus on the first three classes of reticular materials (i.e., MOFs, COFs, and ZIFs).

To summarize the various subclasses of reticular materials, in MOFs and ZIFs, anionic chelating linkers stabilize the cationic metal-containing clusters to form an extended structure, typically combining one type of inorganic building unit with one type of organic building unit.[30] On the contrary, COFs, SOFs, and HOFs contain no metals, except when they are being post-synthetically modified. The covalent bonds in COFs complicate the synthesis of extended structures with long-range order, as these strong chemical bonds leave little room for defect restoration during the synthesis process.[30,31]

To simplify the description of reticular materials, their topology is best described using the "node" and "link" concept from A.F. Wells to classify the seemingly inexhaustible variety in which polynuclear clusters (hereafter referred to as secondary building units or SBUs) can connect to organic linkers, from which the final framework is constructed.[32] In the remainder of this paragraph, we will explain the concept of topologies of reticular materials using MOFs as a representative example. The atomistic structure of a MOF can be translated to a mathematical graph by equating the SBUs to nodes (or equivalently, vertices) and the organic linkers to edges. A net is a simple graph (i) with at most one undirected edge connecting any pair of vertices, (ii) with every vertex linked to every other vertex by a continuous path of edges and (iii) in the explicit absence of edges connecting a

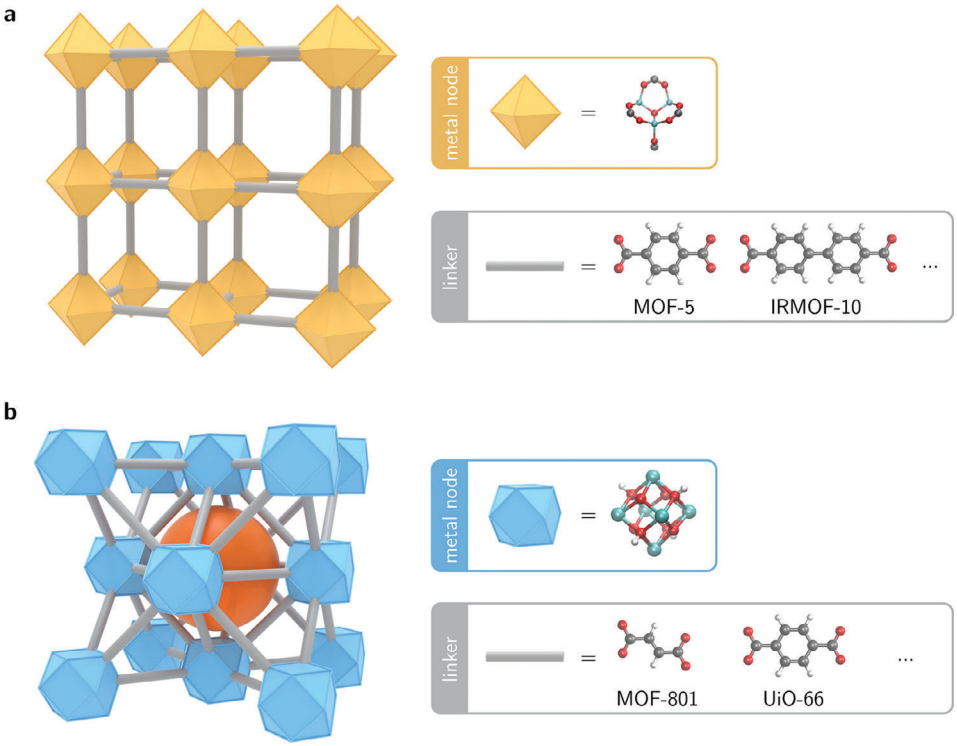

Figure 2. a) Schematic representation of the pcu topology alongside the building blocks of MOF-5 and IRMOF-10. b) Schematic representation of the fcu topology alongside the building blocks of MOF-801 and UiO-66. The octahedral pore of the framework is indicated with an orange sphere. Figure reproduced from ref. [37] with permission from Ghent University, Copyright 2024.

vertex to itself.[33] According to the Reticular Chemistry Structure Resource (RCSR), topologies are identified with three-letter identifiers (lower case and boldface).[34] **Figure 2** shows examples of the translation between the atomistic structure of a MOF and the corresponding topological description. Different MOFs can possess the same underlying topology and form a so-called isoreticular series, see Figure 2.[35,36] The coordination geometry of the SBUs will determine the topology of the extended structure in the reticulation process (Lat.: *reticulum*, meaning netlike) and the strong coordinate bonds of the anionic organic linkers to the SBUs impart chemical stability to the resulting extended structure. The chemical stability is supplemented with architectural stability stemming from the directionality of the coordinate bonds of the organic linkers to the SBUs.

The remarkable properties of these materials quickly attracted global attention from researchers aiming to explore the enormous application potential of reticular materials in fields such as heterogeneous catalysis, gas separation and storage, contaminant removal, drug delivery, water harvesting, chemical sensing, biological applications, and others.[38] Whereas the enormous versatility in chemical elements, topologies, porosities, and consequently properties provide a major strength for material design, it also poses a challenge on how to meticulously design materials for a particular application. Within this area, modeling has become ubiquitous and an essential component to move from serendipitous discovery to rational design. However, to make any realistic prediction on the behavior of reticular materials, it is essential to follow a modeling approach that mimics materials in experimental set-ups as closely as possible. This means that it is essential to model materials in their operating environment and with all their intricacies, thus accounting for defects on various length scales and presence of disorder. Within the MOF field, defect engineering has been exploited as an additional toolbox to introduce functionalities in the framework.[39,40] Striking examples are found within the field of catalysis.[41–43] To fully exploit these concepts, e.g., for catalysis, separation, and gas storage, both experimental and computational techniques are required which enable a precise characterization of the MOF structure from the nanometer to the mesoscale range (2–50 nm). As will be shown in this review, providing such modeling techniques for reticular materials poses enormous challenges. Furthermore, spatial gradients in the crystal, the size of the crystal and its morphology largely affect dynamics of various processes taking place at the crystal particle.[44] For example, the ability of soft porous frameworks to switch between various crystal phases upon exposure to external stimuli is critically dependent on the size of the crystal and defect density. Downsizing MOF crystals from the macro- to the mesoscale substantially suppresses their ability to morph between various phases.[45–53] Major experimental efforts have been undertaken to learn the time scales of this switching behavior. This entanglement of the dynamics of the material with its spatial properties has been defined as spatiotemporal behavior of the material and is crucial to understand the functional behavior of reticular materials.[17,54–56] In our endeavor to model reticular materials at length and time scales comparable to experimental set-ups, availability of increasingly strong computer infrastructure

Table 1. Overview of theoretical and computational methods applied in modeling of reticular materials in Section 2 of this review.

Section	Computational techniques
2.1 Building structural models for reticular materials	Unit cell optimization, geometry optimization, melt-quenching, reverse Monte Carlo, polymerization-based modeling, Bravais-Friedel-Donnay-Harker method, Wulff construction method, reverse topology approach
2.2 Potential energy surface	Electronic structure methods, density functional theory, classical force fields, machine learning potentials, transfer machine learning, Δ-machine learning, coarse-graining methods
2.3 Phase Space Sampling	Statistical thermodynamics, harmonic approximation, quasi-harmonic approximation, anharmonicity, vibrational correlation, ensemble averages, molecular dynamics simulations, Monte Carlo sampling, kinetic Monte Carlo, free energy methods, enhanced sampling, collective variables, free energy error estimation
2.4 Physical properties	Green-Kubo method, Müller-Plathe method, Tauc analysis, GW approximation, Bethe-Salpeter equation

is one key element. In this respect, it is noteworthy that recently the first exascale computers have been taken in operation, which open a lot of perspectives to bridge the length-time scale gap between theoretical modeling and experiment.[57] However, having access to massive computing power is not sufficient to close the length-time scale gap between simulations and experiments. New theoretical algorithms and innovations are necessary to reconcile the macroscopic experimental observations with atomistic simulations. As we will illustrate in the next section, the discrepancy in the attainable length/time scales between experiment and theory is a major challenge in modeling reticular materials for important technological applications.[57]

The structure of this review closely follows the typical workflow of a computational study. First, Section 2.1 will discuss methods to build structural models of reticular materials, how to build or find atomistic structures suitable for theoretical studies. Second, Section 2.2 will discuss the central quantity of any computational modeling study, the potential energy surface (PES). The PES is, by definition, calculated at 0 K and extensions are necessary to account for finite temperature effects or pressure. Accounting for these thermodynamic conditions is equivalent to a conversion of the PES to a free energy surface (FES) and different techniques for operando modeling will be discussed. Third, Section 2.3 will discuss the exploration of the PES (or FES) which is necessary to understand the spatiotemporal evolution at realistic thermodynamic conditions. As the fourth and final step in a computational study, Section 2.4 will explain how the results from the PES/FES exploration can be used to predict a multitude of properties, suitable for comparison with experiment. In Section 3, the importance and relevance of computational modeling in reticular chemistry will be highlighted through a curated selection of case studies. In each of these case studies, it will be shown how state-of-the-art computational techniques, in close synergy with experimental expertise, result in unique insights in the governing physical principles. This review will conclude by providing a future outlook in Section 4 and identify opportunities for further developments in computational modeling of reticular materials. As a final note to this introduction, we wish to highlight that the intention of this review is not to discuss every method itself in depth. However, to the best of the authors' knowledge, necessary references have been given to guide the interested reader on specific methodologies. To guide readers interested in a specific topic, all theoretical and computational methods that will be discussed in Section 2 are collected in **Table 1**.

2. State-of-the-Art in Computational Modeling of Reticular Materials

Given the wide variety in the composition, structure, and properties of reticular materials situated at the crossroads of various disciplines, the field of computational modeling of reticular materials is necessarily very broad. To clearly structure the various components in modeling reticular materials and to lower the entry barrier of researchers in this interdisciplinary field, we have structured the discussion in this section following the typical workflow of a computational study as illustrated in **Figure 3**. A typical molecular modeling exercise consists of four steps: (i) Building a structural model for reticular materials that is suitable for in silico experiments, (ii) modeling the potential energy surface, the central quantity of a molecular modeling exercise, (iii) exploring the phase space defined by the potential (or free) energy surface and (iv) predicting physical properties to connect theoretical and experimental results. Within this section, we discuss each of the components and illustrate the theoretical concepts with examples taken from the field of reticular chemistry. Due to the extensive body of literature on the theoretical modeling of reticular materials, it is not possible to comprehensively cite all literature works, however many references are given to specialized in-depth literature both on the applications and theoretical background.

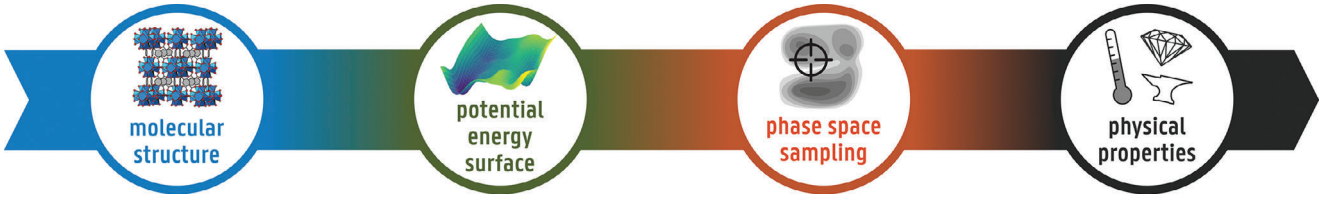

Figure 3. The sequence of a molecular modeling exercise, from left to right: building a structural model, modeling the potential energy surface, phase space sampling, and deriving target physical properties. Reproduced with permission.[58] Copyright 2023, Royal Society Publishing.

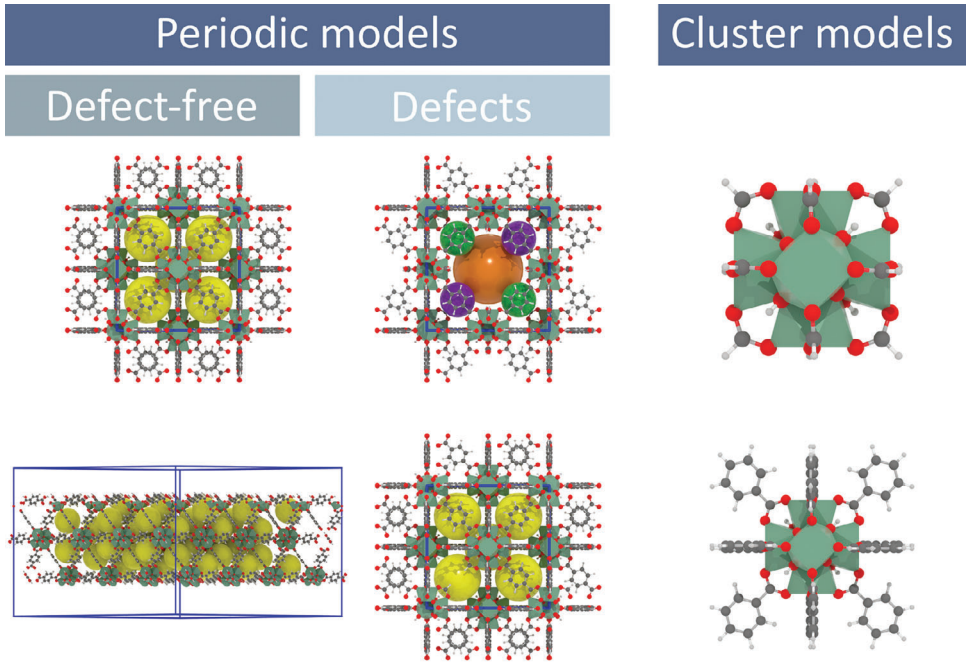

Figure 4. Illustration of different structural models of UiO-66 suitable for computational studies. A structural model can be (a)periodic with or without defects. Top left: pristine periodic model, bottom left: membrane periodic model with added vacuum above and below the membrane. Top middle: periodic model with missing inorganic node, bottom middle, periodic model with missing organic linker (bottom left of the model). Top right: aperiodic cluster model of an inorganic node capped with formate groups, bottom right: aperiodic cluster model of an inorganic node capped with benzoate groups. The unit cells of the periodic models are shown in blue. The spheres, colored by size, fill the cavities in the periodic models for clarity.

2.1. Building Structural Models for Reticular Materials

This section will discuss the construction of structural models of reticular materials. The theoretical atomistic models must accurately represent the real material and account for the crystallinity, flexibility, disorder and the external surface of the target reticular material. As stated in the Introduction, crystallinity and porosity are not a requirement for a material to be classified as a MOF (or ZIF). We remind the reader of the IUPAC definition of a MOF: "A coordination network with organic ligands containing potential voids". The other classes of reticular materials, i.e., COFs, SOFs, and HOFs, strictly speaking do not possess any metals and therefore any ligands, but perhaps the term "network compound" is the most general term which is applicable to all reticular materials. The IUPAC project, started in 2014, to recommend a precise terminology is still on-going (latest update June 2024).[59] **Figure 4** shows a schematic overview of the different structural models which will be discussed in this section. To provide clarity in all the possible structural models of reticular materials, crystalline and amorphous periodic structural models will be discussed in two separate subsections. As a special case of a crystalline aperiodic MOF, we will highlight the case study of TRUMOF-1.[60] Next, the discussion will move from idealized pristine structural models to cluster models, defective and disordered structural models ending with the inclusion of surface effects to more closely simulate real materials. This section will conclude by discussing the discovery of new materials with high-throughput screening methods to accelerate the discovery of viable candidate materials.[61] In the second to last subsection, we provide a non-exhaustive list of databases where structural models of reticular materials are made available by researchers to any interested party.

2.1.1. In Silico Design of Reticular Materials

Modeling reticular materials requires an in-depth knowledge of the structure at the atomistic scale. Information on the material's structure can come from experiments that typically follow a top-down approach, where one tries to zoom into the material using advanced characterization techniques before, during or after synthesis and post-synthetic modifications.[62–64] Empirical characterization techniques include microscopic imaging methods to visualize the structure or spectroscopic techniques to determine unique spectral fingerprints, which can be compared with spectra of known materials to determine the atomistic structure. Computational scientists, on the other hand, build their structural models atom by atom in a bottom-up approach. The in silico design of reticular materials requires a solid foundation both in molecular modeling as well as reticular chemistry.[30]

Reticular materials are comprised of atoms connected by a variety of chemical bonding interactions. In MOFs and ZIFs, the cationic metal nodes bind to the anionic organic linkers through coordinate bonds and charge transfer processes. The chemical environment is different in COFs due to the absence of the metal nodes, but most reticular materials are characterized by large cavities enveloped by structural elements of the framework. The high porosity leads to a significant contribution of long-range van der Waals dispersion interactions which are challenging to describe accurately in first principles calculations.[65] A second

consequence of the high porosity in reticular materials are the resulting large unit cells in periodic calculations, easily leading to hundreds of atoms per unit cell. For example, MOF DUT-49 crystallizes in the $Fm\bar{3}m$ (225) space group and contains 1728 (432) atoms in the conventional (primitive) unit cell (contracted pore phase, cubic conventional unit cell, $a \approx 35$ Å).[46] Another example is MOF MIL-100(Cr), crystallizing in the $Fd\bar{3}m$ (227) space group, containing 11 152 (1394) atoms in the conventional (primitive) unit cell (cubic conventional unit cell, $a \approx 73$ Å).[66,67] The terms primitive and conventional unit cell will be discussed in more detail below.

2.1.2. Crystalline Structural Models

Periodicity is inherently present at the atomic level of most reticular materials, which can be exploited to simplify the atomistic description. Ignoring surface effects, a crystalline solid can be represented as an infinite periodic extension of a minimal collection of building blocks (i.e., a periodic unit cell) reticulated into a wide variety of topologies. Two different types of unit cells can be used to reproduce the extended structure of a reticular material: conventional and primitive unit cells. In crystallographic terms, a primitive unit cell is the unit cell corresponding to a single lattice point, i.e., the smallest possible unit from which the entire periodic structure can be reconstructed by periodic extensions of the unit cell along the lattice vectors. The primitive unit cells will have the lowest number of atoms (and thus the lowest number of electrons) which need to be accounted for during cumbersome first principles calculations. A second type of unit cell is the conventional unit cell, reflecting the symmetry properties of the lattice. Conventional unit cells are constructed according to a strict set of rules which differ for each of the seven lattice systems. These rules, as well as a detailed theoretical background on the different types of unit cells, can be found in the International Tables For Crystallography, Volume A.[68–70] Conversion from the primitive unit cell to the conventional unit cell can facilitate visualization of the cavity or the pore structure of the periodic crystalline material. If the space group of the crystal structure is known (e.g., from powder X-ray diffraction measurements), the primitive and conventional unit cells can be readily interconverted using the unique transformation matrix belonging to one of the 230 space groups.[70] A third type of commonly encountered unit cells are supercells, which are periodic extensions along one or more lattice vectors of an arbitrary, but finite, number of primitive (or conventional) unit cells. A description of the crystal lattice with primitive unit cells limits the possibilities to study any long-range disorder in the system, which is intertwined with defects and flexibility in MOFs.[71] Additionally, the size of the crystal has been shown to either promote or inhibit flexibility of the reticular material, an effect that cannot be captured using only the primitive unit cell in periodic calculations.[72,73] As a concrete example of a size effect in MOFs, Bon et al.[74] showed that the particle size of flexible MOFs DUT-8(Ni) and SNU-9 decreases during the cycling of the sorption process, attributed to the sorption stresses, and the crystal size continued to decrease until the fragmented domains could tolerate the adsorption stresses.

After selecting the target unit cell, the next step is to obtain a structural model that is suitable for periodic calculations. Structures obtained from experimental data or structural databases often require preprocessing steps, which may include, but are not limited to: removing partial occupancies, removing solvent molecules, imposing charge neutrality by adding hydrogen atoms or counter ions, restore disorder, etc. The cleaned target structure is relaxed starting from a reasonable input structure, e.g. from experimental powder X-ray diffraction measurements or taken from a structural database (vide infra). Starting from the optimized structure, the volume is varied over a small range (at most a few hundred $Å^3$) in the elastic regime below and above the equilibrium volume, optimizing the ionic positions and unit cell parameters at each fixed volume. A finite differencing scheme can be applied to find the bulk modulus of the structure as the second-order derivative of the energy with respect to volume. To mitigate numerical inaccuracies, an energy-versus-volume equation of state can be fitted to the discrete set of data points. A least-squares fit of a parametrized energy-versus-volume equation of state provides the energetically most stable volume and the optimized unit cell parameters. Popular choices of equations of state for flexible reticular materials include the Birch-Murnaghan[75,76] and the Rose-Vinet[77,78] equations of state, although the latter is preferred when modeling flexible materials like MOFs and COFs.[79] The bulk modulus, relating the decrease in volume with an increase in pressure, is one of the fitting parameters that follows from the energy-versus-volume equations of state (see also Subsection 2.4.1).

Crystalline reticular materials with non-default topologies can be synthesized with the use of twisted, bent or zigzag organic linkers.[80] However, crystallinity of a material does not require periodicity.[81,82] A small, but quickly growing, subclass of reticular materials lack long-range order and are classified as aperiodic crystals. Simulating aperiodic crystals is not trivial, whereas periodic first principles calculations rely on Bloch's theorem, which states that the solutions to Schrödinger's equation can be expressed as plane waves modulated by periodic functions, its application to aperiodic crystals is more cumbersome. It requires the definition of superspace groups and becomes exceedingly difficult due to the high number of degrees of freedom for both the electronic and vibrational states.[83] A full explanation on aperiodic crystals and superspace is considered outside the scope of this review and can be found in Janssen and Janner.[83] In 2022, Meekel et al.[60] reported the synthesis of a MOF-5, commonly referred to as IRMOF-1, derivate by replacing the linear *para*-1,4-benzenedicarboxylate (bdc) linkers with bent *meta*-1,3-bdc linkers. The lower symmetry of the bent organic linkers leads to an aperiodic crystalline material, which they called TRUMOF-1. The pore structure of the derivate can be described using rotationally asymmetric Truchet patterns (hence the name TRUMOF-1 as an IRMOF-1 derivate) and the authors showed that adsorption of guests is sensitive to the disordered pore network.[84] In a follow-up paper, they compared the elastic stability of the aperiodic crystalline TRUMOF-1 to the periodic crystalline MOF-5 and showed a superior resistance of TRUMOF-1 to pressure-induced framework collapse, which was attributed to the aperiodic network topology of TRUMOF-1.[85] **Figure 5** compares the topologies of MOF-5 (**pcu** topology) and the aperiodic crystalline TRUMOF-1 (**fcu-6** topology) as well as the $F\bar{4}3m$ (216) space group of the configurational average structure.

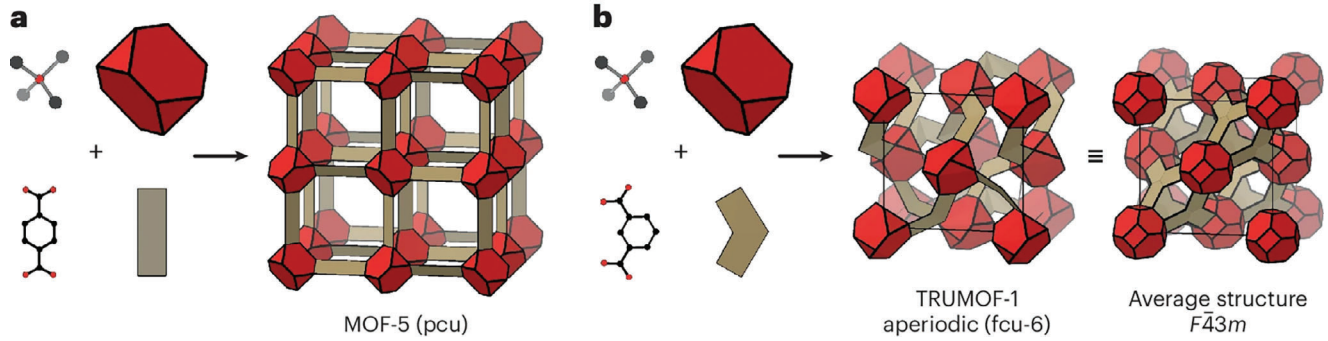

Figure 5. a) In MOF-5, tetrahedral OZn_4 clusters (red polyhedral) are connected by 1,4-bdc linkers (beige panels) to form a network structure with the simple cubic pcu topology. b) The structure of TRUMOF-1 is generated by similar components, except that the linear 1,4-bdc linker is replaced by the bent 1,3-bdc isomer (beige angled panels). Clusters are arranged on a face-centered cubic lattice, with each cluster connected to six of its 12 nearest neighbors (topology fcu-6). The connectivity in TRUMOF-1 is aperiodic. Shown in the center of this panel is a representation of one possible $1 \times 1 \times 1$ approximant. The configurational average of the TRUMOF-1 structure, which is periodic but with partial site occupancies, is represented on the right-hand side. Reproduced with permission.[85] Copyright 2023, Springer Nature.

2.1.3. Amorphous Structural Models

Reticulating building blocks in extended structures implies crystallinity. However, as discussed in the Introduction, the IUPAC definition of MOFs excludes crystallinity as a necessary condition for a reticular material to be classified as a MOF. Consequently, reticular materials can also exist in amorphous phases like liquids, gels, and glasses.[86] Amorphous MOFs can be produced by either preventing crystallization during reticulation of the building blocks or collapsing the crystalline structure by pressure- or temperature-induced amorphization, melt-quenching, or ball milling.[87] The long-range disorder in an amorphous MOF will translate to an absence of well-defined Bragg peaks in their X-ray or neutron diffraction patterns.[88] The lack of periodicity and/or symmetry in amorphous reticular materials makes them much more difficult to model accurately.[89–91] To avoid finite-size effects in the computational results, the size of the periodic unit cell should be sufficiently large with respect to the largest correlation length of the system.[92–94] As the correlation length is strongly dependent on the system under study, there are no clear rules as to the appropriate size of the model. Therefore, it is recommended to verify the absence of finite-size effects by executing multiple simulations at increasing sizes of the periodic unit cell, a recommendation that is valid irrespective of the amorphous or crystalline character of the structural model.[95,96] Structural models of amorphous materials can be generated with (i) melt-quenching with molecular dynamics simulations, (ii) reverse Monte Carlo sampling based on experimental input and (iii) polymerization-based modeling.[90] Hereafter we briefly give some more information on each of the methodologies.

The first approach relies on molecular dynamics simulations to generate amorphous structural models, either with reactive force-fields[97] or with electronic structure methods such as density functional theory (DFT).[86] While force-fields allow to model reticular materials at larger time and length scales, there is an ongoing discussion on whether force fields can adequately model amorphous reticular materials.[91,97] Gaillac et al.[86] used ab initio molecular dynamics (AIMD) simulations to study the structure of ZIF glasses (ZIF-4, ZIF-8, and SALEM-2) starting from a structural model of the crystalline solid state. They melted the ZIF by running AIMD simulations at 1500 K and used the free diffusion or cleavage frequencies of Zn-N bonds to make a distinction between solid (crystalline) and liquid (amorphous) phase. Multiple configurations of the ZIF liquids were quenched to room temperature by running consecutive 4 ps constant temperature AIMD simulations at 200 K intervals from 1500 K to 300 K to deliver the structural models of the solid amorphous glass.

A second way to generate amorphous structural models of gels and glasses is reverse Monte Carlo (RMC), which works as follows: (i) the radial distribution function of an initial guess of the structure is calculated, (ii) a new configuration is generated by random movement of a particle, (iii) the radial distribution function of the new configuration is calculated, (iv) the two χ^2-statistics[98] are computed, comparing each radial distribution function with the experimental radial distribution function and (v) the configuration leading to the lowest χ^2-statistic becomes the new starting configuration until the χ^2-statistic converges to an equilibrium value or a predetermined threshold.[99] However, it should be remembered that analysis of Bragg reflections of experimental samples to validate the computational structure considers only the long-range configurational average structure, while the RMC procedure will only deliver one possible structural model through the minimization of differences between calculated and observed data.[100] Structural models generated with this method will largely depend on the initial configuration of the crystalline model as well as on constraints imposed during the RMC procedure itself.

The third approach to model amorphous MOFs takes inspiration from the field of polymer chemistry. Bechis et al.[101] studied the effect of defects and disorder in amorphous MOFs by generating structural models using a polymerization algorithm consisting of four steps: (i) random packing, (ii) polymerization, (iii) saturation and (iv) annealing. Initially, constituent building blocks of the target MOF glass are randomly packed in a periodic unit cell at a low initial density, which ensures sufficient mobility for the building blocks during the assembly process. Next, the building blocks are polymerized by allowing bond formation between reactive sites on adjacent building blocks. When a reactive site cannot find a building block with which to react, the site can be saturated (e.g., with hydroxyls or water) which results in defects

in the structural model. To relax the final structural model, the structure is annealed with MD simulations, typically densifying the final structure.

2.1.4. Cluster Models to Study Local Phenomena

Depending on the properties of interest, i.e., local versus non-local phenomena, a structural model needs to be defined that fits the needs. For example, when interested in catalytic reactions on isolated active sites, it might be interesting to use a cluster model to represent the structure, rather than a periodic one.[102] However, it should be carefully tested in how far the extended environment impacts the local property of interest. For some catalytic reactions, it may at first instance be assumed that only the local environment plays a role, however, in many cases, neighboring interactions with other guest species or implicit long-range interactions due to the impact of the lattice may affect the catalytic activity. Many cluster calculations have been performed in literature with clusters of increasingly larger sizes. In this sense, even with a cluster model, it is possible to a given extent to capture parts of the extended lattice. A cluster model can be constructed starting from a relaxed periodic model. First, a narrow region of interest is identified and all atoms outside this region are removed (e.g., by defining a cutoff radius around one or more atoms). In the next step, the cluster model needs to be saturated (e.g., with H atoms) to avoid dangling bonds and the terminal atoms can be frozen in place to mimic the constraints of the original periodic model, as shown in Figure 4 (right-hand side).[103] Careful convergence tests of the property of interest with respect to the size of the cluster model are necessary, as the optimal cluster size is likely to change according to the problem in question. The great advantage of cluster models lies in the ability to use computationally more expensive electronic structure methods having a higher accuracy compared to DFT, as will be discussed in more detail in Subsection 2.2.1.

In 2019, Gagliardi and coworkers used cluster models to study the activity of Fe(II) species for the hydroxylation of methane (ethane) to methanol (ethanol) in MIL-type MOFs.[104] In their cluster models, the metal Fe node was capped with formate groups to simulate the structural units of various MOFs, including MIL-100(Fe), MIL-101(Fe), MIL-127, and PCN-250, and the authors concluded that MOFs based on a tri-iron oxide node can potentially serve as catalysts for the conversion of light alkanes to alcohols. Two years later, in 2021, some of the same authors again used cluster models to study CO and NO adsorption in iron-based MOFs.[105] The authors characterized the adsorption behavior of CO and NO on the same tri-iron oxide nodes to accurately assign the vibrational infrared bands in iron-based MOFs. In 2022, Lyu and Maurin also used iron-based cluster models to study the activity of coordinatively unsaturated sites in MOFs for the catalytic reduction of CO_2.[106] The authors studied metal-oxo trimer nodes (Fe_2M, M = Cu(I), Cu(II), Fe(II), Co(II), Ni(II), Zn(II), Cd(II), Ti(III), Y(III), and Ce(III)) existing in MIL-88, MIL-100, MIL-101 and PCN-250 for the reduction of CO_2. The study showed that Cu(II)-, Co(II)-, and Ni(II)-doped metal oxo-trimers could exhibit superior catalytic activity than Fe(II), with Ni(II) the most active one. In 2023, Tofoni et al.[107] studied the conversion of methane to methanol over a Fe(II) site in MIL-100(Fe) to hypothesize a catalytic cycle and the authors used cluster models in DFT calculations to conclude that the Fe(II) centers in the nodes of MIL-100(Fe) can dissociate O_2 to catalyze the production of methanol.

2.1.5. Disorder in Structural Models

Modeling reticular materials with pristine unit cells (or supercells) ignores the presence of defects, always present and unavoidable in real materials, as well as surface effects.[108] This subsection focuses on defects and disorder in reticular materials; surface effects will be discussed in the following subsection. Defects do not necessarily have a negative impact on the material's function and defect engineering can be used as a tool to promote catalytic activity or diffusion in reticular materials.[101,109,110] The length scale of defects and disorder in crystalline reticular materials can be classified according to their length scale, making a distinction between short-, mid- and long-range heterogeneities.[54] The upper part of **Figure 6** shows experimental Scanning (Tunneling) Electron Microscopy (S(T)EM) images of UiO-66, illustrating the continuous efforts of experiment to probe materials at smaller length scales. In the computational bottom-up approach (lower part of Figure 6), computational scientists continuously expand idealized structural models to improve correspondence with real materials.

The main point defects, the typical example of short-range heterogeneities, in reticular materials concern the absence or modification of either the organic linkers, the nodes or both, as shown in Figure 4 (middle) and the bottom middle of Figure 6.[112] In 2018, Fischer and coworkers highlighted efforts (at the time) to model defective metal-organic frameworks.[112] These computational studies tackled the interdependency of missing linker defects and physical properties such as gas sorption and mechanical stability. More recently, in 2022, Möslein et al. combined computational modeling and experiment to study the connection between local defects and the nanoscale mechanical properties of ZIF-8.[113]

Again in 2018, Sholl and coworkers used molecular simulations to show diffusion in ZIF-8 is facilitated by water-induced point defects such as dangling linkers and linker vacancies.[114] In a recent follow-up publication (2024), researchers from the Sholl group used a combination of DFT calculations, force-field molecular dynamics, and Grand Canonical Monte Carlo simulations to show that point defects can promote the nucleation of water clusters and may change the adsorption properties of MOFs in a significant way.[115] At a larger length scale, a sufficiently high number of point defects will alter the surface area, leading to mesoporosity in the crystalline structure.[71] In 2022, Cui et al.[116] studied the degradation of ZIF-8 and ZIF-71 by defect propagation using the kinetic Monte Carlo[117] method. In this study, the ZIF structures were approximated as a 2D square lattice and DFT calculations were used to estimate the energy of defect formation and the interaction energy between defects. These energies were subsequently used as parameters for their kinetic model and the time evolution of the defect concentration was obtained from averaging multiple kMC trajectories. The authors predict, in correspondence with experimental results,[118] a much slower defect formation for ZIF-71 compared with ZIF-8 and concluded that

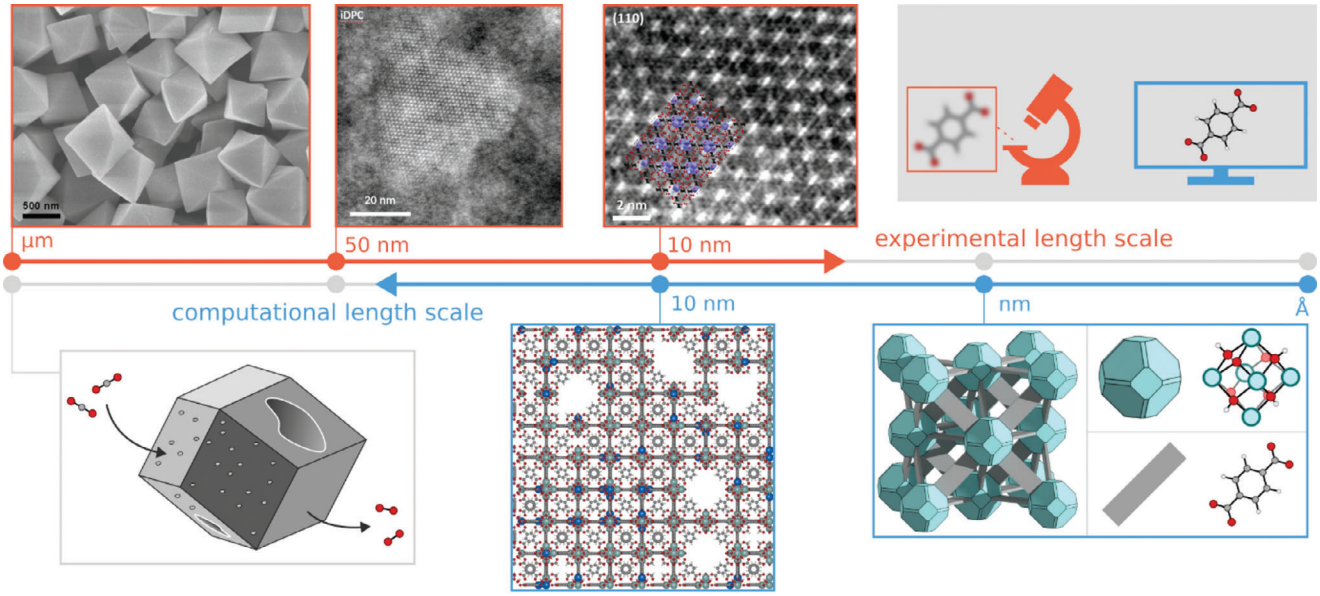

Figure 6. Top part, left to right experimental images of UiO-66: Scanning Electron Microscopy (SEM) image (Reproduced with permission.[111] Copyright 2018, American Chemical Society), low-dose Scanning Transmission Electron Microscopy (STEM) image showing the framework structure, low-dose STEM image showing the linkers. Lower part, right to left: Organic and inorganic building blocks of UiO-66 and its framework structure, randomly generated defective structure with ca. 25 000 atoms, schematic representation of a MOF crystal particle with point defects and mesopores, where external guest molecules can enter.

neighboring defects lead to autocatalytic growth of the defect density which in turn leads to the formation of defect clusters.[116] As an illustrative example of long-range disorder, in 2023, Rogge et al.[119] studied correlated nanoregions in MOFs and predicted a higher amorphization pressure for defective UiO-66 due to cooperative interaction of point defects. Beside local point defects, extended defects like dislocations and interfacial areas of polymorphic materials are responsible for global displacive or reconstructive modes of flexibility.[120,121]

2.1.6. Surface Chemistry of Reticular Materials

Previous sections focused on the modeling of the bulk of reticular materials. In reality, crystal particles have a finite size, with sizes ranging from the nanometer to the micrometer scale and a certain morphology, as shown in the bottom left illustration in Figure 6. Furthermore, the external surface area has a certain chemical composition. Apart from these finite-sized effects at the crystal particle level, reticular materials need to be embedded in supports or fabricated as monoliths to be usable in any practical application.[122–125] Modeling reticular materials within their supports is clearly beyond the current capabilities of molecular modeling. However, simultaneously accounting for the finite size, shape and chemical termination of the external surface, may come soon within reach of molecular modeling efforts. The properties of the external surface will determine the interactions between the nanoparticles as well as with their surroundings.[126,127] Micron-sized MOFs cannot be used as synthesized as the fine particles would cause a large pressure drop in fixed-bed reactors or adsorption vessels. Therefore, industrial deployment of MOFs will necessarily involve MOF/binder composites which are shaped to larger pellets to guarantee sufficient throughput of the feedstock.[128] Functionalization of the external surface of reticular nanoparticles with polymers and lipids is therefore an active focus in the field of reticular chemistry.[129] To identify the optimal binder material and thoroughly understand the interactions between the crystalline material and the binder, accurate structural models of the external surface of reticular materials are required.

Slab models are constructed starting from geometry-optimized supercells of the crystal structure. The periodic model is cleaved along favorable crystallographic planes, typically identified with the Bravais-Friedel-Donnay-Harker (BFDH) method,[130] which uses a geometric argument to argue that the growth rate of a crystallographic plane is inversely proportional to the interplanar distance. While this measure may not be sufficiently accurate to identify the finite crystal shape,[131] the BFDH method relies only on the geometry of the lattice and can be immediately applied to any periodic structural model. Alternatively, crystal surfaces can be identified using the Wulff[132] construction method, which states that finite crystals are bounded by faces located at distances proportional to their surface formation energies. Using this energetic argument, the crystal shape can be determined by minimizing the total surface energy for a given volume. However, calculation of the surface energy may prove challenging in large unit cells with many atoms (e.g., DUT-49 and MIL-100) in which case the BFDH method may prove useful. A third and final approach is to construct finite-sized crystals using the specific topology of the reticular material, as was done by Keupp and Schmid (vide infra).[120] To avoid dangling chemical bonds or exposed metal ions after cleaving a periodic crystal along a crystallographic plane, the surface can be terminated based on chemical intuition or experimental input (e.g., OH^-

ions or H_2O molecules in case of synthesis with an aqueous solvent). By convention, slab models are typically periodic in the *xy*-plane, with the *z* axis perpendicular to the surface. To avoid interactions with periodic images in the *z*-direction, a vacuum box is added above the slab model to construct the final structural model. When using a plane waves basis set, a sufficiently large amount of vacuum should be added above the surface to prevent periodic interactions along the surface normal. The resulting large lattice constant leads to a short reciprocal lattice vector, necessitating a large number of plane waves within a given kinetic energy cutoff for an accurate description of the electronic structure. Jaffe et al.[133] showed that density functional theory for two- and three-dimensional periodic systems may be expressed using localized Gaussian basis functions. As these basis functions naturally go to zero in vacuum, such a description may be beneficial in 2D slab models of reticular materials. Figure 4 (bottom left) shows an example of a UiO-66 membrane where the BFDH method was used to identify the most favorable crystallographic plane and hydrogen atoms were added to impose charge neutrality of the final structural model. Obtaining experimental information (e.g., surface termination, mesoporosity, ...) with atomic resolution of the external surface is extremely challenging and the construction of accurate surface models from a modeling perspective remains an open challenge for now.

To the best of the authors' knowledge, the earliest computational studies that used slab models for metal-organic frameworks came in 2012, when Zhang et al.[134] studied H_2/CO_2 separation in a mixed-matrix membrane (MMM) consisting of polybenzimidazole (PBI) and ZIF-7. Amirjalayer et al.[135] studied the surface termination of HKUST-1 in 2016, which was followed in 2016 by a computational study by Dürholt et al.,[136] who used slab models to model the deformation of the [111] surface of HKUST-1. In 2020, Thompson et al.[137] used slab models of DUT-8(Ni) to study the external surface of nanoparticles and the influence of different surface groups on the gate-opening mechanism with GCMC simulations driven by classical force fields. The authors showed that, while the external adsorption sites depend on the capping group, the different groups capping the external surface have only a minor contribution to the gate-opening mechanism of the switchable MOF. Around the same time, Maurin and coworkers published a series of computational studies on MOF/polymer composites for a selection of MOFs, such as UiO-66,[138] ZIF-67[139] and CALF-20,[140] in which slab models were used to represent the reticular materials. In the latter study on CALF-20, the authors studied the adhesion of four binders to slab models of CALF-20 and evaluated the CO_2 capture performance of the composite system. To construct the slab models, the energetically most favorable[100] surface was identified using DFT calculations. As no experimental evidence was available regarding surface termination, the authors terminated the exposed Zn metal ions with water molecules based on the synthesis process of CALF-20. The binder materials (polymers) were added to the crystal surface and the composite system was relaxed by averaging over several independent MD simulations. The authors concluded that the shaping of CALF-20 with the polymer carboxymethyl cellulose as binder material maintained a high CO_2/N_2 selectivity with similar CO_2 uptake and transport compared to pure CALF-20.

Whereas a few computational studies of MOFs using slab models are available in literature, similar studies on COFs are scarce. In 2021, Luo et al.[141] constructed slab models of charge transfer processes in COFs with triphenylamine and triazine units to study electrochemiluminescence. As another example, Yu et al.[142] constructed models of MOF/COF hybrids by matching the interfacial facets of a MOF (UiO-66-NH_2) and a COF (tri(4-pyridylphenyl)amine TPPA).

So far, the number of computational studies on the surface chemistry of reticular materials remains limited. In late 2023, Zhang et al.[143] published a tool, written in Python, called the "MOF-membrane constructor" to generate MOF membranes with reasonable surface terminations and to automatically identify preferred exposed crystal planes, based on the BFDH method (vide supra). Notably, the authors provide options to the user with respect to surface termination. No termination is applied if the exposed metal center is deemed reasonably stable or alternatively, the exposed metal can be terminated with -OH/-H groups, modulators like acetate or solvent molecules. It is expected that tools like these, along with others which will certainly be developed in the future, will accelerate the development and understanding of surface chemistry of reticular materials.

In contrast to modeling the external surface of reticular materials via slab models, the most realistic representations would be to simulate the materials as true finite-sized crystallites, having a certain shape and morphology. So far, the number of contributions reporting simulations on finite-sized crystallites in the field of reticular materials is extremely scarce. Keupp and Schmid[120] modeled finite-sized nanocrystallites of DMOF-1(Zn) using the reverse topology approach,[135,144–146] by extending the **pcu** topology and slicing the periodic model along specified *hkl*-planes to generate nanocrystallites of around 230 000 atoms (diagonal distance ~ 23.3 nm). The reverse topology approach will be discussed in more detail in the following subsection. The surfaces of the nanocrystal were terminated with either 1,4-diazabicyclo[2.2.2.]octane (dabco) pillars ([001] plane) or phenyl groups ([100] and [010] planes) as shown in **Figure 7**.

2.1.7. High-Throughput Screening of Reticular Materials

Whereas in Subsection 2.1.1 the focus was set on the construction of structural models for one particular material, one can also use the principles of reticular chemistry to generate a nearly inexhaustible variety of hypothetical reticular materials from the possible (super)molecular building blocks, which can be organic, inorganic or both. Experimental screening is often too time-intensive as well as expensive to characterize all possible candidates and high-throughput methods are needed to quickly and accurately explore the design space of reticular materials.[147]

An early attempt to automate the discovery of reticular materials came in 2011, when Wilmer et al.[148] generated a library of over 300 MOFs by recombining building blocks of previously synthesized MOFs. The authors predicted the CH_4 uptake for all possible candidates and their computational results suggested the promotional effect of methyl functional groups on CH_4 uptake. From their computational results, they identified MOF

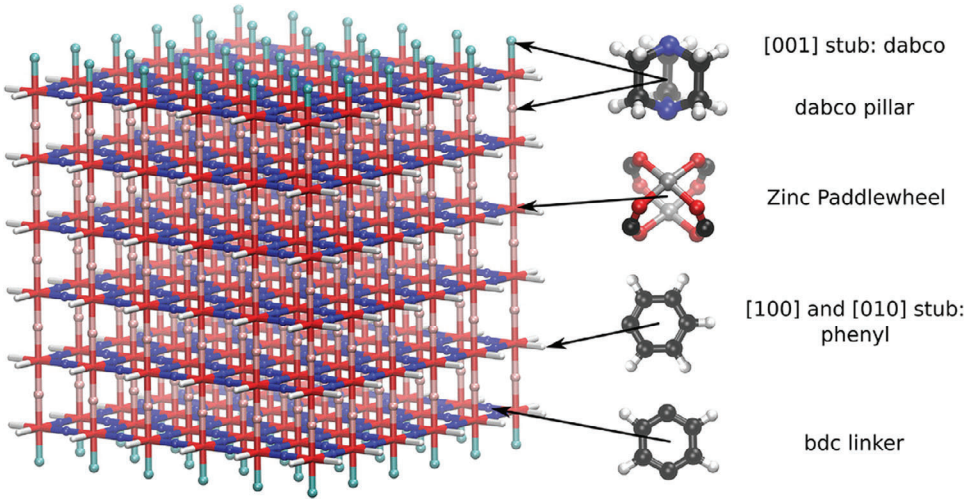

Figure 7. Construction of a MOF nanocrystal from the corresponding blueprint for the case of DMOF-1 NC of size 6 × 6 × 6. Reproduced with permission.[120] Copyright 2019, John Wiley and Sons.

NOTT-107, with a high structural similarity to the MOF with the highest methane storage capabilities known at the time, PCN-14.[149] After the synthesis of NOTT-107, the authors found that the methane storage capacity was 8% lower than what had been predicted by simulations, which was attributed to incomplete pore activation of the synthesized material. To the best of our knowledge, this was the first success story that showcases how theoretical predictions can guide experiments.

Inspired by the success of Wilmer et al., researchers quickly explored different ways to generate hypothetical reticular materials for gas storage.[150,151] Nowadays the most popular way to explore the hypothetical design space is to use known topologies as a starting point for the exploration of the design space, referred to as the reverse topology approach (vide supra). This method starts from a target topology in which building blocks (linkers/SBUs for MOFs or organic building blocks for COFs) are reticulated to the target topology, either by applying symmetry operations of target space groups or iteratively until a unit cell is formed. After structural optimization of the hypothetical MOF/COFs, different candidates can be compared by predicting performance-property relations from which the most promising hypothetical reticular materials can be selected for synthesis.

Currently, there are multiple protocols and software packages (e.g., ReDD-COFFEE,[152] pyCOFBuilder,[153] TOBACCO,[154] TOBASCCO,[150] GFlowNets,[155] Pormake,[156] Weaver,[145] Zeo++,[157] AuToGraFS[158] and others) available to aid the in silico design of MOFs and COFs. The structural models generated by these computational tools, supplemented with those from experimental characterization techniques like X-ray diffraction, are collected and made available in various databases such as: Reticular Chemistry Structure Resource (RCSR),[34] Cambridge Crystallographic Data Centre (CCDC),[159] the ToposPro Topological Collections,[160] the Materials Project,[161] Novel Materials Discovery (NOMAD),[162] the Computation-Ready Experimental MOF (CoRE MOF) database,[163] the Quantum MOF (QMOF) database,[164,165] the Wilmer database,[148,166] the ab initio REPEAT charge MOF (ARC-MOF) database,[167] the CURATED[168,169] COF database and others.

Reticular materials exist in an immense design space, complicating a comprehensive screening of reticular materials due to (i) the potentially prohibitive computational overhead to accurately compute properties of interest for every possible candidate and (ii) the overwhelming amount of data generated through the exploration of the compositional, physical and chemical properties.[170,171] These challenges are emerging in all branches of materials science and new techniques are needed to process the large amount of information in an efficient way.[61,172] In a recent review by Moghadam et al.,[173] the authors discuss the predictive power of computational modeling by describing the development of new MOFs that were computationally designed before being experimentally synthesized, such as NU-100 and NU-800. A thorough discussion on data science and machine learning in reticular materials discovery is considered outside the scope of this review, as many excellent dedicated reviews are already available in literature, see for example the following references.[165,174–182]

2.1.8. Inverse Design of Reticular Materials with Machine Learning Techniques

Recently, significant progress has been made in leveraging machine learning techniques for the inverse design of MOFs. Traditionally, the structure of a MOF is first defined, after which its various properties are predicted. Inverse design attempts to reverse this process; generating MOFs that satisfy given input properties. In 2021, Yao et al.[183] proposed a variational autoencoder (VAE) based approach to encode and decode MOF structures with a latent space of a graph-based representation of MOFs. A Gaussian process is trained on properties of MOFs in the latent space, enabling a search through this space for the top-performing MOFs.

Park et al.[184] more recently proposed a deep reinforcement learning method based on a generator agent that creates MOF structures and a predictor that evaluates them for specific properties (CO_2 heat of adsorption and CO_2/H_2O selectivity). The agent iteratively improves its design based on a reward from the predictor. The predicted top performers were shown to be competitive

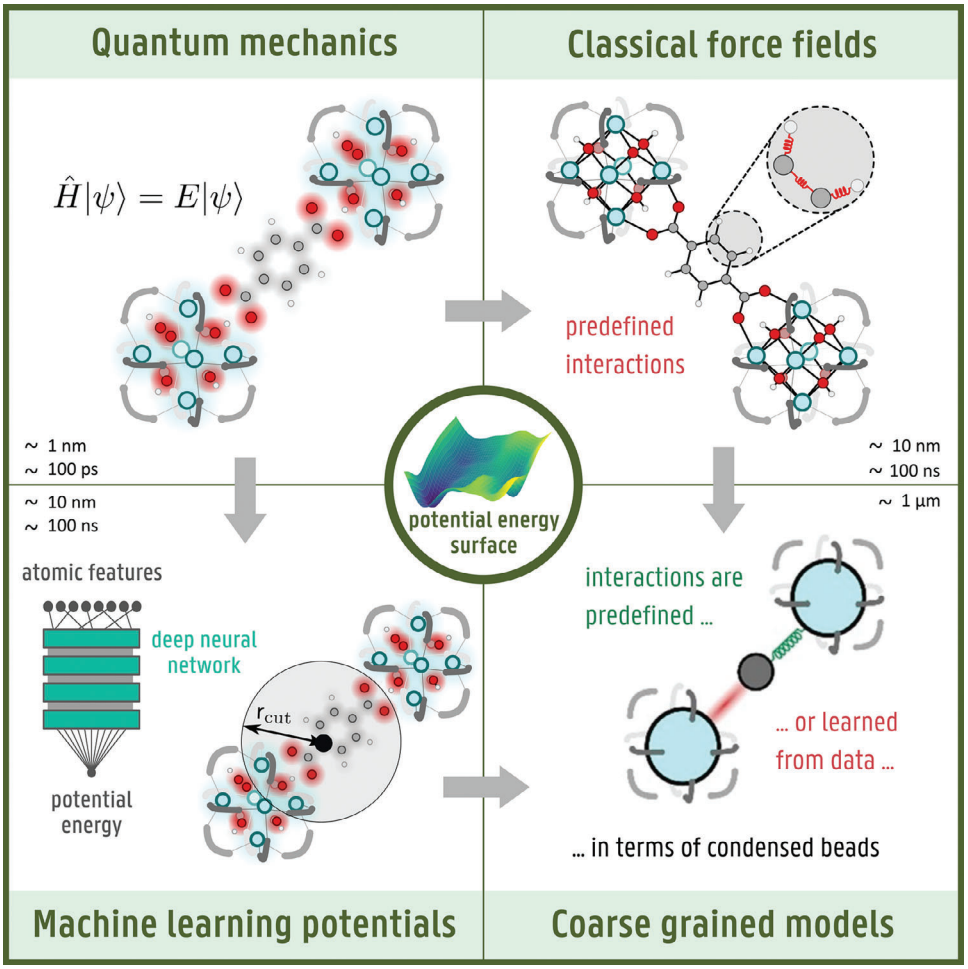

Figure 8. The central quantity in a molecular modeling exercise is the potential energy surface (PES), which can be modeled by solving Schrödinger's equation with quantum mechanical methods (top left). To access larger time and length scales, interatomic potentials can be derived either with machine learning methods (bottom left) or approximating the PES with analytical expressions (top right). Coarse-graining methods (bottom right) group atoms in interacting beads. Reproduced with permission.[121] Copyright 2024, Royal Society Publishing.

with top-performing MOFs reported previously in the literature for direct air capture.

Compared to this reinforcement learning-based approach, Fu et al.[185] proposed the diffusion-based MOFDiff model (analogous to image-generating models) to predict high-performing MOFs for carbon capture applications. In their model, coarse-grained (vide infra) 3D structures of MOFs are directly generated, maintaining the physical symmetries using equivariant and invariant networks. These machine learning-based methods for inverse design of MOFs appear highly promising in generating novel MOF structures targeted specifically for the applications of interest.

2.2. Potential Energy Surface

Once a structural model for the material has been defined, the next step of a molecular modeling exercise models the Potential Energy Surface (PES), connecting the atomic configuration of a many-body system to the potential energy of the system. This section will discuss four different methods to estimate a single point on the PES: quantum mechanical methods, classical force fields (FFs), machine learning potentials (MLPs), and coarse-grained models. Other methods, such as quantum mechanics/molecular mechanics (QM/MM) are viable alternatives which have been successfully applied to study reticular materials.[186–188] A detailed discussion of this method is considered to be outside the scope of this review and we refer the interested reader to a dedicated introduction on QM/MM.[189]

The method of choice to describe the PES is inextricably linked to the attainable time and length scales of the simulations.[54] **Figure 8** shows the typical simulation limits for each of the different methods. While quantum mechanical (QM) methods will consistently deliver results with the highest accuracy, these methods restrict the accessible length and time scales to hundreds of picoseconds and the nanometer scale due to the extensive computational cost and many degrees of freedom. Both classical force fields and MLPs construct an interatomic potential to approximate the PES, yet the underlying principles are markedly different and therefore these two methods will be discussed in separate

subsections. Both classical FFs and MLPs provide access to much larger time and length scales, enabling the construction of structural models with a higher complexity and thus closer to physical reality. Classical force fields give access to longer length and time scales compared to MLPs, as the latter comprise a more complex functional form with many more parameters. Coarse-grained models abandon the atomistic resolution of the system by grouping atoms in beads. The reduction of the degrees of freedom unlock access to structural models up to a few micrometers, which in turn allows the study of physical phenomena such as mesoporosity and polymorphism. However as one abandons the atomistic scale and removes the highest frequencies in the system, one in principle loses the correct time aspect of the simulations. More details about which properties can be obtained using coarse-grained models can be found in the following reference.[190]

2.2.1. First Principles Calculations

Electronic structure methods can be broadly classified in (i) wavefunction-based methods such as Hartree-Fock (HF) theory and post-HF extensions and (ii) density functional theory (DFT). Among the different electronic structure methods, Kohn-Sham DFT calculations are often the method of choice, typically considered as an optimal balance between accuracy and computational cost. Other DFT methods, such as constrained DFT, time-dependent DFT, and orbital-free DFT will not be discussed in this review. In particular, orbital-free DFT is currently experiencing a renewed interest due to its favorable (almost) linear scaling, as opposed to the cubic scaling of Kohn-Sham DFT.[191–193] Similarly, wavefunction-based methods like HF and post-HF methods are considered to be outside the scope of this review. For a dedicated review of electronic structure modeling in reticular materials, we refer to the references.[194,195]

2.2.2. Periodic DFT Calculations

Based on the Hohenberg-Kohn foundations of DFT, the Kohn-Sham formalism reduces the complex direct description of a many-body system to a (comparatively) simple description of its energy as a functional of the ground-state electron density.[196,197] Using DFT, the electronic energy is variationally minimized by first calculating a trial electron density from trial virtual Kohn-Sham orbitals and subsequently using the electron density as an input to the formally exact energy functional. In theory, DFT is an exact method, clearing the path to an exact solution to Schrödinger's equation for an arbitrary many-body system. In practice however, no exact formulation of the electron exchange-correlation (XC) interaction is known and thus approximations to the XC functional are necessary.[198] Due to the approximate nature of a practical XC functional, the Coulomb energy due to the interaction of an electron with the entire electron density, including its own density, will introduce well-documented self-interaction errors.[199] We refer the interested reader to more detailed information on the approximate nature of exchange correlation functionals.[200–202]

Currently, there are hundreds[203,204] of different XC functionals available, leading to a veritable "zoo" of density functional approximations (DFAs). To introduce order in the chaos of the different approximations, Perdew developed a popular DFA taxonomy, termed Jacob's ladder,[205] separating the available DFAs according to the ingredients and approximations of the XC functional. By far the most popular type of DFA used in first principles calculations of reticular materials are based on both the electron density and its gradient as input to the XC functional, referred to as the generalized gradient approximation (GGA). Popular choices within the class GGA functionals include PBE,[206] revPBE,[207] RPBE,[208] PBEsol,[209] vdW-DF(2),[210,211] HLE16,[212] HLE17[213] and others. The optimal choice of GGA functional will depend on the reticular material under study and validation with experimental data or high-accuracy wavefunction-based calculations is indispensable. More accurate XC functionals are available, accounting for the kinetic energy density (meta-GGA) or including nonlocal Hartree-Fock exchange energy density (hybrid GGAs), which are typically used to calculate electronic properties such as band gap and band structures (see Subsection 2.4.3).[214]

The extended structure of reticular materials is best represented with periodic structural models and thus periodic plane waves are often chosen as basis functions which, contrary to finite atom-centered basis sets, do not suffer from basis set superposition error (BSSE).[215] The susceptibility of finite basis sets to BSSE can be addressed using the counterpoise method to generate BSSE-corrected atom-centered basis sets.[216,217] The electronic core states are highly localized due to the strong Coulomb potential close to the atomic nucleus and the constraint of orthogonality. An accurate description of the oscillatory core states would require many plane waves, yet deep-lying core states can safely be considered to be chemically inert. To mitigate the computational overhead, the effect of the core states can be replaced with a pseudopotential, limiting the explicit description of the electrons to the extended valence states. For a more thorough discussion on the differences between plane waves and localized atom-centered orbitals as basis sets in DFT calculations, see for example Tosoni et al.[218] As was noted by Formalik et al.,[219] MOFs and other reticular materials can be considered as a hybrid class of materials between discrete molecules and periodic bulk materials. The intermediate nature of reticular materials allows atom-centered basis functions to be used in computational studies of reticular materials, which can facilitate the study of reticular materials with large pore sizes.[214,220,221]

The high porosity of most reticular materials increases the relative importance of attractive electronic correlation effects, commonly termed London-dispersion or van der Waals interactions.[222] An accurate description of these effects is critical to approach chemical accuracy and explain a variety of noncovalent interactions (e.g., host-guest interactions in adsorbates, hydrogen-bonding interaction, aromatic π-π stacking and more).[223] In the semiclassical approach, the dispersion energy is evaluated as a pairwise additive interaction between atoms, even though electron correlation has an inherent many-body nature.[224] Post hoc semiclassical correction schemes are readily available, such as the series developed by Grimme and coworkers: DFT-D3, DFT-D3 with Becke-Johnson damping or DFT-D4.[225–227] Other popular correction methods are the Tkatchenko-Scheffler method and the exchange-dipole model (XDM).[228–230] Extensions to three-body-interactions, like the

Axilrod-Teller-Muto method,[231,232] or many-body-interactions, like Tkatchenko's many-body-dispersion (MBD) method,[233,234] are also available.

2.2.3. Force Fields

To increase the accessible time and length scales of the computational model, the computational cost can be mitigated by approximating the PES using parametrized analytical potentials to calculate the energy of a system as a function of the atomic positions. The resulting classical force fields express contributions to the potential energy in terms of internal coordinates, such as bond lengths, bending angles, dihedral angles, torsion angles, and more.[235] London-dispersion and Coulombic contributions to the potential energy can also be included to account for short- and long-range non-bonding interactions in the system. To determine intermolecular parameters between atom types, mixing rules are applied to generate pairwise additive interaction parameters between different atoms from the atomic parameters (e.g., Lorentz-Berthelot[236,237] mixing rules). The parameters of the analytical functions can be obtained either from experimental measurements or from ab initio calculations.

Early computational studies used generic force fields such as DREIDING[238] or UFF.[239] To properly account for the idiosyncrasies of reticular materials, such as framework flexibility or open metal sites, material-specific force fields were derived for reticular materials, such as: UFF4MOF,[240–242] MOF-FF,[243] QuickFF,[244,245] BTW-FF,[246] ZIF-FF,[247] ReDD-COFFEE,[152] VMOF,[248] and others. These force fields have been successfully applied in computational studies of MOFs, yet there is no clear preference for a particular force field and careful validation will always be required. As an illustrative example, force fields failed to accurately capture the host-guest interaction in case of CO_2 and CH_4 adsorption in M-MOF-74 (M = Co, Cr, Cu, Fe, Mg, Mn, In, Ti, V and Zn).[249] To describe chemical reactions with force fields, Goddard and coworkers developed a reactive force field, ReaxFF,[250–253] which includes connection-dependent terms relying on a bond-order formalism, empirically calculating the bond order from the relative atom positions. Furman et al. showed that ReaxFF may experience numerical pathologies due to bond order-dependent discontinuities and introduced the Tapered ReaxFF formulation to improve energy conservation during molecular dynamics simulations.[254,255]

2.2.4. Machine Learning Potentials

In the previous Subsection, it was shown how the PES can be approximated in a closed form analytical expression, resulting in classical force fields. While the physical basis of interaction terms comprising a classical force field is appealing, the usage of force fields depends on a trade-off between desired accuracy, computational efficiency, and transferability. The latter refers to the prediction of properties outside of the conditions or systems for which it was parametrized. As an alternative, the high-dimensional PES can be approximated by a numerical potential that is obtained using a non-linear regression of the potential energy as a function of atomic descriptors or features or with machine learning methods.[256–260] The fitted function, i.e., the machine learning potential (MLP), is trained from a consistent set of first principles training data and does not impose a predefined functional form for the interatomic interactions.

The first MLP was introduced in 1995 by Doren and coworkers, who successfully trained a feed-forward neural network to accelerate simulations of H_2 adsorption on a silicon cluster model.[261] The application of these first-generation MLPs was limited to low-dimensional systems such as cluster models or molecules interacting with a frozen surface. In 2007, Behler and Parinello applied atom-centered symmetry functions as predefined descriptors to construct atomic descriptors with translational, rotational and permutational invariance.[262] In this seminal second-generation MLP, the potential energy is expressed as a sum of atomic energies, accounting for the chemical environment within a predefined cutoff radius.

Truncating the atomic environment beyond a cutoff radius necessarily represents an approximation and any electrostatic or dispersive interactions beyond the cutoff radius are only implicitly accounted for.[263] To address the electrostatic long-range interactions, atomic partial charges can be included in the MLP, as was done with PhysNet, introduced in 2019 by Unke and Meuwly.[264] However, mapping the electron density onto atoms is an ambiguous task and the atomic partial charge will depend on the electron density partitioning scheme, such as Quantum Theory of Atoms in Molecules,[265] Hirshfeld[266] and Hirshfeld-Iterative partitioning,[267] the Density Derived Electrostatic and Chemical (DDEC6) method,[268] Minimal Basis Set Iterative Stockholder,[269] and others. Electrostatic interactions can also be included using maximally localized Wannier functions.[270] One such example is the self-consistent field neural network (SCFNN) published in 2022 by Gao and Remsing.[271] With this MLP, initial maximally localized Wannier centers are estimated, which are iteratively refined using neural networks to obtain a self-consistent electric field. The converged electric field is then used as additional input along with the atomic environment to calculate atomic energies and forces. The inclusion of electrostatic interactions beyond the cutoff radius can to some extent be captured by using message-passing neural networks,[272] in which molecules or periodic systems are described as three-dimensional graph networks consisting of vertices (atoms) and edges (interatomic distances, not bonds) and the interaction energy is obtained by exchanging pairwise and even many-body "messages" with neighboring atoms. In a message-passing neural network, a continuous chain of overlapping chemical environments is required to learn the long-range interactions. While the partial inclusion of long-range interactions is expected to improve the predictions of the message-passing neural network, the underlying physics will not be fully incorporated.[263,273,274] Each atom will be described by a feature vector which is iteratively updated in one or more message-passing layer(s) using message functions that process information about neighboring atoms. In this way, effective long-range physics including electrostatic and dispersion interactions, up to the product of the cutoff radius and the number of message-passing layers, can be (partially) included in the feature vector. In April 2024, Isayev and coworkers published a message-passing neural network, AIMNet2, which determines the charge distribution by accounting for the interaction energies between charge densities, atomic partial charges

and the atomic electronegativities to maximally account for long-range electrostatic interactions.[274,275] Other examples of popular message-passing neural networks include, but are not limited to: SchNet,[276] NewtonNet,[277] NequIP,[278] and MACE.[279,280] The ability of atomic state vectors to pass information beyond the cutoff radius in message-passing neural networks can enable the inclusion of dispersion interactions, depending on the number of message-passing layers.[281] Dispersion corrections like those discussed earlier can either be added to the reference DFT data, such that these interactions are learned by the MLP or added as a post hoc correction in case of additive dispersion correction schemes like Grimme's D3 method or its variants (vide supra).

In March 2024, Csànyi and coworkers released a general purpose MLP called MACE-MP-0[282] which was trained on Materials Project[283] data consisting primarily of inorganic crystal structures. The authors tested their model against the QMOF database to test the transferability of their model and showed a low mean average error of 0.033 eV/atom, despite the pronounced difference between the inorganic crystals of the training data and the complex MOF structures in the QMOF database. While the authors admit their model needs improvement to describe intermolecular interactions and high-pressure simulations, this MLP is, to the best of the authors' knowledge, the first attempt at a general-purpose MLP which can always be improved by adding high-quality reference data of the system of interest.

To reach chemical accuracy (about 1 kcal $mol^{-1} \approx 4.2$ kJ $mol^{-1} \approx 4.3 \times 10^{-2}$ eV $\approx 1.6 \times 10^{-3}$ a.u.), MLPs are preferentially trained to high-level electronic structure methods. However, the cost associated with these reference calculations is often prohibitive. To bridge this gap, Δ-machine learning[284] is a promising method in which the energies learned from a lower level of theory can be corrected with a limited set of calculations performed with high-level electronic structure methods like coupled-cluster (CCSD(T)) or random phase approximation (RPA). For more information on high-accuracy electronic structure calculations such as CCSD(T) and RPA, we refer to textbooks on electronic structure methods (e.g., *Electronic Structure – Basic Theory and Practical Methods* by Richard M. Martin).[202] In 2020 Bogojeski et al.[285] used Δ-machine learning to predict coupled-cluster energies of molecules such as water, ethanol, benzene and others. In their approach, the predicted DFT electron density is used as a descriptor to predict coupled-cluster energies. These authors showed that it was more efficient to learn the difference (hence the name Δ-machine learning) between DFT and coupled cluster energies rather than learning either of the two energies separately. A few years later, in 2024, Δ-machine learning was successfully applied to predict the enthalpy of adsorption of CO_2 in protonated zeolite H-CHA by Herzog et al.[286] These two examples highlight the potential of MLPs to go beyond the accuracy of DFT and applications of Δ-machine learning in reticular materials are expected to appear in literature in the near future.

Interestingly, machine learning networks trained to predict specific properties of a MOF can also be useful outside the narrow task of predicting those properties. For example, in this so-called transfer learning approach, Ma et al.[287] showed a significantly improved result on the prediction of CH_4 adsorption properties when it was first pretrained on the prediction of H_2 adsorption properties, demonstrating how training on one task can be informative for a different task. A more striking example of this was demonstrated by Vandenhaute et al.[288] As the atomic feature vectors of an MLP trained on energies and forces encode the atomic environments, they can also be informative for other properties. By adding a readout layer on the pre-trained atomic features to predict the phase of a MOF, a reaction coordinate of the phase transformation could be constructed based on the internal feature representation of the graph neural network without retraining the feature vectors. These authors showed that this reaction coordinate could then be employed in enhanced sampling simulations to determine the free energy barrier between different phases.

2.2.5. Coarse-Graining Methods

Reticular materials are prime candidates for coarse-graining methods as their reticular nature facilitates a templated representation. Subsection 2.1.2 discussed the reverse topology approach for the templated design of hypothetical reticular materials, which can be considered as a form of coarse-graining in which multiple atoms are mapped on a single interaction site. The simplified representation of the structure can be studied with parametrized force fields at larger time and length scales beyond the capabilities of first principles calculations and classical force fields. There is no unique way to coarse-grain atomistic models and coarse-graining methods are only limited by the imagination and chemical intuition of the researcher.

An early example of coarse-graining applied to reticular materials was published in 2014 by Sarkisov et al.,[289] considering MOFs as mechanical networks of rigid metal oxide clusters and organic linkers connected by flexible joints and employing their model to study the flexibility of MOFs. Another example came in 2016 when Dürholt et al. constructed a coarse-grained force field of HKUST-1[290] to study relative stabilities, lattice parameters, and interfacial phenomena of different topologies.[136,291] In contrast to the approach of coarse-graining MOF building blocks, Rogge[292] developed a two-step procedure to coarse-grain entire MOF unit cells, which the author termed the micromechanical model (MicMec).[293] In the first step, the atomistic unit cells are mapped to coarse-grained nodes which, in the second step, are propagated through time based on a nodal Hamiltonian derived from the elastic deformation energy.

Interactions between coarse-grained beads may require a complex multibody potential even if the underlying atomic interactions consist of simple few-body interactions.[294] For this reason, neural networks are ideally suited to capture inter-bead interactions. In 2019, Wang et al.[295] developed a coarse-grained neural network called CGnet. After coarse-grained coordinates of a system are chosen, the inter-bead interactions are learned by a deep learning network through a force-matching scheme. Such coarse-graining methods are ideally suited to mitigate the high computational cost associated with neural network potentials compared with classical force fields while maintaining high accuracy.

Coarse-graining can also be useful as intermediate representation. In late 2023, Fu et al.[185] developed an approach to generate novel MOFs for CO_2 capture. First, known MOF structures are coarse-grained and encoded using GemNet-OC, a physics-guided neural network.[296] After training the neural network, a

diffusion[297] process is applied by first introducing random noise to the coarse-grained MOF structures to train a periodic GemNet-OC, learning the ability to reverse the diffusion process. Training the denoiser allows the generation of coarse-grained MOF structures from random structures which can then be reverse-engineered to atomistic models and relaxed with the classical force field UFF.

2.3. Phase Space Sampling

This section provides an overview of methods available to explore the phase space, the space defined by the positions and momenta of the atoms in the system, to identify relevant configurations and reveal low-lying transition pathways. As seen from the previous section, the potential energy determines the energetic stability of a system as a function of the atomic structure. However, determining the low-lying states on the PES is by itself too limited as it only yields information in the limit of absolute zero temperature. To include finite temperature effects and determine the physicochemical properties of materials at realistic conditions, the free energy surface (FES), not the PES, is the appropriate quantity to be studied. The terminology "free energy" is often colloquially used but in fact it may refer to the Helmholtz free energy $F(N,V,T)$ when evaluated in the constant temperature T, constant volume V and fixed number of particles or Gibbs free energy $G(N,P,T)$ when both temperature T and pressure P are kept constant. The FES is obtained by starting from the PES but also accounting for proper corrections obtained from the partition functions evaluated in the appropriate thermodynamic ensemble. To this end one needs to use the principles of statistical thermodynamics, where the free energy can be estimated with partition functions, computed from the microscopic degrees of freedom subject to predetermined thermodynamic boundary conditions. More detailed information can be found in dedicated textbooks, e.g., *Statistical mechanics: theory and molecular simulation* by Mark E. Tuckerman.[298]

The vibrational partition function is paramount to include finite temperature effects in static modeling of crystalline materials. The canonical vibrational partition function follows from the discrete (an)harmonic vibrational energy spectrum and provides an estimate of the free energy, entropy, and other thermodynamic properties for a single point on the PES. After the discussion on static modeling, this section will continue by discussing dynamic methods. It will be shown how molecular dynamics (MD) and Monte Carlo (MC) techniques can account for multiple metastable states with comparable free energies. Relevant metastable states may be kinetically trapped by large energy barriers, necessitating enhanced sampling techniques to explore larger regions of the phase space, the discussion of which will conclude this section.

2.3.1. Static Methods

Precise phonon calculations provide a way to estimate a wide variety of lattice properties, such as thermal expansion coefficients, heat capacity, thermal conductivity, bulk moduli and host-host or host-guest interactions.[299–303] The analysis of lattice vibrations can also help explain the flexibility and reversible transitions like the breathing transition in MIL-53[304,305] and the gate-opening mechanism in ZIF-8.[306] The importance of lattice dynamics is not limited to MOFs as phonons have been shown to affect charge transfer processes in COFs due to electron-phonon coupling.[307,308]

The most established static method to calculate phonons in periodic crystalline structures is based on a second order Taylor expansion of the potential energy around the equilibrium configuration. The dynamical matrix, i.e., the mass-weighted Fourier-transformed Hessian matrix evaluated at the equilibrium configuration, yields an eigenvalue equation at a given wavevector in the Brillouin zone.[309] In practice, the large structural models of reticular materials, even in the primitive unit cell representation, justify probing the Brillouin zone at the Γ-point only. The vibrational frequencies follow from the square root of the eigenvalues and the eigenvectors give the collective atomic displacements from equilibrium (i.e., the phonons). The preceding procedure allows for a straightforward discrimination between a saddle point and a minimum of the PES: a saddle point will have at least one imaginary frequency while all frequencies at a minimum of the PES will be real. Using the eigenvalues of the dynamical matrix, the PES is therefore approximated as a superposition of uncoupled quantum harmonic oscillators.

In case of crystalline reticular materials, the low-frequency vibrations (soft mode phonons) can be strongly anharmonic.[16,310] In the phonon-based quasi-harmonic approximation (QHA), the temperature dependence of phonons is assumed to rely only on the crystal structure and volume.[311] Therefore, the anharmonicity is assumed to be restricted to the change in volume and the lattice dynamics are still treated within the harmonic approximation. The QHA can be used to calculate mechanical properties such as the bulk modulus or thermal properties such as thermal expansion, heat capacity and thermal conductivity.[312]

To quantify anharmonicity, cubic or quartic force constants can be calculated with Density Functional Perturbation Theory to estimate the anharmonic contribution to the vibrational energy.[313] Alternatively, the PES can be mapped by performing single point calculations along the collective displacements of the harmonic phonons to obtain anharmonic 1D potentials. A polynomial fit of the anharmonic potential in a basis of Hermite polynomials allows for an analytical calculation of the vibrational anharmonic energy levels.[314] A third way to quantify lattice anharmonicity is to variationally solve the nuclear Schrödinger equation using Vibrational Self-Consistent Field (VSCF) theory,[315] the nuclear counterpart of electronic Hartree-Fock theory.[316] Similar to electronic HF theory, the energy difference between the solution from VSCF and the exact solution is defined as the vibrational correlation energy. To account for vibrational correlation, extensions to VSCF can be included using vibrational perturbation theory,[317–319] vibrational configuration-interaction theory,[320] or vibrational coupled cluster theory.[321] While these methods allow for an estimation of the anharmonicity of the PES, they construct the PES as a function of the harmonic phonons and are therefore anharmonic corrections to the harmonic approximation, rather than inherently anharmonic methods. The size of the structural models of reticular materials, coupled with the

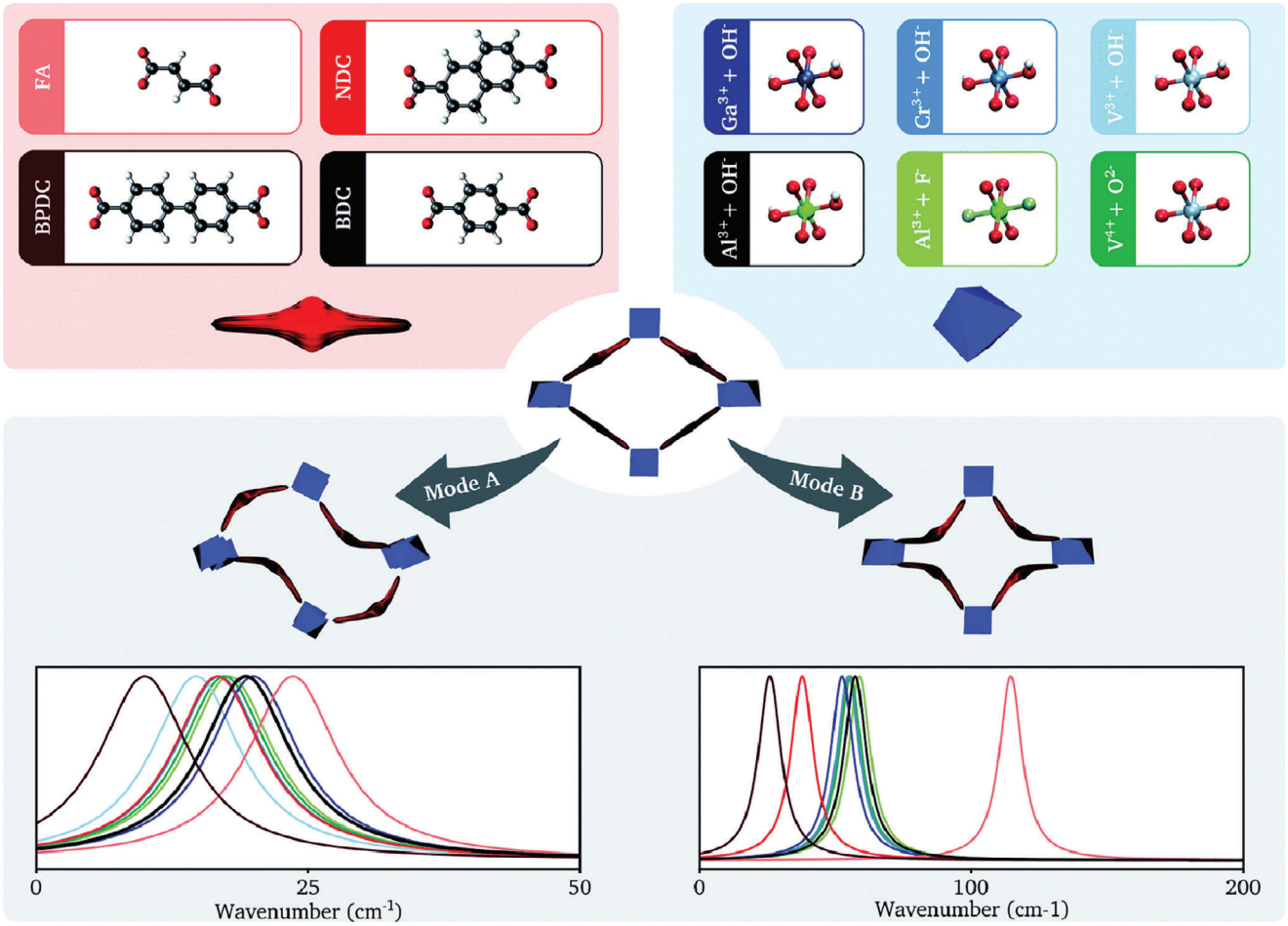

Figure 9. Different linkers are combined with aluminum-oxide octahedra and different inorganic octahedra are combined with BDC linkers to form a winerack framework. These frameworks exhibit general rigid-unit modes (RUMs), i.e., terahertz vibrations with translations and/or rotations of the building blocks. Two of these RUMs are visualized and their theoretically predicted frequencies for the different structures are plotted with Lorentzian lineshapes with the same amplitude. The color of the curve matches the color of the linker or inorganic octahedron that is substituted in the reference structure of MIL-53(Al). Reproduced under terms of the CC-BY license.[326] Copyright 2022, Hoffman et al., published by the Royal Society of Chemistry.

substantial computational overhead, can make these advanced methods challenging to apply to reticular materials using electronic structure methods (e.g., DUT-49 and MIL-100).

Vibrational spectroscopy is a valuable experimental and theoretical tool to study defects and displacive modes of flexibility in reticular materials.[39,301,302,322–325] In 2022, Van Speybroeck and coworkers studied the connection between the terahertz (low-frequency) vibrations and the well-known breathing phenomenon in a series of flexible MIL-53 analogs with different organic linkers and inorganic nodes.[326] As not all low-frequency phonons are Raman active, the authors used static DFT calculations (with the harmonic approximation) to study the effect of linker and inorganic node substitutions on the terahertz vibrations of the MIL-53 series, as shown in **Figure 9**. The combined theoretical/experimental approach in this study provides mechanical insight in the breathing phenomenon and highlights the need for accurate phonon calculations. The advanced static methods of the previous paragraph, combined with classical force fields or MLPs, can be readily applied to extend the study of phonons beyond the harmonic approximation.

2.3.2. Dynamic Methods

The harmonic approximation may prove insufficiently accurate, while the more advanced static methods can quickly become intractable due to the required computational cost. As an alternative, the phase space can be explored with MD simulations, propagating the system through time by integrating Newton's equations of motion, as shown on the left-hand side of **Figure 10**. A second large class of dynamic sampling techniques are MC sampling methods, based on accepting or rejecting random moves based on acceptance rules derived from the partition function of interest (right-hand side Figure 10). The energy evaluations throughout the sampling process can be based on electronic structure methods, classical force fields or machine learning potentials. In both classes of sampling techniques, MD or MC, nuclear quantum effects (NQEs) are typically neglected, which may deteriorate the computational results as shown by Lamaire et al.,[327] who showed that NQEs significantly affected the structural properties of MOF-5. Although rarely applied in practice due to the demanding computational cost, NQEs can be

Figure 10. Illustration of dynamics phase space sampling methods. Molecular dynamics propagates the system through time by integrating Newton's equations of motion (left). Monte Carlo methods are based on accepting random insertion/deletion moves through importance sampling. Reproduced with permission.[121] Copyright 2024, Royal Society Publishing.

accounted for with path integral molecular dynamics,[328,329] which can be accelerated using MLPs.[330–333]

The basics behind these well-established methods are readily available in any textbook on molecular modeling, e.g., *Understanding Molecular Simulation* by Daan Frenkel and Berend Smit.[94]

2.3.3. Sampling Protocol in Monte Carlo Methods

The thermodynamics of both host-guest interactions as well as structural host transitions (e.g., MIL-53(Al), ZIF-8, MIL-88, ...) are difficult to deconvolve experimentally and molecular modeling techniques are therefore ideally suited to understand the thermodynamics of guest-responsive frameworks.[334] Selecting an appropriate sampling protocol to generate a representative ensemble of configurations is crucial to obtain accurate and quantitative results.[121] To highlight the importance of the sampling protocol, the following will discuss a case study on modeling gas adsorption in flexible metal-organic frameworks with Monte Carlo simulations.

In grand canonical Monte Carlo (GCMC) simulations, the framework is typically assumed to remain rigid.[335] However, Witman et al.[336] among others showed the necessity to account for the intrinsic flexibility of the host to accurately model adsorption in metal-organic frameworks. GCMC simulations can also easily become trapped in local free energy minima, increasing the required simulation time until convergence. Transition matrix Monte Carlo (TMMC) methods[337,338] can be applied to address these difficulties, which will be discussed in more detail in Section 3.2. Sampling in the osmotic[339] (μ, p, T) ensemble allows deformations of the host framework by imposing a fixed adsorbate chemical potential μ, the external pressure p and the temperature T to minimize the osmotic potential. In 2010, Maurin and coworkers introduced a hybrid MD/MC scheme to sample the osmotic ensemble and observed guest-induced structural transitions in MIL-53(Cr).[340,341] In the hybrid scheme, the GCMC steps are supplemented with short MD simulations which are propagated in time in the (N_{host}, N_{guest}, p, $\boldsymbol{\sigma}_a = \mathbf{0}$, T) ensemble with a fixed number of molecules (N_{host} and N_{guest}), a fixed pressure $p = \mathrm{Tr}(\boldsymbol{\sigma})/3$ with $\boldsymbol{\sigma}$ the external stress, setting the deviatoric stress $\boldsymbol{\sigma}_a$ to zero ($\boldsymbol{\sigma}_a = \boldsymbol{\sigma} - p\mathbf{1} = \mathbf{0}$) and a fixed temperature T. The model of Maurin successfully reproduced the phase transition from the large pore (lp) to the narrow pore (np) form of MIL-53(Cr) after adsorption of CO_2 at low adsorbate pressure but failed to predict a second phase transition from the np form to the lp form. The breakdown of the model was tentatively attributed to insufficient sampling of the phase space, possibly due to the presence of large free energy barriers. In 2019, Rogge et al.[342] improved the hybrid MC/MD scheme to model adsorption in MIL-53(Al) while fully accounting for the shape and flexibility of the framework. In this second hybrid model, the short MD simulations are sampled in the (N_{host}, N_{guest}, V, $\boldsymbol{\sigma}_a = \mathbf{0}$, T) ensemble at a fixed cell volume V. By performing simulations at the range of all feasible framework volumes V, the authors could probe osmotic potential barriers which can prevent phase transitions from occurring even when a different phase is thermodynamically more stable. The authors showed that the adapted hybrid scheme increased the accuracy of the modeled adsorption isotherms, enabling a quantitative prediction of adsorption-induced metastable states, such as negative gas adsorption in DUT-49.[343] Negative gas adsorption will be revisited in Subsection 2.4.1 in the context of adsorption-induced displacive modes of flexibility.

Earlier in this review, when discussing disorder in structural models in Subsection 2.1.1, we briefly discussed the study of Cui et al.,[116] who used kinetic Monte Carlo (kMC) modeling to study defect propagation in ZIFs. The authors of this review believe that kMC is a powerful technique with substantial future application potential in computational modeling studies. The remainder of this section is dedicated to kMC, focusing on the timescale of crossing energy barriers while coarse-graining the PES minima.[117,344] In the kinetic Monte Carlo approach, a series of stochastic trajectories is generated which propagate the system from one state to the other and afterwards the correct dynamics is retrieved by ensemble averaging over all these trajectories.[345] So far, kMC studies on reticular materials remain scarce.[346–350] To showcase the potential of kMC modeling and promote further

computational studies, we discuss two more recent case studies in which kMC has been successfully applied in computational studies of reticular materials.

Guo et al.[347,351] combined DFT calculations with kMC simulations to study hydrogen storage in COF-8 and showed the promoting effect of fluorine-doping on the hydrogen spillover process. Migration barriers of H atoms were estimated with DFT and kMC simulations were used to study the migration process. The authors concluded that doping F atoms in COF-8 changes the charge distribution on the surface of COF-8, lowering the migration barrier of hydrogen and enhancing the adsorption energy of atomic hydrogen.

Very recently, in early 2024, Le et al.[346] also combined DFT calculations and kMC simulations to study the catalytic conversion of biomass to valuable chemicals and fuels in UiO-66 and focused on the production of γ-valerolactone via catalytic hydrogen transfer. Reaction energies and barrier heights were estimated with DFT and kMC simulations were used to predict rate-determining steps and reaction rates. They assumed the active site to contain both a free Zr open metal site, due to a missing linker defect, and an isopropoxide group, originating from the isopropanol solution used in experiment. The authors benchmarked multiple XC functionals and noted a strong dependence of the reaction rate constants on the chosen XC functional. Comparison with experiment was difficult due to the unknown concentration of active sites in the experimental MOF catalyst. Furthermore, this model neglected diffusion, the inclusion of which could improve the accuracy of the model. Despite these shortcomings, a reasonable agreement was found between experiment and theory.

2.3.4. Enhanced Sampling in Molecular Dynamics

A key aspect of dynamic methods to sample the phase space is the ergodic hypothesis, stating that a sampling protocol will eventually explore the whole relevant phase space of the system. In practice this may not be feasible, as the system may be kinetically trapped in a metastable state, rendering transitions from one state to another a rare event.[96] Sampling all the metastable states to construct a free energy profile may require simulation times beyond the capabilities of the computational resources and thus lead to ergodicity issues. Enhanced sampling protocols enable efficient sampling of low-probability regions of configuration space corresponding to activated regions.[352] A first class of enhanced sampling methods rely on predefined degrees of freedom, i.e., collective variables (CVs), which may be defined based on chemical intuition or identified with machine learning methods.[353] Sampling is enhanced along this degree of freedom rather than sampling freely along all possible degrees of freedom. Examples of this class of protocols include umbrella sampling,[354,355] metadynamics,[356] thermodynamic integration[357] and variationally enhanced sampling.[358] In case of MIL-53(Al), the unit cell volume adequately serves as a collective variable to describe the breathing transition and a free energy profile can be constructed using any enhanced sampling technique.[121,359] When the flexibility modes become more complex, such as the conformational inversion[360] (also called "ring flip") of the organic linker in MOF CAU-13, it is far from trivial to define a proper collective variable, as shown in **Figure 11**.[361]

A second class of enhanced sampling protocols does not require the definition of a CV and relies on the generation of replicas of the system at different thermodynamic conditions. Examples of this second class of enhanced sampling protocols include replica exchange[362,363] and expanded ensembles[364,365] methods. In a third class of methods, the transition path is sampled without prior knowledge of transition states by systemically generating trial paths to create an ensemble of unbiased dynamical trajectories between different basins of attractions in the FES.[352] For in-depth reviews on enhanced sampling protocols and free energy calculations in microporous materials, we refer to literature dedicated to the topic.[352,366–369]

Demuynck et al.[359] studied the breathing behavior of MIL-53(Al) and applied five biased sampling protocols (i.e., free energy perturbation, thermodynamic integration, umbrella sampling, metadynamics and variationally enhanced sampling) to construct free energy profiles as a function of the unit cell volume. The authors showed that umbrella sampling using the weighted histogram analysis[370] (WHAM) method required the minimal computational effort of all methods tested in the study to reach the predefined error threshold and concluded that umbrella sampling was the most efficient free energy method for this system. WHAM is a statistical method to extract free energy differences from umbrella sampling simulations and, like any statistical method, will be subject to statistical errors.[96,371] In 2023, Borgmans et al.[372] developed a protocol to construct accurate free energy surfaces, called the Optimal Grid Refinement (OGRe) protocol.[373] In this protocol, umbrella sampling simulations are iteratively refined to minimize the statistical errors in the WHAM method using ThermoLIB,[374] an in-house developed software package for the construction and analysis of free energy surfaces.

Beyond providing information on the stability of an empty MOF, empty host free energy profiles can be extended towards the osmotic ensemble to gain insight into the adsorbate-induced flexibility of a MOF. As discussed in Subsection 2.3.2, the full osmotic potential as a function of the methane gas pressure and the unit cell volume of DUT-49 was constructed in this way, shown in **Figure 12**a.[343] By walking along this osmotic landscape towards increasing gas pressure (full lines), the phase transition pressure and associated negative gas adsorption step could be quantitatively predicted. In the same way, walking along the landscape from the highest gas pressure towards decreasing gas pressure, the desorption branch could be predicted, giving rise to observed hysteresis between adsorption and desorption, as shown in Figure 12c. From such investigations, the underlying reasons for kinetic trapping in metastable states can be traced back to the presence of osmotic energy barriers.

2.4. Physical Properties

Due to their unique building pattern, reticular materials may respond in an anomalous way to external stimuli such as pressure, temperature, light and guest adsorption and it is one of the reasons why they attracted so much interest from the broader community. From the application point of view their dynamic

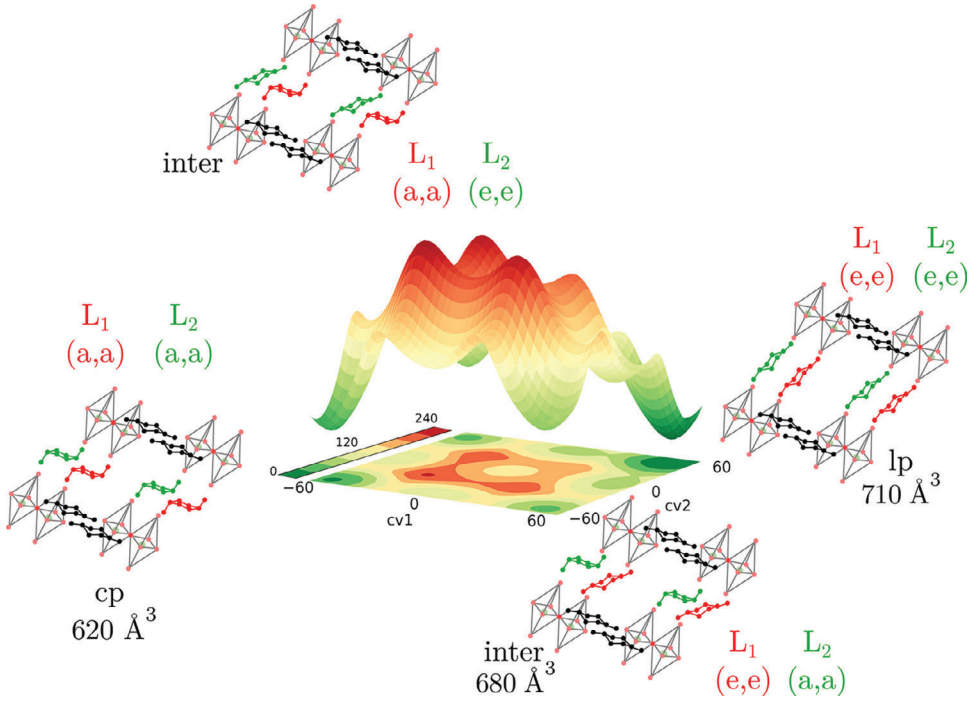

Figure 11. Free energy surface (in kJ mol^{-1} and obtained with variationally enhanced sampling) of CAU-13 at 300 K as a function of the proposed collective variables corresponding to the conformational inversion of the organic linker in CAU-13. Schematic representation of one of the folding pathways of CAU-13 of our simulation cell and the periodic extension. Reproduced with permission.[361] Copyright 2018, American Chemical Society.

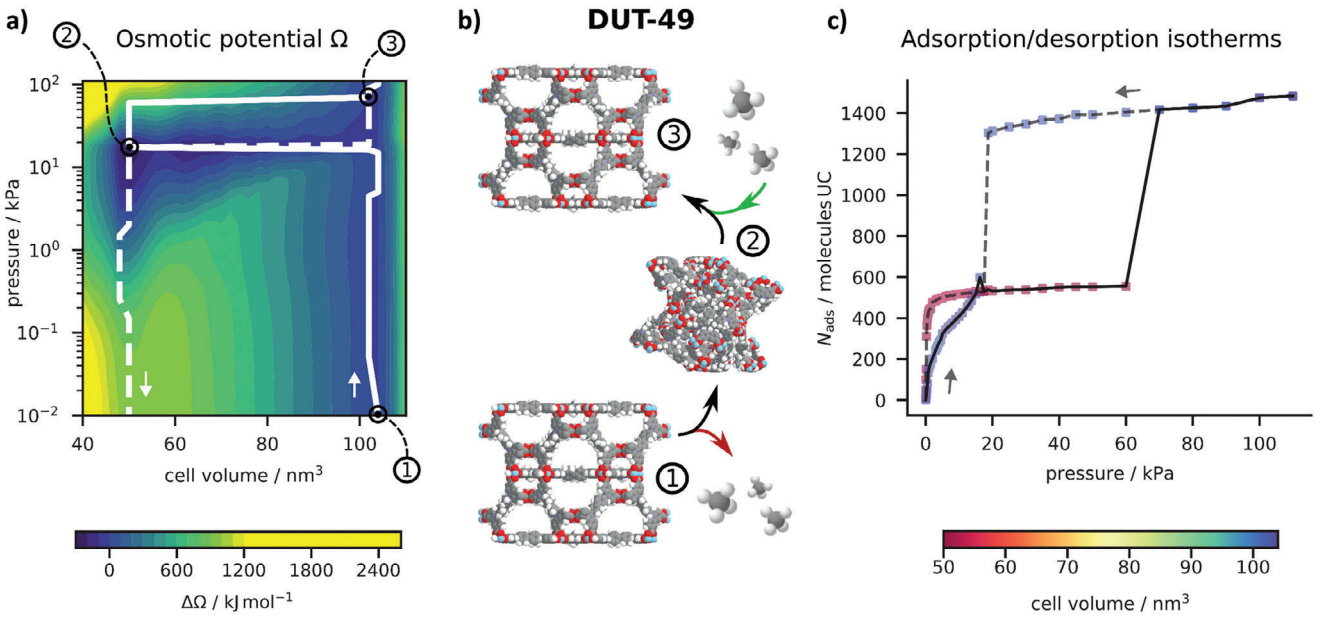

Figure 12. a) Osmotic potential of methane gas adsorption in DUT-49 as a function of the gas pressure and unit cell volume. b) Structures of the open and closed pore phases of DUT-49, along with the observed phase transitions during adsorption. c) The computed adsorption and desorption branches, obtained from walking along the osmotic potential towards increasing and decreasing gas pressure, respectively. Adapted under terms of the CC-BY-NC-ND license.[343] 2021, Goeminne et al., American Chemical Society.

response to external stimuli makes them ideally suited to be used in sensors and actuators. In this section, we will discuss mechanical, thermal and electronic properties and show how insights can be obtained from applying the molecular modeling techniques discussed in the previous sections. To limit our demand on the reader's attention, this section does not aim to give an exhaustive overview of all possible properties and important topics such as effect of pressure, diffusivity, defect engineering, piezoelectricity and pyroelectricity are considered outside the scope of the review.[113,121,375–378] Instead, the focus in this section will lie on the results of important molecular modeling studies to highlight recent progress in reticular chemistry and the rigorous theoretical background of these methods can be found in the references. The examples in this section will highlight the necessity of modeling the spatiotemporal evolution (see Introduction) of reticular materials as close to experimental conditions as possible to capture the dynamic response of reticular materials.[54]

2.4.1. Mechanical Properties

The elastic stiffness tensor is a generalization of Hooke's law in three dimensions and is commonly employed to study the elastic properties, structural stability, phase transitions and phonons of reticular materials.[260,379,380] The elastic stiffness tensor can be used to predict a variety of mechanical properties, such as the volumetric and linear compressibility of a crystal, the bulk modulus, Young's modulus, the shear modulus and Poisson's ratio. The elastic constants, i.e., the 21 unique elements of a $3 \times 3 \times 3 \times 3$ fourth-rank tensor can be calculated at 0 K (adiabatic) or including finite temperature effects (isothermal). To calculate the latter, special care must be taken to sample the system in the appropriate thermodynamic ensemble (see Subsection 2.3.2) and extract elastic stiffness tensors and bulk moduli.[381,382] For a thorough theoretical background on crystal elasticity, see Nye.[383] For an in-depth explanation on the calculation of the elastic stiffness tensor and derived mechanical properties of (flexible) reticular materials, see Rogge.[384]

Reticular materials have been shown to exhibit negative linear or area compressibility[14,385,386] (i.e., during volume compression, the material expands along one or more directions) or auxetic behavior (i.e., during uniaxial tension, the material expands along one or more perpendicular axes). Examples of reticular materials with reports of negative compressibility include HKUST-1,[387] MIL-53(Al),[388] MIL-140A/C,[312] ZIF-3,[390] ZIF-4,[391] ZIF-75,[392] CALF-20,[386] UPF-1,[393,394] DUT-49[395] and others. Giri and coworkers showed that this unexpected behavior is not limited to MOFs or ZIFs and reported a negative Poisson's ratio, i.e., the ratio of transversal strain to axial strain during uniaxial tension, for a series of COFs, such as COF-1, COF-5, TP-COF and a 3D COF with dynamic imine linkages.[396,397] The origins for the negative compressibility were sought at a different length scales. In the case of MIL-140A, MIL-140C, DUT-49 and the COFs, the compression behavior was attributed to the rotational and/or flexural mobility of the linker as a long-range effect. Negative compressibility was also explained by connecting the elastic properties to the terahertz vibrations linked to symmetric collective deformation mechanisms, as was the case for HKUST-1.[302,387,398] At an even larger length scale, the global topologies of MIL-53(Al) and CALF-20 were used to explain the anomalous mechanical behavior. In the case of CALF-20, Fan et al.[386] used molecular dynamics (classical force field as well as MLP) simulations to show reversible switching from auxetic to non-auxetic deformation behavior by applying uniaxial tension along the [001] direction. Moreover, the authors used static DFT calculations to predict low energy barriers between different phases of CALF-20. These results agreed with the conclusions of Chen et al.,[399] who used both experimental results and classical force field molecular dynamics simulations to show a reversible structural transformation in CALF-20 following changes in atmospheric humidity.

A second surprising characteristic in reticular materials we wish to highlight are the adsorption-induced displacive modes of flexibility, structural transformations in which chemical bonds are distorted, but not rearranged (e.g., breathing transformations found in the MIL-53(Al) family), following the definition from Vanduyfhuys et al.[121] This phenomenon was already briefly discussed in Subsection 2.3.2, in which it was shown how a hybrid MD/MC scheme was able to adequately sample the phase space, leading to the successful prediction of negative gas adsorption in DUT-49.[15,343] Negative gas adsorption (NGA) is a novel phenomenon in which adsorption of guest molecules induces a contraction of the framework, which in turn releases adsorbed gases and thus increases the external pressure.[400] In such a displacive mode of flexibility, the guest-loaded open phase is considered a long-lived metastable state with a high free energy barrier between the open and close phases.[401] The large unit cell of DUT-49 prohibits DFT calculations beyond a simple geometry relaxation and limited energy evaluations. To apply more advanced techniques, one option can be to resort to cluster models. As an alternative solution, MLPs can be applied to periodic structural models, as was recently done by Goeminne et al.[402] to model CO_2 adsorption in a series of ZIFs and Mg-MOF-74.

Displacive modes of flexibility are not limited to MOFs and can also be found in COFs.[403] In 2018, Zhao et al.[404] showed experimental evidence for adsorption-induced reversible dynamics in urea-linked 2D COFs, COF-117 and COF-118, using powder X-ray diffraction measurements. Activating the samples by solvent removal rendered COF-117 amorphous, which the authors attributed to the flexible nature of the urea linkers. Crystallinity was regained when the samples were treated with solvents, which was explained by the disruption of interlayer interactions by the adsorption of guest molecules. While some computational studies on guest adsorption in COFs are available in literature (e.g., Aksu et al.,[405] Zhao et al.[406]) adsorption-induced structural dynamics in COFs remains an open challenge for computational modeling.

2.4.2. Thermal Properties

A material's volumetric expansion is not limited to mechanically driven processes, and the thermal expansion can, like the compressibility, be positive or negative in reticular materials. Already as early as 2007, Dubbeldam et al.[407] studied thermal expansion in IRMOF-1 with molecular simulations and observed negative thermal expansion (NTE). The authors explained the NTE phenomenon by highlighting the competitive response of bond lengths and thermal movement of the organic linkers to changes

in temperature. As the temperature rises, the bond lengths will increase (local effect) but the thermal movement of the organic linkers can decrease the average length between the inorganic nodes (long-range effect). A few years later, in 2010, Lock et al.[408] also used molecular dynamics to study NTE in IRMOF-1 and the authors proposed, in agreement with Dubbeldam et al., that the transverse normal modes of the organic linkers counteract the lattice-expanding longitudinal modes, resulting in an overall contraction of the lattice.

This explanation is in line with the conclusions from the previous subsection, in which negative compressibility was explained using the rotational and flexural mobility of the organic linkers. Nowadays, low-frequency phonons, phase transitions[409] and defects[410] are commonly accepted as important driving mechanisms of NTE in crystalline solid materials and NTE is more likely to be observed in materials with a high porosity and in the presence of non-covalent bonds, i.e., properties commonly found in MOFs.[411,412]

Heat transport plays a critical role in any heterogeneous catalytic process and a thorough understanding of the heat capacity and thermal conductivity of reticular materials is critical in industrial applications such as pressure swing adsorbers.[413] Wieme et al.[414] studied the heat of adsorption of CO_2 and CH_4 in a series of MOFs, including MOF-5, HKUST-1 and UiO-66. These authors used path integral molecular dynamics with force fields to predict the heat capacity and the thermal expansion coefficient. The authors acknowledged that the idealized models likely overestimated the temperature rise, yet they predict idealized temperature increases between 100 and 250 K at high-pressure adsorbate loading of 100 bar CO_2 adsorption. This computational study supports the hypothesis that large temperature swings could be present during the adsorption/desorption process risking material degradation, in case of a sharp temperature rise, or adsorbate condensation in case of a large temperature drop.

The final thermal property we discuss is thermal conductivity, which can be calculated using either non-equilibrium or equilibrium MD simulations.[415,416] To understand thermal conductivity in MOFs, we turn (once again) to the study of phonons. A large mass difference between the inorganic node and the organic linker in MOFs will result in a small overlap in the phonon density of states, leading to minor phonon scattering[311] and an increased relative thermal conductivity.[417] Naturally, the high porosity characterizing MOFs will still lead to a low absolute thermal conductivity. In 2020, Babaei et al.[418] used equilibrium force field MD simulations with the Green-Kubo method,[419,420] in which the thermal conductivity is expressed using an integral of the heat current autocorrelation function, to study the effect on thermal conductivity due to the presence of adsorbates in HKUST-1. The authors argued that adsorbed gas molecules can provide additional pathways for heat transfer, but this effect must be balanced against the additional phonon scattering in the framework. When guest molecules enter the pores of a MOF, they will collide with the framework, increasing phonon scattering and thus decreasing the thermal conductivity.

In the summer of 2024, Yamaguchi et al.[421] used force field MD (UFF) simulations to study water adsorption in MOF Cu-TCPP. The thermal conductivity of the MOF was calculated using non-equilibrium MD simulations with the Müller-Plathe[422] method, a non-equilibrium method to predict thermal conductivities in which a temperature gradient is imposed across the simulation cell, and the authors showed that aggregated clusters of water in the MOF pore play a critical role in heat conduction with an analysis of the phonon density of states before and after adsorption of water. The conclusion of the study was that a network of adsorbed water molecules will provide additional vibrational modes to facilitate heat dissipation and increase the thermal conductivity of the combined guest-host system. Contrary to this conclusion, Sezginel et al.[423] used equilibrium MD simulations to calculate the thermal conductivity in a series of idealized breathing porous crystals with the Green-Kubo method and the authors predicted a decreasing thermal conductivity in the presence of adsorbed gases due to increased phonon scattering. In 2023, Cheng et al.,[424] used molecular simulations (Green-Kubo method) to study the heat transfer in three topological ZIFs by calculating the phonon density of states and supported the conclusions of Babaei et al. by highlighting the delicate balance between (i) additional pathways for heat dissipation and (ii) increased phonon scattering after guest adsorption. The resulting increase or decrease of the thermal conductivity after guest adsorption depends on the dominant phenomenon and is tied to the topology of the framework and the type of adsorbate molecules.

In a recent Perspective on thermal conductivity in COFs by Kwon et al.,[425] the authors highlight the current limitations of molecular modeling techniques capable of accurately probing the thermal properties of COF. Nevertheless, the principles of the previous paragraph are generally transferable. One major difference which can be highlighted is the length of the organic linker. In the previous paragraph, a short organic linker increased the mass mismatch between the inorganic node and the organic linker, which in turn reduced phonon scattering and is expected to increase thermal conductivity in MOFs. As COFs do not contain any heavy metal atoms, this argument is no longer applicable. Instead, Rahman et al.[426] studied 2D COFs using equilibrium MD simulations, with the Green-Kubo method to compute thermal conductivities, to show that short linkers give rise to a greater coupling between acoustic and optical phonons, which reduced the thermal conductivity along a 2D plane. Furthermore, the authors propose that larger nodes, with an increased number of covalent bonds, are beneficial for heat transport, leading to a higher thermal conductivity.

2.4.3. Electronic Properties

To aid the design of an efficient electro- or photocatalyst, computational modeling can be used to study and optimize electronic properties such as band gaps, band structure, polarizability and charge transfer processes.[345–348] In solids, the electronic (or fundamental) band gap is the energy difference between the top of the valence band and the bottom of the conduction band, whereas the optical band gap refer to the lowest electronic excitation energy after photon absorption.[427] In the latter case, the photoexcited electron-hole pair will experience additional Coulombic stabilization, resulting in an lower band gap. The high porosity of reticular materials translates to a low dielectric constant,[428] which in turn leads to a high binding energy of the photoexcited electron-hole pair (i.e., the exciton). The exciton can spontaneously recombine (with photon emission) or dissociate into

free charge carriers to promote catalytic activity.[429] The interest in reticular materials as potential electro- and/or photocatalysts is quickly growing, but computational studies are hampered by the often very large unit cells and the necessity to use hybrid functionals to obtain accurate results from DFT calculations.

Fabrizio et al.[430] studied optical band gaps in MOFs using DFT calculations (i) to critically evaluate the difference between Gaussian fitting and Tauc analysis[431,432] for assigning optical band gaps to MOFs and (ii) release a series of recommendations to calculate optical band gaps. The authors opted for a hybrid-GGA functional (HSE06 sometimes also called HSE-HJS)[433] which has been shown to systematically correspond well with experimental values of electronic properties.[195] Recently, Yu et al.[434] studied the electronic properties in a series of COFs of the Lieb lattice, a two-dimensional square lattice which has been theorized to facilitate the tuning of electronic properties.[435,436] The authors used static DFT calculations (HSE06 functional) to study the optical band gap, exciton binding energy (using the G_0W_0[437] approximation and the Bethe-Salpeter[438] equation) and chemical structure of the COF series and concluded that (i) narrowing the band gap and (ii) increasing the dielectric screening[439] effect suppressed the exciton binding energy, which resulted in an increased photocatalytic activity. An interesting example of the application of the GW method and the Bethe-Salpeter equation to MOFs is the work by Kshirsagar et al.,[440] in which the authors combined theoretical calculations with experimental results to show the strong excitonic effects in MOF-5. Using DFT calculations, this time with a GGA functional (PBE), Rahman et al.[426] showed that the pore size is a major structural descriptor controlling the band gap in COFs. These authors also used MD simulations to show a positive correlation between mass density and thermal conductivity (vide supra). Additionally, it was shown that functional groups can localize the charge and thereby alter the band gap. Similarly, Ling et al.,[441] showed a positive correlation between pore size and band gap using static DFT calculations (HSE06 functional) in a series of MIL-53-type MOFs with different metal cations (Al, Ga, In, Sc, Ti, V, Cr and Fe). It was observed that the correlation between the pore size and band gap decreased as the presence of metal d states in the band edges increased and the authors also showed the major influence of breathing transitions on the electronic properties.

3. Selected Case Studies Showing the Potential of Modeling Reticular Materials for Technological Applications

This section highlights a curated selection of reticular materials with application potential in modern technologies such as (i) carbon capture[442,443] to address climate change due to anthropogenic CO_2 emissions, (ii) water harvesting[444,445] to extract atmospheric moisture in arid environments and (iii) renewable energy conversion to replace depleting fossil resources by converting solar energy to chemical energy with photocatalysis.[446] Obviously, the examples illustrated in this section are limited, but were selected to show how reticular materials have evolved into an extremely versatile platform of materials offering the potential to contribute to technologically important solutions in many fields, such as climate change, health and sustainable energy solutions. Biological applications of reticular materials can be found in fields such as drug delivery, volatile organic compound (VOC) sensing, biocatalysis and biomedicine.[447–450] Simulations of biomolecules by themselves are complicated due to the presence of slow degrees of freedom (e.g., rotation, diffusion and conformational changes). Modeling the encapsulation of large biomolecules by reticular materials requires large pore sizes in the host and necessitates the use of large structural models which are difficult to model using first principles methods.[451,452] Additionally, enhanced sampling methods (vide supra) are required to overcome the disparity in time scales between biomolecules and reticular materials.[54] A number of computational studies on biological applications such as drug storage are already available, which are concisely summarized in the review by Demir et al.,[453] yet new methods are needed to fully characterize and understand the interactions between bioactive molecules and reticular materials.[335,452]

3.1. Carbon Capture

MOFs have long been investigated for their potential to capture CO_2.[442,443,454–456] While a wide variety of MOFs exhibiting excellent CO_2 sorption properties have been reported in the literature, many suffer from the competitive adsorption of water and acid gases at elevated temperatures encountered in flue gases.[457–462] Therefore, the reporting on CALF-20 (Zn_2(1,2,4-triazolate)$_2$(oxalate)), an exceptionally stable MOF under typical flue gas conditions, attracted great interest as a powerful candidate for CO_2 capture.[463,464] CALF-20, shown in **Figure 13**, is composed of layers of 1,2,4-triazolate-bridged zinc(II) ions pillared by oxalate ions and preferentially adsorbs CO_2 up to a relative humidity (RH) of 40%, with the presence of CO_2 in the framework even suppressing water sorption. Moreover, the low-cost synthesis procedure (aqueous methanol solution at room temperature) and the wide availability of raw materials (zinc acetate and oxalate salt) are ideally suited to scale up the production of this MOF in an economically viable way.[460,461]

To gain fundamental insight into the origin of CALF-20's exceptional hydrophobic CO_2 uptake capacity, a variety of computational tools were used. The adsorption of water in CALF-20 was investigated by GCMC simulations employing a static framework by Lin et al.[464] At 20% RH, where the water uptake is half the saturation loading, the pores of CALF-20 were observed to be either (i) filled, forming a hydrogen-bonded network or (ii) completely empty, suggesting rapid water condensation. These findings were supported from calculations of the self- and corrected diffusion coefficients (D_s and D_0) of water in CALF-20 as a function of the relative humidity, as computed with the Green-Kubo relation from force field MD simulations. For water, D_s and D_0 are approximately equal up to 20% RH, indicating negligible cross-coupling between adsorbates.[466] At 20% RH and higher, a clear difference is observed, indicating the formation of hydrogen bonds. Interestingly, no cross coupling is observed for CO_2 at any gas pressure.

Moreover, at the most probable binding sites of water with the framework, no hydrogen bonds are formed with the oxalate linkers and low binding energies were observed. Instead, molecules are oriented away from the oxalate linkers, poised to make

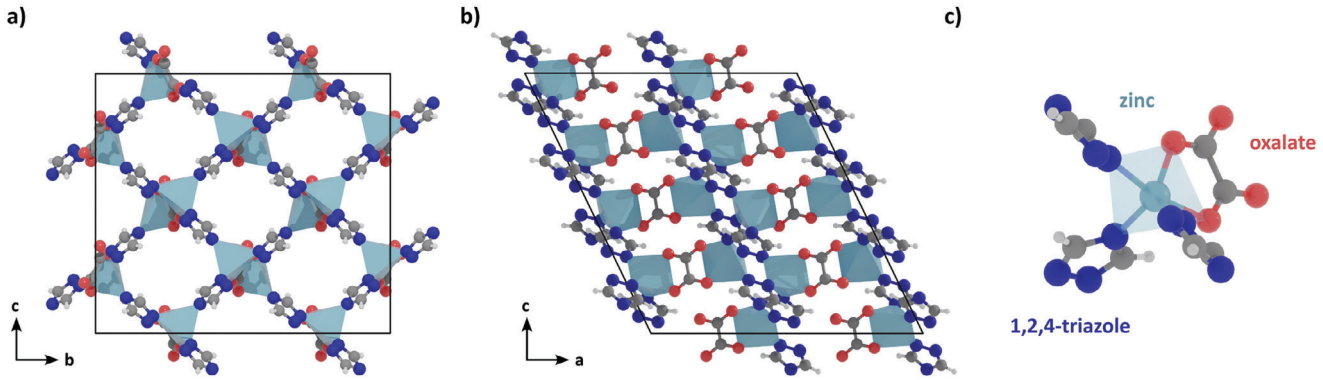

Figure 13. a) Structure of the CALF-20 zinc triazolate grid. b) Structure of the oxalate pillaring of the triazolate-bridged zinc ions. c) View of the coordination environment of the zinc ions.

hydrogen-bonding interactions with other water molecules. The largest cavity diameter (LCD) and pore limiting diameter (PLD) of CALF-20 are equal to 4.3 Å and 3 Å. Compared to the relatively small kinetic diameter of CO_2 of 3.3 Å, this provides a tight fit for these molecules.[454,467] Additionally, force field MD simulations revealed that CO_2 and H_2O molecules compete for the same binding sites, as shown in **Figure 14**. This results in more confined water hydrogen-bonded networks in the presence of CO_2, decreasing water entropy.[468]

Shortly after the reporting on CALF-20, experimental results indicated that structural flexibility can be reversibly induced in this material under the influence of humidity, resulting in a second, structurally similar polymorph.[399] To investigate such guest-induced flexibility in CALF-20 at the atomic scale and its influence on adsorption, the dynamic behavior of CALF-20 under the presence of CO_2 and H_2O molecules was investigated by means of MLPs which were trained to enhanced sampling DFT MD simulations.[467] With the trained NequIP MLPs,[278] the free energy profiles of CALF-20 as a function of the unit cell volume for a range of guest-loadings were determined with dynamic MLP-based umbrella sampling simulations. For CO_2, a monotonic increase in the equilibrium volume is observed with increasing guest-loading. However, for water, a non-monotonic behavior is observed in which the unit cell first shrinks until intermediate water-loadings, after which the unit cell volume increases to a value larger than the empty framework volume. From equilibrium MLP-MD simulations it was also observed that the presence of water induces a significant rotation of the triazolate linkers, while this rotation is less pronounced for CO_2.

Aiming to further improve the CO_2 and H_2O adsorption properties of CALF-20, Maurin and coworkers built an in silico series of five linker-substituted MOFs.[469] The adsorption properties of a CO_2/N_2 binary mixture and a $CO_2/N_2/H_2O$ ternary mixture were characterized in the five linker-substituted MOFs with multi-component GCMC simulations. Among the five MOFs, SquCALF-20, which consists of a squarate linker, was demonstrated to have a larger CO_2 uptake (3.6 mmol g^{-1} versus 2.8 mmol g^{-1} at a pressure of 0.15 bar) and higher CO_2/N_2 selectivity (500 versus 180) when compared to CALF-20. While this does come at the cost of a slightly more hydrophilic behavior (competitive higher CO_2 adsorption at 10% lower RH due to a higher water enthalpy of adsorption of −38.7 kJ mol^{-1} compared to −33.4 kJ mol^{-1} for CALF-20), this trade-off might be advantageous in certain applications. This study demonstrates how insight obtained from computational insights can be leveraged to further optimize MOFs for their target application. In this sense,

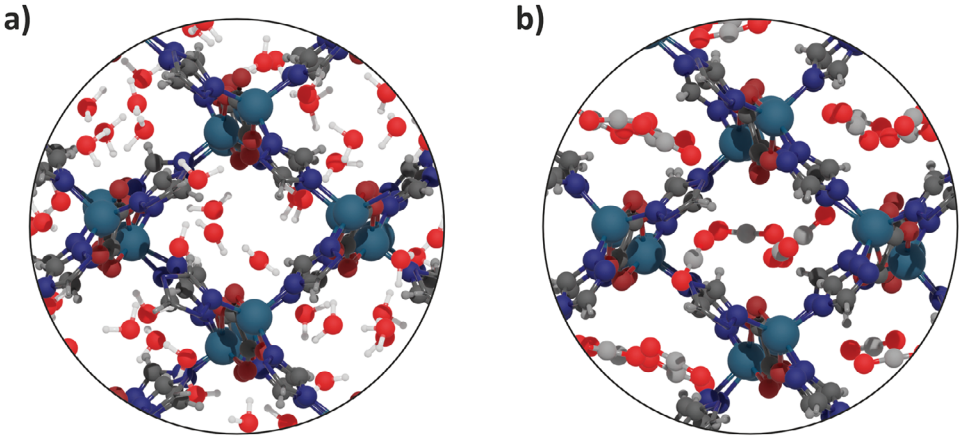

Figure 14. Snapshots of DFT NPT MD simulations of a) H_2O and b) CO_2 molecules in flexible CALF-20 at saturation loading. Structural models taken from ref. [467].

a close feedback loop between simulations and experiments has proven invaluable to exchange new insights to rationally design MOFs. CALF-20 clearly exemplifies the path of a MOF from the laboratory to the industrial scale, where attention is not only paid to the optimal theoretical performance of a material, but also to in-the-field implementations of the technology to de-risk further steps up the technology readiness level ladder.

3.2. Water Harvesting

Computational modeling of water adsorption in MOFs is highly challenging, both in terms of the description of the intermolecular interactions, as well as the simulation sampling procedure. Water-water interactions can be accurately modeled with force fields.[470–472] However, these potentials need to be supplemented with additional terms to account for the MOF-water interactions, which can reduce the accuracy of the simulation results. Generic MOF force fields may not be sufficiently accurate and the combined force field will require careful benchmarking to ab initio reference data or refitting to experimental data.[473–476] Even for water-water force fields, predicted saturation vapor pressures differ significantly, leading to ambiguity in the reference of the obtained adsorption isotherms. In general terms, obtaining chemically accurate adsorption isotherms is extremely challenging as a very accurate level of theory is necessary to describe the potential energy surface. Recently some new developments are taking place to describe the adsorption isotherm based on machine learning potentials, however also here extreme care is necessary to generate the MLPs from chemically accurate underlying quantum mechanical training data.[476] Apart from the difficulties in describing the molecular interactions, also the sampling procedure can largely influence the obtained isotherm. In terms of sampling, the commonly employed GCMC simulations can be hindered by metastability, especially for hydrophobic MOFs where the formation of stabilizing hydrogen bonded water clusters is required for uptake. Due to the sequential nature of insertions in GCMC simulations, reaching convergence can be extremely difficult.[338,477–479] Additionally, framework flexibility is neglected in GCMC simulations. While this approximation intuitively breaks down for MOFs with large-scale structural changes such as the swelling mode of MIL-88, it has also been shown to qualitatively affect the isotherm shapes in MOFs exhibiting only subtle local flexibility.[474,480] Recently, some of the current authors proposed a new methodology based on transition matrix Monte Carlo simulations and efficiently trained MLPs to fully account for the framework flexibility while keeping chemical accuracy. The method was validated for some typical water harvesting systems like MOF-303, MOF-333 and MOF-LA2-1.[476]

Only quite recently, it was recognized that MOFs can act as effective extractors of atmospheric moisture from arid air using only natural cooling and sunlight, to subsequently release it for human consumption.[481–485] In this respect, significant interest developed in MOF-303 (Al(OH)(PZDC), with PZDC = 1-H-pyrazole-3,5-dicarboxylate), shown in **Figure 15**a. Tested in an arid environment (32% RH, 27 °C), a MOF-303 based water harvester generated 1.3 L kg^{-1} day^{-1}, or 0.7 L kg^{-1} day^{-1} in the more extreme conditions of the Mojave desert (10% RH, 27 °C).[484,486] This performance represented a significant improvement on the previous state-of-the-art.

Interestingly, MOF-303 does not exhibit a single-step isotherm (shown in Figure 15c), a desired component of an efficient water harvester.[143,487] Instead, an S–shaped adsorption behavior is observed. By performing DFT optimizations of water molecules in the framework, it was revealed that the water seeding initiates at the pyrazole functionalities of two neighboring PZDC linkers (see Figure 15b), strongly binding the first water molecules.[485]

In subsequent work by Chheda et al.,[474] the adsorption behavior in MOF-303 was probed by means of Gibbs ensemble Monte Carlo simulations. First, various force fields were selected and benchmarked on their ability to accurately capture the interaction energy on the primary adsorption site. However, even after selecting an appropriate force field, the S-shape of the adsorption isotherm could not be accurately reproduced when using the rigid DFT-optimized framework without guest molecules. Only when employing the framework geometry optimized in the presence of water molecules could the S-shape of the adsorption isotherm be captured. Interestingly, this was explained by small local distortions in the primary adsorption site, in which the distance between pyrazole functionalities of neighboring PZDC linkers expands from 3.4 Å to 3.9 Å, as shown in Figure 15b. This work highlights how adsorbing water can significantly influence the flexibility of the host MOF, an observation that has been made before. For example, water adsorption in (Al)MIL-53(OH) is associated with phase transition of the framework with pronounced hysteresis between the adsorption and desorption branch.[488] In Co_2Cl_2(BTDD), water adsorption on the open metal sites leads to a decrease of the pore diameter from 21 Å to 17 Å.[488] Water adsorption in MIL-88 is even associated with a near doubling of the cell volume.[480] The necessity to include these effects significantly complicates an accurate computational modeling of the adsorption properties of these materials, as typical GCMC simulations neglect the flexibility of the framework. Moreover, a second complication arises when modeling water adsorption is related to the employed sampling procedure in GCMC in which molecules are sequentially added, as simulations can remain stuck in local free energy minima, sometimes requiring months of simulation time to reach convergence, due to the strong stabilization of clusters of water molecules.[477,478]

To overcome these difficulties, recent interest has developed in TMMC simulations (see Subsection 2.3.2). In these simulations, NVT Monte Carlo trajectories are performed at every relevant loading of guest molecules. On these trajectories, virtual insertions and deletions of adsorbates are performed and the unbiased acceptance probabilities are accumulated to compute the macrostate probability distribution.[337,338] From this, the adsorption isotherm at every gas pressure can be computed, avoiding the convergence problems associated with GCMC simulations. This method was used to compute the adsorption properties of MOF-303 over a continuous range of pressures and temperatures, providing rich insight into the thermodynamic landscape of gas adsorption.[489] However, this approach still employs a rigid framework. Therefore, Goeminne et al.[476] trained machine learning potentials on the flexible MOF-303 in the presence of water molecules, to further employ it in MD-based TMMC simulations. In this way, the flexibility of the framework during guest adsorption is sampled and all adsorption

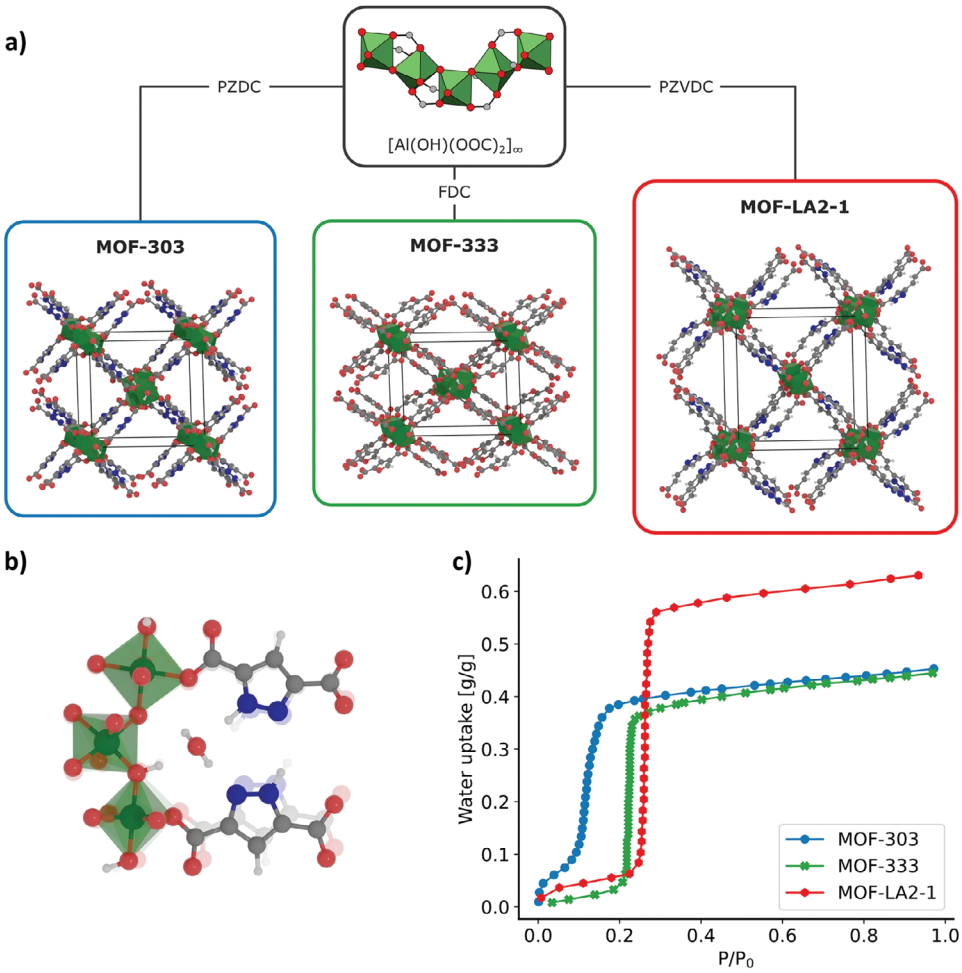

Figure 15. a) View of the structure of MOF-303, MOF-333 and MOF-LA2-1. b) Structure of the primary adsorption pocket of MOF-303. The optimized geometry in the presence of a water molecule is shown with opaque atoms, while the same geometry optimized in the absence of water is overlaid with transparent atoms. c) The experimentally observed adsorption isotherms for all three MOFs.[485,490]

energetics are treated at the DFT level of theory, yielding quantitative agreement when using the rPBE-D3(BJ) level of theory.

From these simulations, the importance of the local as well as the global (unit cell) flexibility on the computed adsorption properties was clearly established. Moreover, contrasting the density profiles of water at different loadings in MOF-303 with those in MOF-333 demonstrated the impact of a less hydrophilic FDC linker composing MOF-333 (FDC = 2,4-furandicarboxylate, shown in Figure 15a), resulting in two less strongly interacting adsorption pockets between two linkers instead of one strongly interacting adsorption pocket as the case for MOF-303.[476,485] For MOF-333, this gives rise to a single-step adsorption isotherm instead of the S-shaped adsorption isotherm observed in MOF-303. Alternatively, instead of modulating the hydrophilicity of the linker, a linker extension strategy was recently employed in MOF-LA2-1 to yield a larger working capacity, as seen from the adsorption isotherm in Figure 15c.[490]

While the water clustering behavior computed from MD-based TMMC simulations was observed to be very consistent across the use of different DFT levels of theory used as training data, the energetics and resulting adsorption behavior was observed to heavily depend on the level of theory. As the use of machine learning potentials in computational adsorption studies can be expected to rise over the coming years, further work will be needed in either developing more accurate functionals or employing highly accurate wavefunction-based methods to derive MLPs. In any case as previous discussion reveals, to accurately predict adsorption isotherms, one needs to employ methodologies where the energy can be calculated at or above chemical accuracy in combination with methods where the flexibility of the materials is accounted for.

3.3. Renewable Energy Conversion with Photocatalysis

Abundant solar energy can be converted to chemical energy using photocatalysis, producing green hydrogen without the need for renewable electricity. In this context, COFs as photocatalysts have attracted interest for their advantages in pore structures, high surface areas and tunable functionalization.[491,492,7,493–499] Photocatalytic water splitting stands out as a crucial process wherein green hydrogen and oxygen are produced in an environmentally friendly manner. **Figure 16a** shows a schematic representation

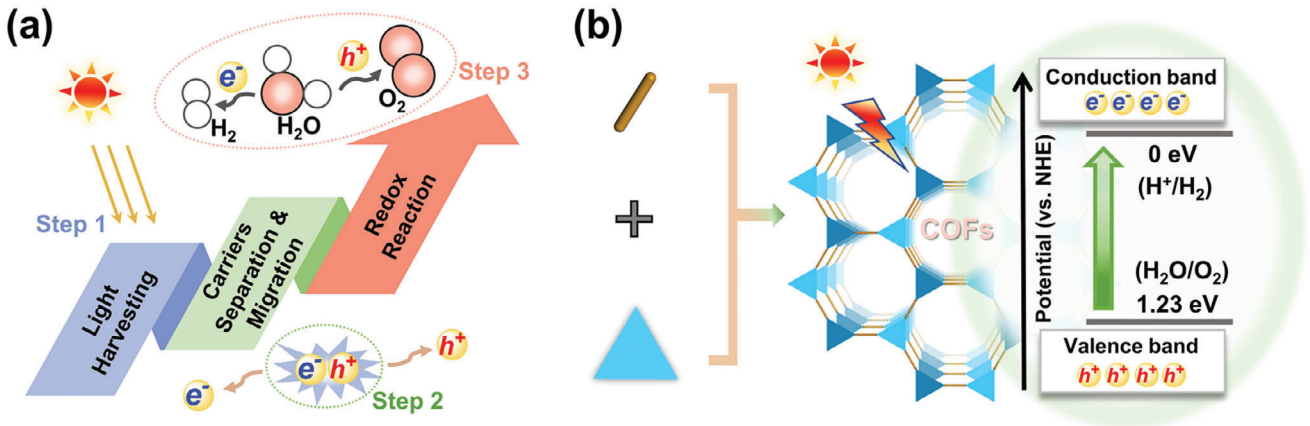

Figure 16. a) Critical factors and steps affecting the photocatalytic water splitting performance. b) Schematic diagram of the general synthesis of COFs and redox potentials for photocatalytic water splitting. Reproduced with permission.[500] Copyright 2024, American Chemical Society.

of photocatalytic water splitting as a three-step process: (i) light is harvested, i.e., the generation of excited electron-hole pairs through photon absorption, (ii) separation and migration of charge carriers and (iii) chemical oxidation and reduction mediated by these charge carriers. Optimizing these processes in COFs requires an understanding of the optical absorption, the ground and excited state properties, charge carrier lifetimes and band alignment.

To serve as a suitable photocatalyst, the valence band maximum (VBM) of the COF must be more negative than the water oxidation potential (O_2/H_2O; −5.67 eV versus vacuum at pH = 0) which leads to the oxygen evolution reaction (OER), and the conduction band minimum (CBM) must be more positive than the proton reduction potential ($H+/H_2$; −4.44 eV versus vacuum at pH = 0) which is the hydrogen evolution reaction (HER), as shown in Figure 16b. In the first step of the photocatalytic water splitting process, absorption of a photon with sufficient energy to bridge the band gap can photoexcite an electron to create an exciton. In efficient photocatalysts, recombination of the exciton with concomitant photon emission should be slow and the exciton should easily dissociate in free charge carriers. The π-conjugation in COFs promotes both charge separation and long-distance charge transportation.[501–503] After optimizing key parameters such as the band gap, band edge alignment, charge separation and charge transport, the adsorption of intermediates on active sites becomes crucial in the overall reaction. The OER (oxidation reaction) and the HER (reduction reaction) each have distinct adsorption requirements on the COF surface. Consequently, efficient photocatalytic water splitting requires that adsorption sites for OER intermediates align with the hole transport sites, while adsorption sites for HER intermediates align with the electron transport sites. We will first introduce orthogonal electronic structure engineering (OESE) as a useful concept to optimize the electronic properties of reticular materials. Next, we will discuss computational studies of the active sites for photocatalytic water splitting and discuss the potential advantages of employing donor-acceptor strategies in COF-based photocatalysts.

3.3.1. Orthogonal Electronic Structure Engineering

High-porosity MOFs are generally expected to exhibit low electrical conductivity, typically explained by the (both spatial and energetic) orbital mismatch between redox-inactive organic linkers and the hard metal ions of the organic nodes: the low orbital overlap leads to a low electron delocalization and thus reduces charge carrier mobility (i.e., electrical conductivity).[504–507] Throughout this review, we have expressed the continuous challenge of modeling at larger length and time scales to understand and explain plethora of fascinating properties of reticular materials. However, in this subsection we highlight the concept of orthogonal electronic structure engineering (OESE) to simplify the study of electronic properties of reticular materials. The OESE principle, introduced by De Vos et al.,[508,509] reduces reticular materials to an assembly of building blocks and considers the electronic structure of reticular materials as a sum of independent (orthogonal) contributions. The authors first applied the new concept to UiO-66(Zr). **Figure 17** shows the density of states (DOS) of pristine UiO-66(Zr) as a representative 0D MOF, following Férey's classification of MOFs (see Introduction).

The DOS of pristine UiO-66(Zr) can be separated in three contributions from the organic linkers (−1 eV to −0.2 eV, 2.8 eV to 3.6 eV and 4.7 eV to 5 eV, blue background Figure 16) and two contributions from the inorganic nodes (−0.2 eV to 0 eV and 4.4 eV to 4.7 eV, green background Figure 16). In the photocatalytic process in UiO-66(Zr), absorption of a photon with energy ΔE_{abs} will excite an electron of the linker to create an excited electron-hole pair. Next, after charge separation and electron transport to the inorganic node (energy barrier ΔE_{LMCT}) the Zr ion in the inorganic node will be reduced ($Zr^{4+} + e^- \rightarrow Zr^{3+}$) and the electron is available for the reduction reaction. A high photocatalytic activity will necessitate a low (or even negative) energy barrier ΔE_{LMCT}, which is clearly not the case for pristine UiO-66(Zr), as shown in Figure 17. The energy barrier ΔE_{LMCT} can be lowered through defect engineering (vide supra, Subsection *Disorder in structural models* and Figure 6).[510] Additionally, the authors showed that isovalent metal substitution of Zr with Ti enhances charge

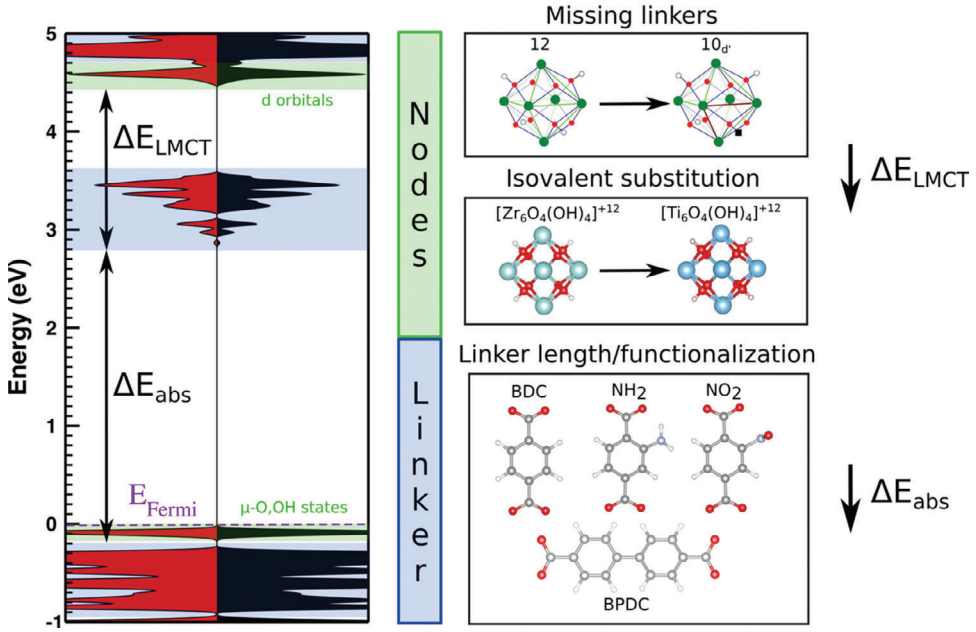

Figure 17. Orthogonal tuning of the electronic structure of UiO-66(Zr) (left) where red and black curves represent different spin channels and blue and green indicate linker and node states, respectively. Linker alteration affects the absorption wavelength, ΔE_{abs}, and therefore controls the energy needed to excite the linker (BPDC = biphenyl dicarboxylate). The position of the unoccupied d orbitals (ΔE_{LMCT}) is changed by node modification and is important for an efficient ligand-to-metal charge transfer (LMCT). Reproduced with permission.[509] Copyright 2017, American Chemical Society.

transfer capabilities to lower the energy barrier ΔE_{LMCT}. MOFs isoreticular to UiO-66(Zr) can exhibit superior photocatalytic activity by tuning the nature and length of the organic linker and replacing the benzene dicarboxylate linker of UiO-66(Zr) with higher conjugated organic linkers is expected to reduce ΔE_{abs} and improve the absorptive properties. Finally, functionalization of the organic linker with electron-donating groups (e.g., -NH_2) and an increased aromaticity of the linker can also improve photon absorption. The increased electron-donating character of the functional group as well as the improved delocalization of the π-electrons has been shown to be positively correlated with a reduction in the band gap.[428,511]

2D COFs are of particular interest in photocatalysis, as the layered stacking improves the aromatic π-π stacking to better delocalize electrons, which in turn increases the mobility of the charge carriers. In a follow-up study (2019), some of the same authors of the previous study applied the OESE principle to COFs to evaluate the photocatalytic activity.[512] The authors studied 2D covalent triazine frameworks (CTF), whose high thermal and chemical stability show great promise in photocatalytic applications.[20,497,513–515] The introduction of triazine groups in the scaffold naturally incorporates nitrogen atoms in the framework, increasing the basicity of the material to stabilize extra-framework metal complexes and intercalated metal ions (i.e., an example of the heteroatom effect).[516,517] In the computational study, the authors studied three photocatalytic Ru complexes, in which a Ru^{2+} ion was octahedrally chelated by three bidentate nitrogen-containing ligands, as shown in **Figure 18**. Embedding the extra-framework complex into the CTF, one of the linkers will be shared between the framework and the complex, while the other two chelating ligands extend into the pore (right-hand side Figure 18). The authors first studied the DOS of the Ru-complexes in vacuo and showed that the complex has a Ru-centered highest occupied molecular orbital (HOMO) and a ligand-based lowest occupied molecular orbital (LUMO). Next, the authors compared the electronic properties of the Ru-complexes before (left column) and after (three right columns) incorporation in the CTF framework and showed that the properties of the complex are mostly conserved. The HOMO of the Ru-complex is superseded by the highest occupied crystal orbital of the CTF-centered framework and the Ru-complexes maintained a high photocatalytic activity after incorporation in the CTF. Additionally, the metal-to-ligand charge transfer (MLCT) is predominantly directed towards the ligand containing the highest number of nitrogen atoms. By altering the nitrogen content, it is possible to steer the direction of excitation towards either the framework or the pore, depending on the specific requirements of the catalytic process (right-hand side Figure 18b). The authors concluded that further tuning of the Ru-complexes is available by modifying the CTF linkers and the OESE principle is expected to be applicable to other materials beyond the two case studies discussed in this subsection.

3.3.2. Active Sites for Photocatalytic Water Splitting

Yang and co-workers explored a series of two-dimensional (2D) COFs for water splitting driven by visible light.[518] These COFs employed various linkages and building unit combinations to achieve bifunctionality for the HER and the OER. Nitrogen-containing linkages (imine (I), azine (Ai), and azo (Ao) groups) were strategically incorporated to promote HER catalysis as shown in **Figure 19a**, as previous studies have shown the efficacy of lone pair electrons on the nitrogen atom

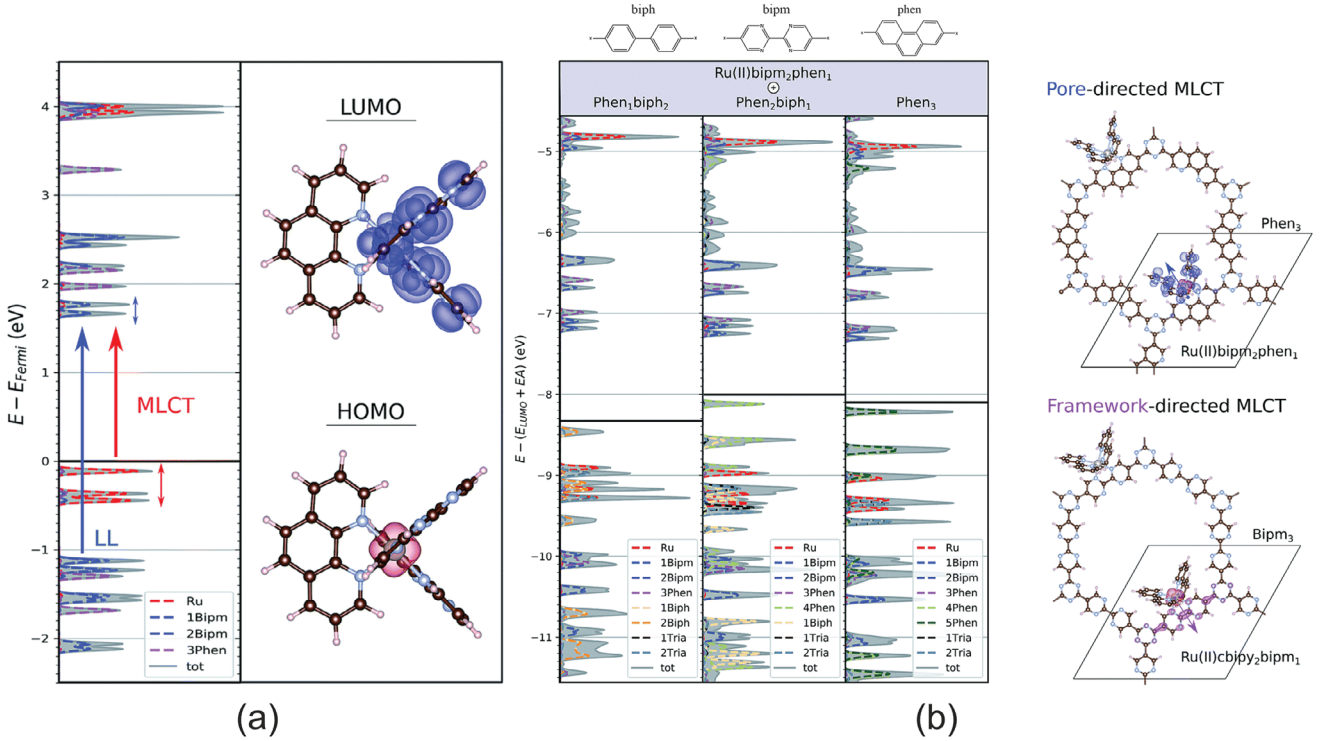

Figure 18. a) Metal-to-ligand charge transfer (MLCT) and ligand–ligand (LL) transitions in Ru(II)bipm$_2$phen$_1$ together with the corresponding orbitals. b) Electronic states of the Ru(II)bipm$_2$phen$_1$ complex in vacuo and when anchored on a phen$_n$biph$_{3-n}$, (n = 0, 1, 2, 3) framework (left). Depending on the Ru(II)L$_3$ complex and CTF scaffold, the charge transfer upon light absorption can be directed either towards the pore or towards the framework (top and bottom right). Bipm = bipyrimidine, phen = phenanthroline and biph = biphenyl, see also top of figure. Adapted with permission.[512] Copyright 2019, Royal Society of Chemistry.

in accepting the protons.[515,519] On the other hand, benzene ring-based groups (benzene (BZ), triphenylamine (TA), 1,3,5-triphenylbenzene (TBZ) and 2,4,6-triphenyl-1,3,5-triazine (TST)) were chosen as an active site for OER, supported by both computational and experimental investigations.[513,520] Using these two combinations, a total of 12 different 2D COFs were investigated for photocatalytic water splitting and the electronic properties were calculated with static DFT calculations using the HSE06 hybrid functional to assess their suitability for overall water splitting, as shown in Figure 19b. This involved aligning the band edges of the COFs with the reaction potentials of H^+/H_2 and O_2/H_2O. The calculated band edges indicate that COFs constructed with BZ, TBZ, or TST have CBM positions higher than the reduction potential of protons (H^+/H_2) and VBM positions lower than the oxidation potential of water (O_2/H_2O), making them suitable candidates for overall water splitting, while the TA-based COFs did not fulfill the necessary conditions. The authors calculated the band gap and attributed discrepancies with earlier reported optical band gap values (see Table S1 in ref. [518]) to the importance of the stacking pattern in 2D COFs.[521–523] 2D COFs are characterized by strong covalent bonding of building blocks within an individual layer and the relative position of successive layers is governed by weak non-covalent interactions. The layer offset leads to various stacking patterns in 2D COFs, significantly impacting the physical and chemical properties of 2D COFs and their derived materials.[521] Therefore, investigating various stacking configurations and their impact on the band gap and band edge is critical for identifying suitable COFs for photocatalytic water splitting.

Moreover, the authors also investigated free energy changes for all the elementary steps of HER and OER for I-TST, Ai-TST, and Ao-TST. The four-electron OER mechanism was considered using the single-site and dual-site pathways on the TST segment of the COFs as shown in Figure 19c. The first two intermediates, OH* ($H_2O \rightarrow OH^* + H^+$ with the asterisk symbol representing adsorption on an active site) and O* ($OH^* \rightarrow O^* + H^+$) are similar for both pathways. The final intermediate is OOH* ($O^* + H_2O \rightarrow OOH^* + H^+$) for the single-site pathway, which leads to the formation of final product O_2 ($OOH^* \rightarrow O_2 + H^+$). For the dual-site pathway, the third intermediate O*OH* ($O^* + H_2O \rightarrow O^*OH^* + H^+$) binds on two active sites rather than one and the final intermediate is OO* ($O^*OH^* \rightarrow OO^* + H^+$) which further leads to the formation of final product O_2 molecule and completes the OER. In the absence of induced light (U = 0, pH = 7), the calculated Gibbs free energy change suggested that the formation of OOH* is the rate determining step for the single-site pathway as shown in Figure 19d. While the formation of OH* is the rate determining step for dual-site pathways, all dual-site pathways are more energetically favorable compared to single-site pathways. At a light-induced bias potential *U*, i.e., the energy difference between the VBM and the hydrogen reduction potential, of 1.83 eV for I-TST, all the elementary steps are energetically feasible for dual-site pathways. The reduction reaction

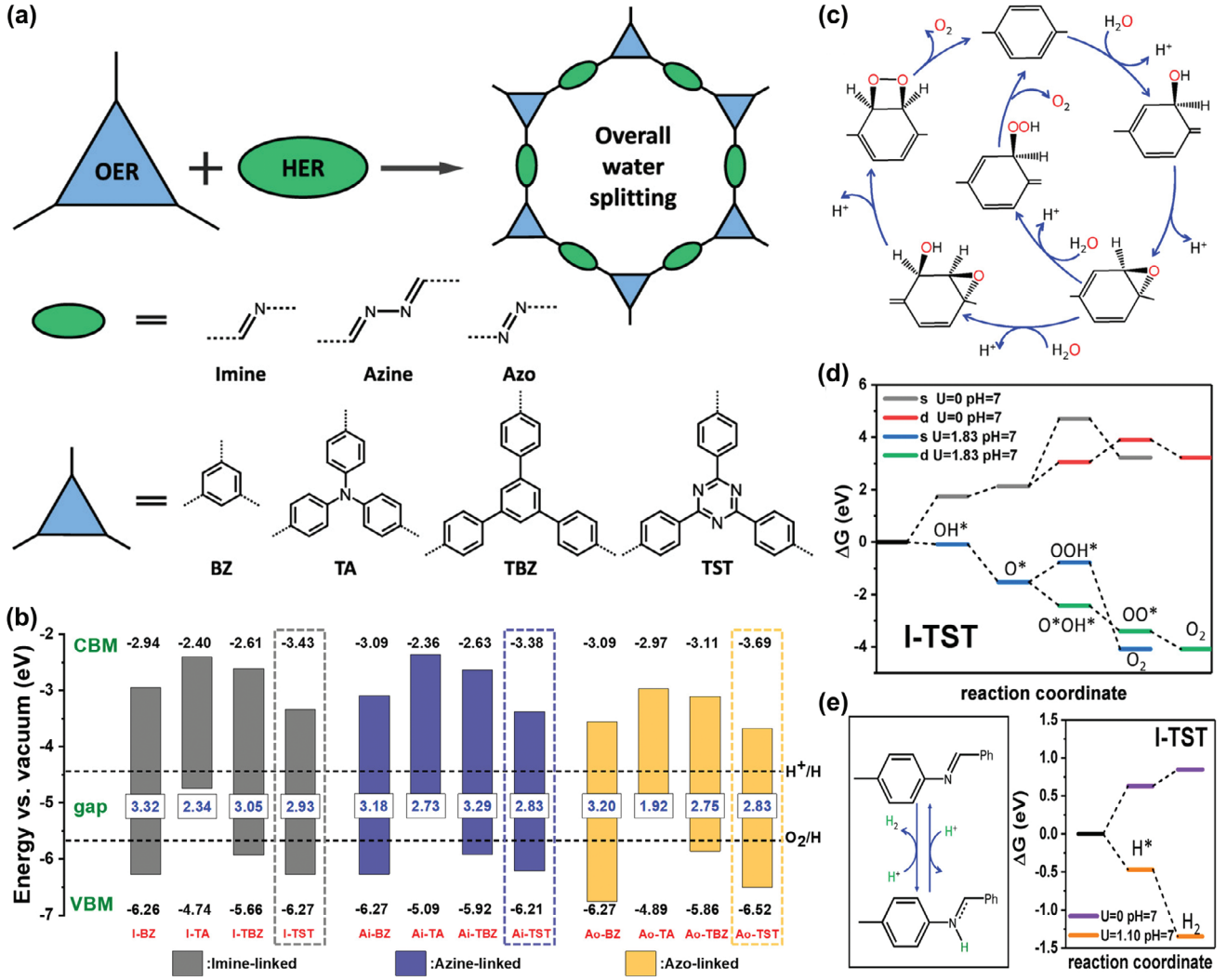

Figure 19. a) Schematic illustration of the structure and design principles of 2D COFs for photocatalytic overall water splitting. b) The calculated band positions of the COFs relative to the vacuum level as numbers alongside water redox potentials at pH = 0 as horizontal dashed lines. c) Possible OER pathways on the TST segment. d) Calculated Gibbs free energy changes for OER intermediates on I-TST. e) HER process on the imine linkage and corresponding intermediate Gibbs free energy changes for I-TST. Reproduced with permission.[518] Copyright 2020, American Chemical Society.

of water splitting was also investigated for HER by calculating the free energy of adsorption of a proton (H*) at the nitrogen atom of the COF. Similar to the OER, the free energy change of HER (see Figure 19e) becomes spontaneous in the presence of a light-induced bias potential ($U = 1.10$ eV). The computational prediction of photocatalytic water splitting under visible light into O_2 and H_2 was experimentally confirmed for I-TST COF, making this study an instructive example of close synergy between theory and experiment to gain insight in photocatalytic water splitting in 2D COFs.

3.3.3. Donor-Acceptor COFs

In efforts to reduce the recombination of photoexcited electrons and holes in COFs, researchers have explored combinations of donor-acceptor (D-A) units for photocatalysis.[524,525] D-A COFs consist of both electron-rich donor groups and electron-withdrawing acceptor groups. Upon light absorption, an electron is excited from the donor's highest occupied molecular orbital (HOMO) to the acceptor's lowest unoccupied molecular orbital (LUMO). This process is most efficient when the HOMO is situated on the donor and the LUMO on the acceptor. Tuning the strength of these D-A interactions is crucial for developing efficient COF-based photocatalysts.

Jiang and co-workers reported a computational study on seven D-A COFs to study the impact of the D-A framework on the photocatalytic performance and efficiency.[526] Their detailed time-dependent density functional theory (TD-DFT)[527] analysis assessed the D-A interaction strength by calculating the optical band gap, from which the exciton binding energy (E_b) can be estimated as an important parameter to evaluate the excitonic effect of a photocatalyst (see Subsection 2.4.3).[528–531] The E_b was calculated by subtracting the optical band gap from the fundamental

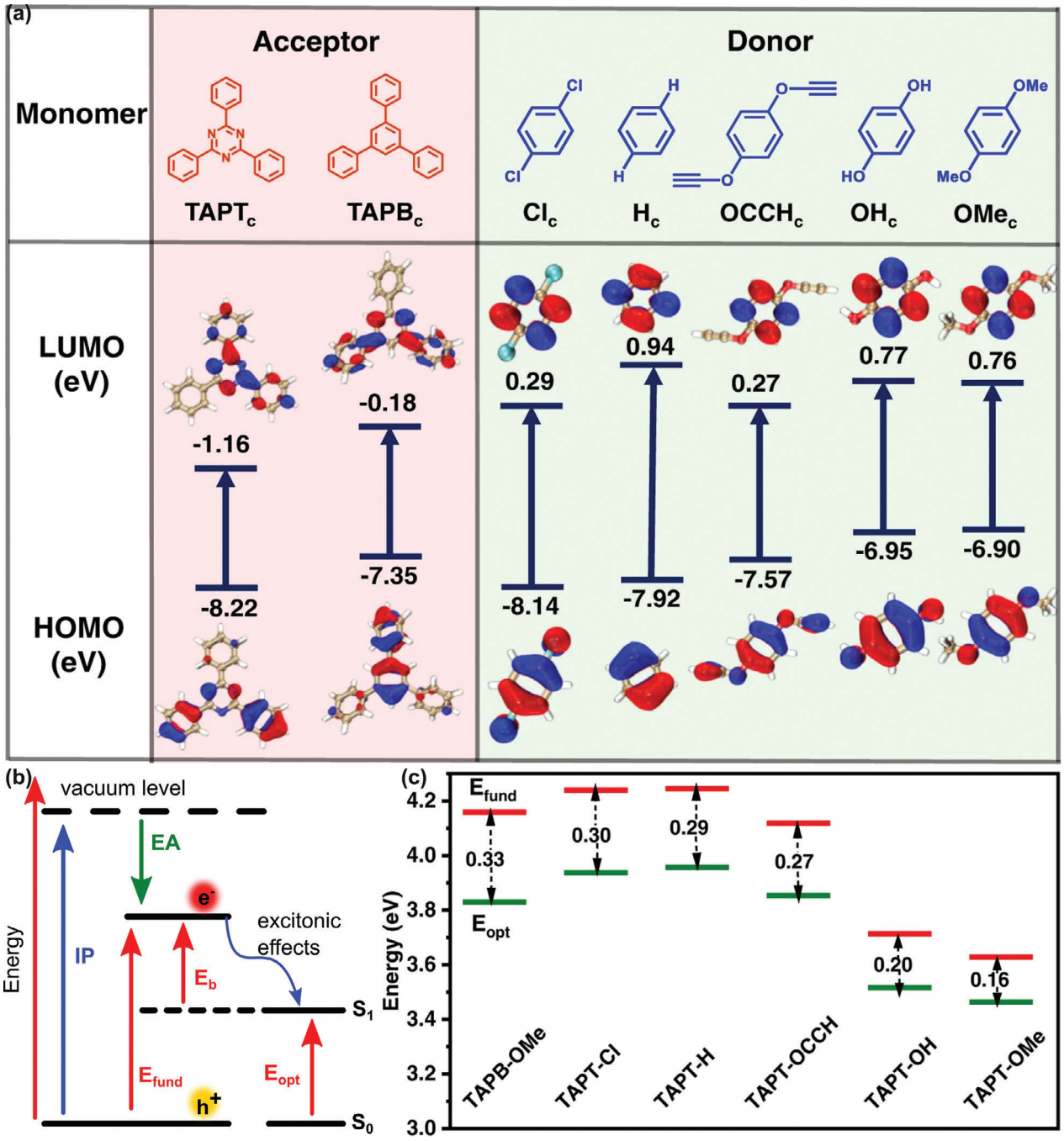

Figure 20. a) The HOMO and LUMO energy level diagram for the two types of building blocks used to construct donor-acceptor (D-A) pairs is shown. TAPT$_c$ and TAPB$_c$ represent the core structures of the amino-based monomers (TAPT and TAPB) without their amine groups. Similarly, Cl$_c$, H$_c$, OCCH$_c$, OH$_c$, and OMe$_c$ represent the core structures of the terephthalaldehyde-based monomers without their aldehyde groups. b) Illustration of various energy gaps in the molecular base: S0 and S1 denote the electronic ground state and the lowest excited state, respectively. IP: ionization potential; EA: electron affinity; E$_{fund}$: fundamental band gap; E$_{opt}$: optical band gap; E$_b$: exciton binding energy. c) The calculated exciton binding energy E$_b$ (double arrows) for all the COFs. Reproduced under terms of the CC-BY license.[526] 2023, Qian et al., published by Springer Nature.

band gap (**Figure 20b**) where a lower E$_b$ value signifies a stronger D-A interaction, ultimately improving the photocatalytic efficiency. For a detailed explanation on the application of TD-DFT, we refer to the supplementary information in the original publication.[526] Consequently, a stronger D-A interaction leads to a lower exciton binding energy, ultimately improving the photocatalytic efficiency. The researchers selected TAPB and TAPT as amine-based acceptor groups and five functionalized terephthalaldehydes with C$_2$ symmetry to serve as donor units as shown in Figure 20a. Analysis of the calculated molecular orbitals revealed

that TAPT exhibits suitable characteristics for D-A interactions with all the investigated aldehyde-based monomers. Conversely, TAPB can only form effective D-A structures with aldehydes containing electron-donating groups like -OH and -OMe. Among the designed COFs, TAPT-OMe displayed the lowest E_b of 0.16 eV, indicating the strongest D-A interaction as shown in Figure 20c. Furthermore, the researchers successfully synthesized these COFs and compared the results from photoelectrochemical characterization techniques to validate the theoretical predictions, i.e., the suppression of exciton recombination and the promotion of exciton dissociation. The TAPT-OMe COFs demonstrated the highest hydrogen production, highlighting the effectiveness of this approach. The successful application of computer-aided design for targeted chemical tailoring of COFs presents a highly efficient approach to optimize COF-based photocatalysts by (i) calculating properties from first principles, (ii) synthesizing the most promising candidates to confirm the theoretical predictions and (iii) optimizing the stability and performance using computational insight.

4. Future Outlook in Modeling Reticular Materials

Initially the field of reticular chemistry had to mature, but today, 30 years since its inception, the possibilities offered by the field have clearly been demonstrated. So far, we probably have only seen a fraction of the opportunities offered by these materials in technological applications. Initially, reticular materials such as metal-organic frameworks were perceived as laboratory curiosities, but the case studies in this review show that reticular materials have matured to an extremely versatile class of materials which can be modulated to play an essential role in technological solutions in fields such as health, sustainable and clean energy production, mitigation of climate change, combat of environmental, damage clean air and the availability of water resources. In our opinion, the challenge for the upcoming decades in the field of reticular chemistry will be the full integration of reticular materials into technological applications and deployment at an industrial scale. Initially the attention was focused on constructing as many materials as possible to prove the generality of the reticulation concept by combining various building blocks, topologies, nets etc. Currently it is generally accepted that with the reticular concept, one can make almost any material with desired functions. The true challenge is now to further evolve towards integrating these materials into the innovation chain and to fully exploit their potential to provide solutions for urgent societal problems related to energy, health and water resources. This will require more focus towards upscaling, towards exploring the properties at the crystal particle level, exploring properties induced by shaping, morphology and integration of reticular materials into larger units with the help of binders or construction of monoliths. Developments along this trajectory will truly revolutionize the innovation chain where one goes from molecules to materials to engineering solutions for societal and technological innovations. Given these evolutions and opportunities, the main question we like to address within this outlook section is "*Where does modeling fit into this exploration cycle towards technological innovation based on the reticular concept?*"

4.1. Open Challenges in Computational Modeling of Reticular Materials

Reticular materials have evolved into a platform to design materials with desired functions and properties up to any liking. In parallel to the rise of the field of reticular chemistry, modeling also matured substantially and hereafter we try to put both evolutions into perspective and highlight particular modeling aspects, we believe are important in the computational modeling of reticular materials. To understand the potential role of modeling, it is essential to refer back to their unique building pattern where molecular building blocks with specific functions are stitched together into a framework with almost perfect control on the positions of the molecular building blocks. In contrast to any other material class, the whole periodic table of elements becomes a playground for reticular chemistry as one can start from "any building block". Reticular chemistry is an interdisciplinary field, combining aspects of organic and inorganic chemistry, molecular and solid-state physics and chemistry. Modeling these materials also requires concepts from modeling organic, inorganic, isolated molecules and solid-state materials. Unlike any other material class, reticular materials provide a unique opportunity to construct scaffolds with desired functions in various applications. Besides the almost boundless number of chemical elements and building blocks, the almost unlimited number of possibilities is also rooted in the architectures to combine the blocks, giving access to periodic, aperiodic, disordered structures, etc. Modeling such structures is far from trivial as we illustrated in this review and further method developments will be necessary to model these structures as realistic as possible. Apart from the flexibility offered by the molecular building blocks, the way these building blocks are stitched together provides opportunities to include additional functions, dynamics and properties invoked by the architecture itself. A very recent example of such higher order architectures are infinite catenane frameworks synthesized by Yaghi and co-workers in which discrete adamantane-like polyhedra are catenated to construct the extended crystalline structure, as shown in **Figure 21**.[532]

Interpenetrated frameworks were recently simulated by us to study flexible COFs and we found that the number of phases present depends on the degree of interpenetration.[533] The properties of these newly synthesized materials are largely unknown, yet these materials exhibit application potential as molecular motors, efficiently converting chemical energy into mechanical movement.[534,535] These two examples are a first step towards making materials that can flex and potentially can stiffen in response to external stimuli, leading to elastic porous materials with rubber-liker properties.[536]

4.1.1. Importance of Accurately Modeling Interatomic Interactions

In the last three decades, reticular chemistry evolved into a strong material's design principle, while at the same time modeling also matured substantially. About two decades ago, modeling was rather an explanatory field, to help experimentalists in understanding their experimental observations. The approaches used around the year 2000 did not allow to model realistic materials with realistic sizes capturing defects, disorder, nor was it possible

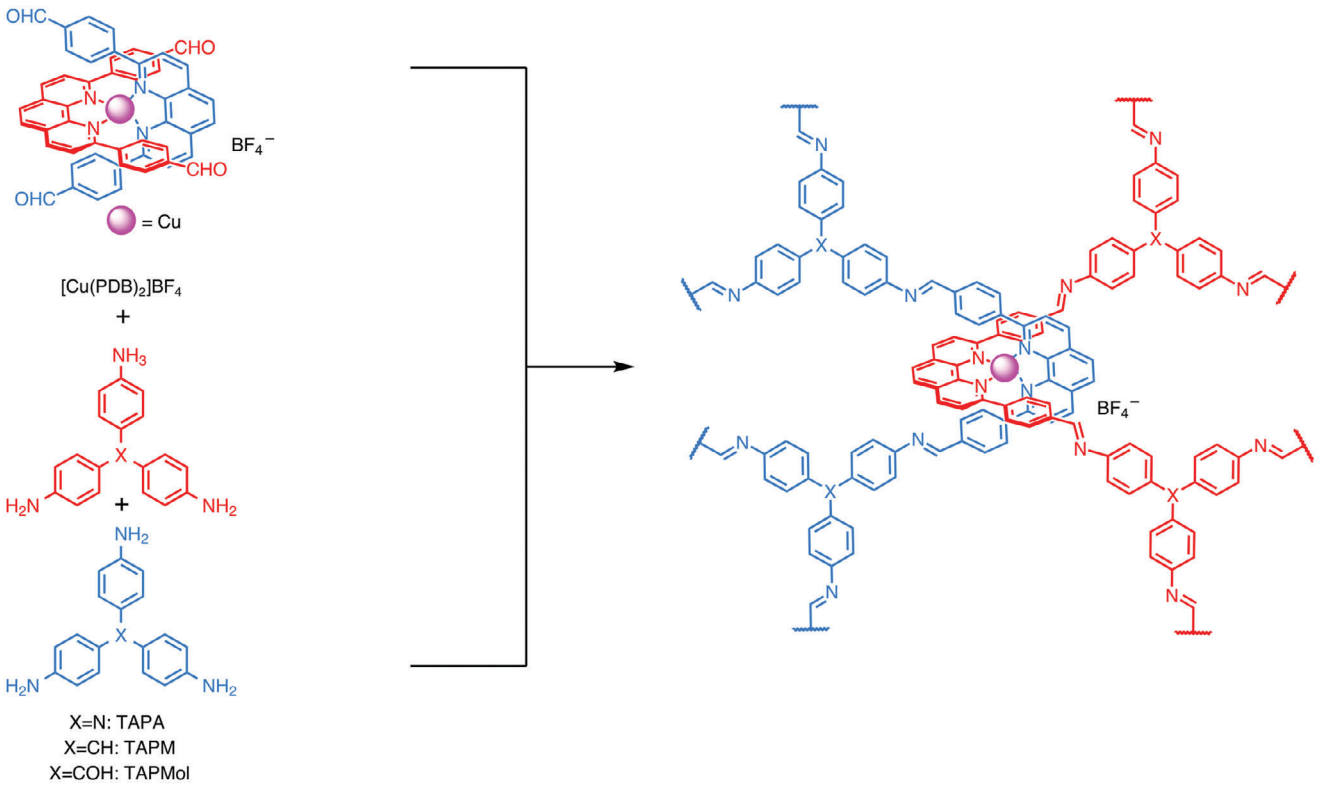

Figure 21. The building block of an infinite catenane, or catena-COF, consists of two crossed molecules with a copper atom at the center. When mixed, they link up to create an extended, 3D material of interlocking molecules. Reproduced with permission.[532] Copyright 2023, Springer Nature.

to study the dynamic behavior of materials and their response to external triggers or interactions with guest species in a way that allows a direct comparison with experimental data. Since reticular materials are governed by a broad variety of interactions going from strong covalent bonds to coordination bonds but also weak interactions, e.g., to model host-guest interaction, interactions between layers in covalent organic frameworks, or π-interactions between linkers in winerack frameworks, it is critical to model all these interactions with high accuracy. The last 30 years, the modeling field evolved substantially and currently it has become possible to model at the local level (0.1 to 1 nm) both strong covalent interactions but also weaker interactions with higher accuracy. Additionally, the proper modeling of the metal-coordination bond is not-trivial for quantum mechanical models especially when elements are involved prone to strong electron correlation. More detailed information on how to model these systems is given in Section 4.2.1. From a modeling perspective, fundamentally new models have been developed that allow to model strong and weak interactions, including van der Waals interactions. These new models have now found their way into the field of reticular chemistry. Certainly for materials like layered covalent organic frameworks governed by π-interactions and dispersive interactions between such layers, those models are critical. Despite this progress, modeling the quantum mechanical many-body problem accurately for the whole periodic table of elements and for the whole set of materials accessible within the field of reticular chemistry remains an important field of study.

4.1.1.1. Importance of Having Access to Representative Structural Models: As outlined in Section 2.1 of this review, the first step of any molecular modeling exercise is the construction of a **representative structural model** with atomic resolution. Furthermore, as explained in previous paragraphs, there is a need to model not only local phenomena but model realistic scaffolds of reticular materials up to the mesoscale. In Section 2.1, we elaborated on various methodologies to propose structural models for realistic reticular materials. The strength of reticular materials is not only invoked by their particular building concept but also their potential to incorporate defects at various length scales into the framework in a structured way. Defect engineering offers major possibilities if it can be controlled in an atomic precise way. Furthermore, we should obtain more control of the outer surface. While techniques exist to construct disordered models for these mesoscale structures, without any experimental input the number of potential structures becomes infeasibly large. Therefore, a close synergy with experiments is crucial to precisely determine the structure of defective finite-sized reticular materials from the nano- to the mesoscale. Many spectroscopic techniques may give input on the structure, but a direct comparison with atomistic models requires spatially resolved measurements. One interesting technique to directly observe individual defects in real space with atomic resolution is offered by high-resolution electron microscopy.[537–540] However some reticular materials like metal-organic frameworks are beam-sensitive and new low-dose electron-microscopy acquisition methods need to be developed

to overcome the beam-sensitivity in MOFs or other related beam-sensitive reticular materials. Even when such high-resolution images come available, electron microscopy modeling and quantification tools need to be developed to translate the high-resolution TEM images to atomistic structural models. Ideally an integrated experimental-modeling approach would be developed for structure characterization of tunable reticular materials with varying building blocks, architectures, defects, and disorder.

4.1.2. Which Length and Time Scales Need to be Modeled with Atomic Resolution?

As length and time scales span various orders of magnitude when going from the atomistic to the application level, a pertinent question is to what length and time scales and for which phenomena do we need to model with atomic resolution? We refer to Figure 8 earlier in this review for the achievable time and length scales of the different methods discussed throughout this review. When interested in understanding all processes from the crystal particle level to the atomic level, it is potentially not necessary to model the whole crystal particle level with atomic precision. At the same time, it is important to define realistic goals on accessible time windows with quantum mechanical methods. With the rise of machine learning models, it will likely become possible to model reticular materials up to 50 nm at a microsecond time scale in the near future. Clearly, this is a huge step forward compared to what is possible today, but it still does not allow a direct comparison with experimental data. A realistic goal for modeling could be to follow the time evolution of realistic materials, having (finite) sizes of minimum 10–50 nm in presence of defects and potentially guest species, all at quantum mechanical accuracy. When using methods of atomistic resolution, time scales could be restricted from the picosecond to the microsecond level. To reveal time aspects in larger spatiotemporal windows one should resort to overall kinetic models such as kinetic Monte Carlo models or other yet-to-be-developed kinetic models which are able to deduce the kinetics on longer time scales, based on underlying atomically revolved data. When aiming to address also longer length scales, one should reside to coarser models where not all atomical interactions are described with quantum accuracy.

4.1.3. Modeling Spatiotemporal Phenomena

As reticular materials form architectures at longer length scales, modeling needs to capture not only local phenomena but also non-local events typically important for transport of molecules through the pores of the materials, modeling framework transitions, phenomena related to the mesoporosity or dynamics invoked by higher order architectures as mentioned above. Within the last 30 years, modeling has evolved substantially, and attainable length scales or feasible number of atoms add up to a few thousand atoms when describing energies with Density Functional Theory or up to a million atoms when using classical force fields.[220,221] Referring back to future directions in the field of reticular chemistry, i.e., their integration within larger macroscopic units to be used in technological applications, a critical point for modeling reticular materials is to **bridge the length scale gap** between molecular structures at the nanoscale to architectures at the mesoscale or micrometer scale. Despite the fact that longer time scales are now within reach with the development of more accurate methods at a computationally affordable cost to describe the energies and interactions, it remains a formidable challenge to **bridge the time scale gap** to understand the kinetics of all phenomena taking place within reticular materials. An illustrative example is the switching behavior of metal-organic frameworks between various crystal phases upon exposure to external stimuli. Major experimental efforts have been undertaken to get track of time for this switching behavior. Only very recently, the kinetics of switchable MOFs upon butane adsorption could be measured. A critical dependence of the kinetics on the crystal size was observed, which was ascribed to butane intracrystalline diffusion, however a clear molecular explanation was not given.[541] Modeling has now evolved to a point where we can estimate the kinetics of local phenomena, e.g., reactions, but kinetic theories to understand the kinetics of intertwined local and global phenomena or phenomena with strongly disparate time scales are yet to be developed.

Future modeling efforts should further focus on modeling interactions within the framework and with guest molecules with greater accuracy yet at an affordable cost and on methodologies to bridge length and time scales to pursue the modeling of realistic scaffolds of reticular materials and their dynamics. It is important to realize that **spatial properties are intertwined with time properties**, e.g., the ability of soft porous frameworks to switch between various crystal phases upon exposure to external stimuli is critically dependent on the size of the crystal and defect density.[45–53] Acknowledging this coupling leads to the concept of spatiotemporal phenomena, referring to the entanglement between the dynamics and spatial heterogeneities. Embracing the coupling between spatial heterogeneities present in the crystal from the nanoscale local level to the crystal particle level and the dynamics of the framework as well as its environment may lead to new design principles where both the spatial and time axis can be explored. One could imagine that based on the spatiotemporal concept, it could become possible to build materials that can selectively capture molecules in multiple time windows, or materials that have a memory. This concept of spatiotemporal design was first postulated by Stefan Kaskel and co-workers in a recent perspective paper.[56]

4.1.4. Understanding the Dynamics of Reticular Materials

A critical point to understand the function of a material under realistic operating conditions is to unravel the material's **dynamics** and its interaction with its environment. Reticular materials are intriguing dynamic scaffolds with the ability to respond to external triggers in an anomalous way. Understanding the time aspects of the framework and the phenomena taking place when being exposed to temperature, pressure and guest interactions is critical to understand the function of reticular materials. Yet today, time aspects of reticular materials and their interaction with their environment is not well understood, neither from experimental nor from modeling point of view. About 30 years ago the first fully quantum mechanical-based molecular dynamics simulations appeared, however due to the enormous computational cost of evaluating energies and forces at the QM level, accessible

time scales were initially restricted to a few picoseconds. The field has now substantially evolved, and currently even when energies and forces are evaluated at the DFT level, one can access time scales of the order of hundreds of picoseconds. Clearly this is still too short to describe slower events, therefore the field of machine learning potentials provides a great promise to access much longer length and time scales. With classical force fields microseconds are already feasible, however more research is necessary to also access these time scales with machine learning potentials.

As discussed in this review, enhanced sampling molecular dynamics methods have become a strong vehicle to study **rare events** for example associated with framework transitions and chemical reactions taking place in reticular materials. However, challenges remain on how to define collective variables as in many cases today these are based on chemical or physical intuition. For example, for a phase transformation in soft porous reticular materials where a large volume change occurs, the volume is most often chosen as a collective variable. For more complex materials exhibiting a complex configuration space due to the presence of flexible linkers (e.g., CAU-13, ZrCDC and NOTT-300), more complex collective variables are necessary beyond the volume to fully describe their free energy landscape.[361] New methods are actively being developed to learn the collective variables in an automated way based on data-driven methodologies, yet their applications in the field of reticular materials are few and far between.[542,543] As a recent example from our own group, we mention Vandenhaute et al.[288] Consequently, one area of future growth concerns the further development and application of data-driven methods within the field of complex chemical and physical transformations taking place in reticular materials. A second opportunity in the study of rare events involves the development of methods to efficiently sample paths for activated processes without defining collective variables and without prior knowledge of transition states. Within this respect transition path sampling methods provide an interesting route, in which an ensemble of unbiased dynamical trajectories between various stable minima is created by systematically generating new trial paths through modification of previous paths in a Monte Carlo fashion. When resorting to variants like transition interface sampling (TIS) or replica-exchange transition interface sampling (RETIS), these methods offer the opportunity to also obtain rates.[544–547] Such methods have not yet been explored in the field of reticular materials, as one needs thousands of trajectories to obtain reliable quantitative data. However, when methods become available that allow to calculate the energies and forces with quantum accuracy at a much lower computational cost, transition path sampling methods will become viable. Consequently, the integration of machine learning potentials and transition path sampling methods is a highly promising avenue. Access to such methodologies would open the perspective to answer following questions relevant for the field of switchable reticular materials: What is the mechanism behind a phase transformation? Do phase transformations nucleate locally at defects? How are phase transformations impacted by crystal size, crystal morphology, and spatial heterogeneities? Do transformations occur collectively or semi-collectively with domain formation? Can we predict transformation rates?

The answers to these questions will unlock fundamental insights and are crucial to design spatiotemporal controlled processes.

4.2. Specific Challenges and Opportunities in Modeling Reticular Materials

In this subsection, we identify and enumerate specific challenges in modeling reticular materials and hope that their identification will inspire future model developments, which will eventually lead to modeling new reticular materials in a realistic way. Each of the following outstanding problems is highly challenging and we highlight recent efforts by distinguished researchers in the field who are actively working towards a solution.

4.2.1. Highly Accurate Quantum Mechanical Methods for all Elements of the Periodic Table of Elements

The strength of reticular materials is their versatility in terms of chemical elements to be included in the scaffold, however some of these elements have **challenging electronic structures**. As an illustrative example, we mention MIL-53 materials, containing different metal oxide $[M^{3+}(OH)^{-}]_n$ chains that are connected by benzene dicarboxylate linkers, have been synthesized, for which the M^{3+} metal cations can either be 3p metal cations like Al^{3+},[548] Ga^{3+},[549,550] In^{3+},[551] or transition metal cations like Sc^{3+},[552] Cr^{3+},[553] Fe^{3+},[554] etc. A second example are rare-element MOFs with attractive applications in photocatalysis, such as UiO-66 materials made of $Zr_6(\mu_3\text{-}O)_4(\mu_3\text{-}OH)_4$ bricks connected through organic ligands, where one or more Zr ions are substituted by Ti, Ce or lanthanide metal ions (see also Subsection 3.3.1 Orthogonal Electronic Structure Engineering).[555–557]

An accurate description of the electronic structure of reticular materials exhibiting **strong electron correlations and various possible spin configurations** requires computationally more expensive methods beyond DFT, which can be broadly classified in methods from many-body perturbation theory and nonperturbative methods. Many-body perturbation theory includes methods such as the random phase approximation (RPA),[558–561] constrained RPA (cRPA)[562] and the GW approach (see also Subsection 2.4.3),[563,564] while nonperturbative methods include dynamical mean-field theory (DMFT)[565–567] and density matrix embedding theory (DMET).[568–571] Application of the preceding advanced methods to better account for electron correlation remain scarce, although recent computational studies are already available on 1D MOFs such as MIL-53(Al)[558] and 2D kagome[572] lattice MOFs such as Cu-dicyanoanthracene (DCA-Cu).[573–575]

4.2.2. Future Direction for Machine Learning Methodologies within the Field of Reticular Chemistry

Within this review, we have mentioned a few times the opportunities offered by the rapidly evolving field of data science and machine learning. Moreover, we particularly highlighted the potential of machine learning potentials to predict energies and forces

with quantum mechanical accuracy. Apart from this specific target, machine learning is transforming all branches of molecular simulations with applications in the extraction of free energy surfaces, methods to sample phase space, rapid screening of chemical space, etc. We refer the interested reader to dedicated reviews on the impact of machine learning in the field of molecular simulations and materials science.[190,576]

Within this subsection, we particularly highlight some future directions that are relevant for the field of reticular chemistry and their computational modeling. Firstly, when we introduced the sequence of a molecular modeling exercise, the determination of the PES and its exploration via sampling methods were introduced as two different steps. Currently by the introduction of active learning schemes, where the MLP itself is used to generate new configurations ready to be subjected to DFT evaluations, these two steps are merged to some extent. In this case, one starts from a small training data set to derive an initial MLP, which is then used to explore configuration space along some specific collective variables.[577] From these runs new configurations are extracted, which are subjected to new DFT calculations that can be used to train a next-generation MLP. This procedure is repeated until the interesting part of phase space has been seen. Most of these active learning schemes still rely on the definition of predefined collective variables, for example, the volume in case of flexible MOFs. Future interesting directions would be to develop an integrated engine to simultaneously derive the MLP as well as identify important collective variables or reactive paths. In this case, the graph neural networks should learn simultaneously the energy, forces but also important reactive paths or collective variables.

The simulation of realistic reticular materials may generate very large structural models (see the discussion in Subsection 2.1.1). For such mesoscopic systems having spatial gradients, like external surfaces or internal regions where defects are present, it might become very difficult to perform DFT calculations on the mesoscopic systems with periodic boundary conditions. In this case, it might be interesting to explore a cluster-based approach for generating the MLP. By inspecting atomic representations in feature space, it could be learned which atomic environments need to be added to the training data. For such new environments, a cluster could be carved from the mesoscopic system to subject it to quantum mechanical data and generate training data.

Lastly, one can ask the question whether it is necessary to build a new MLP for every material at hand. As mentioned earlier in this review general-purpose foundation models, i.e., machine learning models which are trained on data broadly distributed across the chemical design space such that it can be applied across a wide range of systems, are now becoming available. Such models could serve as a good basis to train more dedicated system-specific MLPs. Specifically for reticular materials, the opportunity exists to explore the building block concept to train MLPs for a broad set of materials made up of similar building blocks. In Vandenhaute et al.[578] a proof of principle was shown for constructing a universal MLP in the field of MOFs. In this case a set of ten well-known aluminum- and zirconium-based frameworks similar to MIL-53(Al) and UiO-66(Zr) in either the topology of the framework or the organic ligand were considered, however the pristine MIL-53(Al) and UiO-66(Zr) were not included. The model was trained on a data set with a significantly larger variety in atomic environments and achieved relatively low force and stress MAEs, even for the frameworks not included during training. Furthermore, the model correctly predicted the expected flexibility of MIL-53(Al). Such universal MLPs, based on the building concept in combination with data-efficient equivariant message-passing neural networks, provide promising routes to easily and quickly explore the space of reticular materials with greater accuracy compared to universal classical force fields.

From a methodological point of view, systematically newer and more efficient machine learning mathematical architectures are continuously being developed. It is of utmost importance that those working in the field of reticular chemistry closely keep up with these methodological evolutions, to capture as much information as possible from the delivered training data. Currently, strong networks are equivariant neural networks, such as NequIP and MACE, which are currently considered state-of-the-art in terms of accuracy and data-efficiency across the periodic table.[278,280,579] However recently new architectures, e.g. SO3KRATES[580] which combines equivariant and invariant features, have been launched to make them even more efficient for very long molecular dynamics runs or systems of increasing size.

Evidently this section on future directions in machine learning methods is not comprehensive but gives only a few future directions from our perspective, and which we think are relevant for modeling reticular materials. As many scientists are now exploring these directions, intriguing new insights in the field of reticular materials and machine learning are to be expected.

4.2.3. High Throughput Screening at Higher Levels of Accuracy

High throughput screening has been instrumental for finding new materials in the large design space of reticular materials. However so far, most screening is performed with relatively "cheap" computational methods, given the large number of structures under consideration. Within the review it became clear that machine learning potentials are highly promising to extend the accessible length and time scales within molecular simulations, however the question raised in how far they are also applicable for high throughput screening.

Earlier in this Review, we discussed MACE-MP-0 as a **general-purpose foundation model**, i.e., a machine learning model which is trained on data broadly distributed across the chemical design space such that it can be applied across a wide range of systems (vide supra Subsection 2.2.3). With the development of such general-purpose foundation models, the possibility of high throughput screenings being performed at DFT accuracy is rapidly approaching. However, such models are still computationally not competitive with classical force fields as they have many more parameters. This currently renders high throughput screening with these models unfeasible. To overcome this, **merging short-ranged simple neural networks with physics-based models** to accurately account for long-ranged interactions is a promising way forward to approach quantum mechanical accuracy in high throughput screening. To train such hybrid potentials, foundation models are expected to remain valuable to sample the phase space without the need for explicit DFT calculations, gathering data to efficiently train the hybrid potentials.

Such an approach could lead to transferable models maintaining DFT accuracy at computationally tractable expenses and is therefore ideally suited for future highly accurate high throughput screenings.

In the near future, structural, chemical or adsorption-related properties can be expected to be derived from foundation models or fine-tuned MLPs for a large set of reticular materials. In a further step, these DFT quality properties could be used to train deep learning models to learn highly accurate structure-property relationships and employ such models to screen vast sets of hypothetical MOFs. This can reduce the need for laborious and expensive experiments and allows an accurate estimation of the effect of defects, impurities, surface and size effects, as these are always well-defined in molecular simulations. In a feedback loop with experiments, such investigations could furthermore provide insight into the presence, origin and distribution of imperfections present in any real-world material under study, ever deepening our understanding of the rich chemistry of these reticular materials.

4.2.4. Modeling the Crystallization Process of Reticular Materials: a Highly Challenging Goal for Modeling

In this review, we discussed modeling techniques to model extended structures of already formed reticular materials, however a highly challenging goal for modeling is to model the crystallization problem of reticular materials. In contrast to the plethora of literature available on the modeling of already formed reticular materials, the literature on the crystallization mechanism and its characterization is much more restricted. Classical nucleation and growth theories assume the formation of a rigid nucleus, followed by the successive addition of building blocks.[581,582] Both computational[583,584] and experimental[585–587] studies argue in favor of the existence of non-classical nucleation and growth pathways in all classes of reticular materials, although conclusive evidence of the dominant pathway, either from comprehensive kinetic studies or precise microscopic imaging, is currently lacking.[588] As the largest and oldest subclasses of reticular materials, MOFs and ZIFs are the main focus of recent efforts to model the self-assembly process.[584,589–594] In the crystallization process, the system is often assumed to obey Ostwald's rule of stages,[595] sequentially evolving through all available metastable states. Contrary to Ostwald's rule of stages, classical nucleation theory predicts a parallel and independent growth of all possible phases.[596] Regardless of the serial or parallel crystallization process, the system may become **kinetically trapped in a metastable state** thereby arresting the formation of a thermodynamically more stable phase, which, as shown abundantly throughout this review, may heavily depend on external stimuli such as pressure, temperature, and guest molecules. Moreover, the formation of strong bonds, in particular the strong covalent bonding in COFs, limits **self-correction** of the system during crystallization, commonly referred to as the crystallization problem.[597,598]

Additionally, from an experimental point of view, different solvents have been shown to lead to different polymorphs in MOFs,[599] ZIFs,[600] and COFs.[601] Therefore, accurately modeling the early stages of the reticulation process must **account for the solvent**, yet explicitly including solvent molecules in the atomistic models quickly leads to an overwhelming amount of atoms. On the other hand, the implicit inclusion of a solvent is a long-standing open challenge in molecular modeling with frequent new developments.[602,603]

Clearly, modeling the initial phases of formation of reticular material formation and crystallization is highly challenging, given the importance of the conditions, solvent and the huge amount of possible pathways to be considered. Therefore, modeling the solvent problem, serial and parallel polymorphism and defect healing are identified as highly challenging areas in the modeling of the self-assembly of reticular building blocks.

4.3. Final Remarks on the Past, Present, and Future of Modeling Reticular Materials

We finalize this review by answering the question in how far modeling fits in the technological innovation chain invoked by reticular materials. In our opinion, we have currently reached the phase of a synergistic modeling-experimental approach where rational material design becomes within reach thanks to an intimate feedback loop between modeling and experimental insights. In the future, virtual modeling experiments might hopefully be possible where also reverse engineering becomes possible, how can we design a reticular scaffold that shows the right function for the right application. We intentionally use the terminology scaffold to refer to the necessary larger macroscopic bodies to be fabricated to integrate the reticular materials in technological applications. A major challenge for modeling is to step-up towards modeling realistic crystal particles having a finite size, with an external surface, a certain morphology, and shape. Hopefully, such virtual modeling experiments will enable predictive modeling of functional reticular scaffolds. Furthermore, modelers should closely interact with the experimental community to understand the boundaries of experimental synthetic procedures and to validate their predictions. As mentioned in the introduction, reticular materials are situated at the crossroads of disciplines, and in our opinion major steps forward can be achieved from collaborative efforts among theoreticians with various backgrounds on one hand, among modelers and expert experimentalists on the other hand as well as among scientists crossing boundaries of chemistry, physics, computer science, and engineering. In this sense, reticular materials and their design are a showcase example of scientific progress among disciplines without boundaries.

Acknowledgements

All current and former members of the Center for Molecular Modeling are acknowledged for their contributions and discussions, which allowed advancements in the field of modeling reticular materials. All funding bodies that have supported this fundamental research over the years such as the Fund for Scientific Research – Flanders (FWO), the Research Fund of Ghent University (BOF) and the European Research Council are acknowledged. Ghent University is acknowledged for providing the framework to conduct fundamental research. R.G. acknowledges the support from Flanders Industry Innovation Moonshot (MOONRISE, No. HBC.2020.2612), K.S.R. acknowledges the Research Board of Ghent University (BOF) through a Concerted Research Action (GOA010-17). W.T.

acknowledges Prof. Dr. S.M.J. Rogge for fruitful discussions and Aran Lamaire for contributions to figures. Prof. Dr. S. Bals and S. Kavak of the Electron Microscopy for Materials Science (EMAT) at the UAntwerpen are greatly acknowledged for providing us with the Scanning Transmission Electron Microscopy images taken up in Figure 6 and Dr. P. Horcajada is acknowledged for providing the samples.

Conflict of Interest

The authors declare no conflict of interest.

Keywords

computational modeling, free energy, molecular simulation, potential energy surface, reticular materials, structural models

Received: August 14, 2024
Revised: November 22, 2024
Published online:

[1] O. M. Yaghi, M. J. Kalmutzki, C. S. Diercks, *Introduction to Reticular Chemistry: Metal-Organic Frameworks and Covalent Organic Frameworks*, Wiley-VCH, Weinheim, Germany **2019**.
[2] O. M. Yaghi, *Mol. Front. J.* **2019**, *03*, 66.
[3] H. Li, M. Eddaoudi, M. O'Keeffe, O. M. Yaghi, *Nature* **1999**, *402*, 276.
[4] K. S. Park, Z. Ni, A. P. Côté, J. Y. Choi, R. Huang, F. J. Uribe-Romo, H. K. Chae, M. O'Keeffe, O. M. Yaghi, *Proc. Natl. Acad. Sci. U. S. A.* **2006**, *103*, 10186.
[5] J. H. Cavka, S. Jakobsen, U. Olsbye, N. Guillou, C. Lamberti, S. Bordiga, K. P. Lillerud, *J. Am. Chem. Soc.* **2008**, *130*, 13850.
[6] A. P. Côté, A. I. Benin, N. W. Ockwig, M. O'Keeffe, A. J. Matzger, O. M. Yaghi, *Science* **2005**, *310*, 1166.
[7] L. Stegbauer, K. Schwinghammer, B. V. Lotsch, *Chem. Sci.* **2014**, *5*, 2789.
[8] S. R. Batten, N. R. Champness, X.-M. Chen, J. Garcia-Martinez, S. Kitagawa, L. Öhrström, M. O'Keeffe, M. P. Suh, J. Reedijk, *Pure Appl. Chem.* **2013**, *85*, 1715.
[9] B. P. Block, S. H. Rose, C. W. Schaumann, E. S. Roth, J. Simkin, *J. Am. Chem. Soc.* **1962**, *84*, 3200.
[10] E. A. Tomic, *J. Appl. Polym. Sci.* **1965**, *9*, 3745.
[11] P. Z. Moghadam, A. Li, S. B. Wiggin, A. Tao, A. G. P. Maloney, P. A. Wood, S. C. Ward, D. Fairen-Jimenez, *Chem. Mater.* **2017**, *29*, 2618.
[12] R. Freund, O. Zaremba, G. Arnauts, R. Ameloot, G. Skorupskii, M. Dincă, A. Bavykina, J. Gascon, A. Ejsmont, J. Goscianska, M. Kalmutzki, U. Lächelt, E. Ploetz, C. S. Diercks, S. Wuttke, *Angew. Chem., Int. Ed.* **2021**, *60*, 23975.
[13] G. Férey, *Chem. Soc. Rev.* **2008**, *37*, 191.
[14] W. Li, M. R. Probert, M. Kosa, T. D. Bennett, A. Thirumurugan, R. P. Burwood, M. Parinello, J. A. K. Howard, A. K. Cheetham, *J. Am. Chem. Soc.* **2012**.
[15] S. Krause, V. Bon, I. Senkovska, U. Stoeck, D. Wallacher, D. M. Többens, S. Zander, R. S. Pillai, G. Maurin, F.-X. Coudert, S. Kaskel, *Nature* **2016**, *532*, 348.
[16] S. Horike, S. Shimomura, S. Kitagawa, *Nat. Chem.* **2009**, *1*, 695.
[17] S. Kitagawa, in *Flexible Metal–Organic Frameworks: Structural Design, Synthesis and Properties* (Ed.: S. Kitagawa), Royal Society Of Chemistry, London, UK **2024**, p. 396.
[18] P. J. Waller, F. Gándara, O. M. Yaghi, *Acc. Chem. Res.* **2015**, *48*, 3053.
[19] S.-Y. Ding, W. Wang, *Chem. Soc. Rev.* **2013**, *42*, 548.
[20] P. Kuhn, M. Antonietti, A. Thomas, *Angew. Chem., Int. Ed.* **2008**, *47*, 3450.
[21] X. Feng, X. Ding, D. Jiang, *Chem. Soc. Rev.* **2012**, *41*, 6010.
[22] Z. Zheng, Z. Rong, H. L. Nguyen, O. M. Yaghi, *Inorg. Chem.* **2023**, *62*, 20861.
[23] R.-B. Lin, Y. He, P. Li, H. Wang, W. Zhou, B. Chen, *Chem. Soc. Rev.* **2019**, *48*, 1362.
[24] I. Hisaki, C. Xin, K. Takahashi, T. Nakamura, *Angew. Chem., Int. Ed.* **2019**, *58*, 11160.
[25] A. Pedrini, D. Marchetti, R. Pinalli, C. Massera, *ChemPlusChem* **2023**, *88*, 202300383.
[26] X. Song, Y. Wang, C. Wang, D. Wang, G. Zhuang, K. O. Kirlikovali, P. Li, O. K. Farha, *J. Am. Chem. Soc.* **2022**, *144*, 10663.
[27] X.-J. Xi, Y. Li, F. Lang, J. Pang, X.-H. Bu, *Chem. Sci.* **2024**, *15*, 4529.
[28] W. Yang, A. Greenaway, X. Lin, R. Matsuda, A. J. Blake, C. Wilson, W. Lewis, P. Hubberstey, S. Kitagawa, N. R. Champness, M. Schröder, *J. Am. Chem. Soc.* **2010**, *132*, 14457.
[29] Y. He, S. Xiang, B. Chen, *J. Am. Chem. Soc.* **2011**, *133*, 14570.
[30] H. Jiang, D. Alezi, M. Eddaoudi, *Nat. Rev. Mater.* **2021**, *6*, 466.
[31] F. Haase, E. Troschke, G. Savasci, T. Banerjee, V. Duppel, S. Dörfler, M. M. J. Grundei, A. M. Burow, C. Ochsenfeld, S. Kaskel, B. V. Lotsch, *Nat. Commun.* **2018**, *9*, 2600.
[32] A. F. Wells, *Acta Crystallogr.* **1954**, *7*, 535.
[33] M. O'Keeffe, O. M. Yaghi, *Chem. Rev.* **2012**, *112*, 675.
[34] Reticular Chemistry Structure Resource **2024**, https://rcsr.anu.edu.au/, (accessed: July 2024).
[35] M. Eddaoudi, J. Kim, N. Rosi, D. Vodak, J. Wachter, M. O'Keeffe, O. M. Yaghi, *Science* **2002**, *295*, 469.
[36] Y. Liu, M. O'Keeffe, *Isr. J. Chem.* **2018**, *58*, 962.
[37] A. Lamaire, Ph.D. Thesis, Ghent University, **2024**.
[38] B. Li, H. Wen, Y. Cui, W. Zhou, G. Qian, B. Chen, *Adv. Mater.* **2016**, *28*, 8819.
[39] Z. Fang, B. Bueken, D. E. De Vos, R. A. Fischer, *Angew. Chem., Int. Ed.* **2015**, *54*, 7234.
[40] G. C. Shearer, S. Chavan, S. Bordiga, S. Svelle, U. Olsbye, K. P. Lillerud, *Chem. Mater.* **2016**, *28*, 3749.
[41] F. Vermoortele, M. Vandichel, B. Van de Voorde, R. Ameloot, M. Waroquier, V. Van Speybroeck, D. E. De Vos, *Angew. Chem., Int. Ed.* **2012**, *51*, 4887.
[42] F. Vermoortele, B. Bueken, G. L.e Bars, B. Van De Voorde, M. Vandichel, K. Houthoofd, A. Vimont, M. Daturi, M. Waroquier, V. Van Speybroeck, C. Kirschhock, D. E. De Vos, *J. Am. Chem. Soc.* **2013**, *135*, 11465.
[43] M. Vandichel, J. Hajek, F. Vermoortele, M. Waroquier, D. E. De Vos, V. Van Speybroeck, *CrystEngComm* **2015**, *17*, 395.
[44] I. L. C. Buurmans, B. M. Weckhuysen, *Nat. Chem.* **2012**, *4*, 873.
[45] H. Miura, V. Bon, I. Senkovska, S. Ehrling, S. Watanabe, M. Ohba, S. Kaskel, *Dalton Trans.* **2017**, *46*, 14002.
[46] S. Krause, V. Bon, I. Senkovska, D. M. Tobbens, D. Wallacher, R. S. Pillai, G. Maurin, S. Kaskel, *Nat. Commun.* **2018**, *9*.
[47] T. Kundu, M. Wahiduzzaman, B. B. Shah, G. Maurin, D. Zhao, *Angew Chem Int Ed Engl* **2019**, *58*, 8073.
[48] Y. Sakata, S. Furukawa, M. Kondo, K. Hirai, N. Horike, Y. Takashima, H. Uehara, N. Louvain, M. Meilikhov, T. Tsuruoka, S. Isoda, W. Kosaka, O. Sakata, S. Kitagawa, *Science* **2013**, *339*, 193.
[49] S. Krause, F. S. Reuter, S. Ehrling, V. Bon, I. Senkovska, S. Kaskel, E. Brunner, *Chem. Mater.* **2020**, *32*, 4641.
[50] S. Ehrling, H. Miura, I. Senkovska, S. Kaskel, *Trends Chem* **2021**, *3*, 291.
[51] S. Krause, J. D. Evans, V. Bon, I. Senkovska, S. Ehrling, P. Iacomi, D. M. Többens, D. Wallacher, M. S. Weiss, B. Zheng, P. G. Yot, G. Maurin, P. L. Llewellyn, F.-X. Coudert, S. Kaskel, *Chem. Sci.* **2020**, *11*, 9468.
[52] S. Ehrling, I. Senkovska, V. Bon, J. D. Evans, P. Petkov, Y. Krupskaya, V. Kataev, T. Wulf, A. Krylov, A. Vtyurin, S. Krylova, S. Adichtchev, E. Slyusareva, M. S. Weiss, B. Büchner, T. Heine, S. Kaskel, *J. Mater. Chem. A* **2019**, *7*, 21459.

[53] S. Wannapaiboon, A. Schneemann, I. Hante, M. Tu, K. Epp, A. L. Semrau, C. Sternemann, M. Paulus, S. J. Baxter, G. Kieslich, R. A. Fischer, *Nat. Commun.* **2019**, *10*, 346.
[54] V. Van Speybroeck, S. Vandenhaute, A. E. J. Hoffman, S. M. J. Rogge, *Trends Chem* **2021**, *3*, 605.
[55] H. Miura, V. Bon, I. Senkovska, S. Ehrling, N. Bönisch, G. Mäder, S. Grünzner, A. Khadiev, D. Novikov, K. Maity, A. Richter, S. Kaskel, *Adv. Mater.* **2023**, *35*, 2207741.
[56] J. D. Evans, V. Bon, I. Senkovska, H.-C. Lee, S. Kaskel, *Nat. Commun.* **2020**, *11*, 2690.
[57] C. Chang, V. L. Deringer, K. S. Katti, V. Van Speybroeck, C. M. Wolverton, *Nat. Rev. Mater.* **2023**, *8*, 309.
[58] V. Van Speybroeck, *Philos. Trans. R. Soc. Math. Phys. Eng. Sci.* **2023**, *381*, 20220239.
[59] Terminology guidelines and database issues for topology representations in coordination networks, metal-organic frameworks and other crystalline materials, https://iupac.org/project/2014-001-2-200 (accessed: August 2024).
[60] E. G. Meekel, E. M. Schmidt, L. J. Cameron, A. D. Dharma, H. J. Windsor, S. G. Duyker, A. Minelli, T. Pope, G. O. Lepore, B. Slater, C. J. Kepert, A. L. Goodwin, *Science* **2023**, *379*, 357.
[61] E. O. Pyzer-Knapp, J. W. Pitera, P. W. J. Staar, S. Takeda, T. Laino, D. P. Sanders, J. Sexton, J. R. Smith, A. Curioni, *Npj Comput. Mater.* **2022**, *8*, 84.
[62] L. Hanna, J. V. Lockard, *J. Phys. Condens. Matter* **2019**, *31*, 483001.
[63] E. Brunner, M. Rauche, *Chem. Sci.* **2020**, *11*, 4297.
[64] C. Wiktor, M. Meledina, S. Turner, O. I. Lebedev, R. A. Fischer, *J. Mater. Chem. A* **2017**, *5*, 14969.
[65] R. J. Maurer, C. Freysoldt, A. M. Reilly, J. G. Brandenburg, O. T. Hofmann, T. Björkman, S. Lebègue, A. Tkatchenko, *Annu. Rev. Mater. Res.* **2019**, *49*, 1.
[66] G. Férey, C. Serre, C. Mellot-Draznieks, F. Millange, S. Surblé, J. Dutour, I. Margiolaki, *Angew. Chem., Int. Ed.* **2004**, *43*, 6296.
[67] A. Celeste, P. Fertey, J.-P. Itié, G. Blanita, C. Zlotea, F. Capitani, *J. Am. Chem. Soc.* **2024**, *146*, 9155.
[68] J. D. H. Donnay, *Am. Mineral.* **1943**, *28*, 313.
[69] J. D. H. Donnay, H. M. Ondik, U. S. N. B. of Standards, *Crystal Data: Inorganic Compounds*, National Institute of Standards and Technology, Gaithersburg, Maryland, USA **1973**.
[70] M. I. Aroyo, in *International Tables for Crystallography: Space-Group Symmetry* (Ed: M. I. Aroyo), International Union of Crystallography, Chester, England **2016**.
[71] T. D. Bennett, A. K. Cheetham, A. H. Fuchs, F.-X. Coudert, *Nat. Chem.* **2017**, *9*, 11.
[72] A. A. Tiba, A. V. Tivanski, L. R. MacGillivray, *Nano Lett.* **2019**, *19*, 6140.
[73] C. L. Hobday, S. Krause, S. M. J. Rogge, J. D. Evans, H. Bunzen, *Front. Chem.* **2021**, *9*, 772059.
[74] V. Bon, N. Kavoosi, I. Senkovska, S. Kaskel, *ACS Appl. Mater. Interfaces* **2015**, *7*, 22292.
[75] F. Birch, *Phys. Rev.* **1947**, *71*, 809.
[76] F. D. Murnaghan, *Proc. Natl. Acad. Sci* **1944**, *30*, 244.
[77] J. H. Rose, J. R. Smith, J. Ferrante, *Phys. Rev. B* **1983**, *28*, 1835.
[78] P. Vinet, J. Ferrante, J. H. Rose, J. R. Smith, *J. Geophys. Res. Solid Earth* **1987**, *92*, 9319.
[79] D. E. P. Vanpoucke, K. Lejaeghere, V. Van Speybroeck, M. Waroquier, A. Ghysels, *J. Phys. Chem. C* **2015**, *119*, 23752.
[80] V. Guillerm, D. Maspoch, *J. Am. Chem. Soc.* **2019**, *141*, 16517.
[81] I. U. o. Crystallography, *Acta Crystallogr. A* **1999**, *55*, 565.
[82] J. J. Oppenheim, G. Skorupskii, M. Dincă, *Chem. Sci.* **2020**, *11*, 11094.
[83] T. Janssen, A. Janner, *Acta Crystallogr. Sect. B Struct. Sci. Cryst. Eng. Mater.* **2014**, *70*, 617.
[84] C. S. Smith, P. Boucher, *Leonardo* **1987**, *20*, 373.
[85] E. G. Meekel, P. Partridge, R. A. I. Paraoan, J. J. B. Levinsky, B. Slater, C. L. Hobday, A. L. Goodwin, *Nat. Mater.* **2024**, *23*, 1245.
[86] R. Gaillac, P. Pullumbi, T. D. Bennett, F.-X. Coudert, *Chem. Mater.* **2020**, *32*, 8004.
[87] T. D. Bennett, S. Horike, *Nat. Rev. Mater.* **2018**, *3*, 431.
[88] A. F. Sapnik, C. Sun, J. E. M. Laulainen, D. N. Johnstone, R. Brydson, T. Johnson, P. A. Midgley, T. D. Bennett, S. M. Collins, *Commun. Chem.* **2023**, *6*, 92.
[89] T. D. Bennett, A. K. Cheetham, *Acc. Chem. Res.* **2014**, *47*, 1555.
[90] N. Castel, F.-X. Coudert, *J. Phys. Chem. C* **2022**, *126*, 6905.
[91] N. Castel, F.-X. Coudert, *J. Phys. Chem. C* **2022**, *126*, 19532.
[92] D. Frenkel, J. P. McTague, *Annu. Rev. Phys. Chem.* **1980**, *31*, 491.
[93] A. R. Denton, P. A. Egelstaff, *Z. Für Phys. B Condens. Matter* **1997**, *103*, 343.
[94] Frenkel, D., Smit, B., *Understanding Molecular Simulation*, Elsevier, Amsterdam, Netherlands **2002**.
[95] L. R. Pratt, S. W. Haan, *J. Chem. Phys.* **1981**, *74*, 1864.
[96] M. P. Allen, D. J. Tildesley, *Computer Simulation of Liquids*, Oxford University Press, Oxford **2017**.
[97] E. Méndez, R. Semino, *J. Mater. Chem. A* **2024**, *12*, 4572.
[98] K. Pearson, *Lond. Edinb. Dublin Philos. Mag. J. Sci.* **1900**, *50*, 157.
[99] R. L. McGreevy, L. Pusztai, *Mol. Simul.* **1988**, *1*, 359.
[100] T. Proffen, *Z. Für Krist. – Cryst. Mater.* **2000**, *215*, 661.
[101] I. Bechis, A. F. Sapnik, A. Tarzia, E. H. Wolpert, M. A. Addicoat, D. A. Keen, T. D. Bennett, K. E. Jelfs, *Chem. Mater.* **2022**, *34*, 9042.
[102] J. Sauer, *J. Catal.* **2024**, *433*, 115482.
[103] I. Choudhuri, J. Ye, D. G. Truhlar, *Chem. Phys. Rev.* **2023**, *4*, 031304.
[104] J. G. Vitillo, A. Bhan, C. J. Cramer, C. C. Lu, L. Gagliardi, *ACS Catal.* **2019**, *9*, 2870.
[105] J. G. Vitillo, L. Gagliardi, *Inorg. Chem.* **2021**, *60*, 11813.
[106] P. Lyu, G. Maurin, *ACS Appl. Nano Mater.* **2022**, *5*, 17750.
[107] A. Tofoni, F. Tavani, M. Vandone, L. Braglia, E. Borfecchia, P. Ghigna, D. C. Stoian, T. Grell, S. Stolfi, V. Colombo, P. D. Angelo, *J. Am. Chem. Soc.* **2023**, *145*, 21040.
[108] Z. Yu, S. Jamdade, X. Yu, X. Cai, D. S. Sholl, *J. Phys. Chem. Lett.* **2023**, *14*, 6658.
[109] D. S. Sholl, R. P. Lively, *J. Phys. Chem. Lett.* **2015**, *6*, 3437.
[110] X. Feng, H. S. Jena, C. Krishnaraj, K. Leus, G. Wang, H. Chen, C. Jia, P. Van Der Voort, *ACS Appl. Mater. Interfaces* **2021**, *13*, 60715.
[111] H.-Q. Xu, S. Yang, X. Ma, J. Huang, H.-L. Jiang, *ACS Catal.* **2018**, *8*, 11615.
[112] S. Dissegna, K. Epp, W. R. Heinz, G. Kieslich, R. A. Fischer, *Adv. Mater.* **2018**, *30*, 1704501.
[113] A. F. Möslein, L. Donà, B. Civalleri, J.-C. Tan, *ACS Appl. Nano Mater.* **2022**, *5*, 6398.
[114] C. Han, R. J. Verploegh, D. S. Sholl, *J. Phys. Chem. Lett.* **2018**, *9*, 4037.
[115] S. Jamdade, Z. Yu, S. E. Boulfelfel, X. Cai, R. Thyagarajan, H. Fang, D. S. Sholl, *J. Phys. Chem. C* **2024**, *128*, 3975.
[116] K. Cui, S. Nair, D. S. Sholl, J. R. Schmidt, *J. Phys. Chem. Lett.* **2022**, *13*, 6541.
[117] A. F. Voter, in *Radiat. Eff. Solids* (Eds: K. E. Sickafus, E. A. Kotomin, B. P. Uberuaga), Springer Netherlands, Dordrecht **2007**, pp. 1–23.
[118] S. Bhattacharyya, R. Han, W.-G. Kim, Y. Chiang, K. C. Jayachandrababu, J. T. Hungerford, M. R. Dutzer, C. Ma, K. S. Walton, D. S. Sholl, S. Nair, *Chem. Mater.* **2018**, *30*, 4089.
[119] S. M. J. Rogge, S. Borgmans, V. Van Speybroeck, *Matter* **2023**, *6*, 1435.
[120] J. Keupp, R. Schmid, *Adv. Theory Simul.* **2019**, *2*, 1900117.
[121] L. Vanduyfhuys, M. Wahiduzzaman, S. M. J. Rogge, G. Maurin, V. Van Speybroeck, in *Flex. Met. Framew*, (Ed: S. Kitagawa), Royal Society Of Chemistry, London, UK **2024**, pp. 231–303.
[122] B. M. Connolly, M. Aragones-Anglada, J. Gandara-Loe, N. A. Danaf, D. C. Lamb, J. P. Mehta, D. Vulpe, S. Wuttke, J. Silvestre-Albero, P.

Z. Moghadam, A. E. H. Wheatley, D. Fairen-Jimenez, *Nat. Commun.* **2019**, *10*, 2345.
[123] B. M. Connolly, D. G. Madden, A. E. H. Wheatley, D. Fairen-Jimenez, *J. Am. Chem. Soc.* **2020**, *142*, 8541.
[124] T. Tian, J. Velazquez-Garcia, T. D. Bennett, D. Fairen-Jimenez, *J. Mater. Chem. A* **2015**, *3*, 2999.
[125] X. Yu, B. Li, L. Wu, D. Shi, S. Han, *Energy Fuels* **2023**, *37*, 9938.
[126] D. Zacher, R. Schmid, C. Wöll, R. A. Fischer, *Angew. Chem., Int. Ed.* **2011**, *50*, 176.
[127] R. S. Forgan, *Dalton Trans.* **2019**, *48*, 9037.
[128] J. Cousin-Saint-Remi, A.-L. Finoulst, C. Jabbour, G. V. Baron, J. F. M. Denayer, *Microporous Mesoporous Mater.* **2020**, *304*, 109322.
[129] E. Ploetz, H. Engelke, U. Lächelt, S. Wuttke, *Adv. Funct. Mater.* **2020**, *30*, 1909062.
[130] J. H. Donnay, D. Harker, *Am. Mineral. J. Earth Planet. Mater.* **1937**, *22*, 446.
[131] D. Winn, M. F. Doherty, *AIChE J.* **2000**, *46*, 1348.
[132] G. Wulff, *Z. Für Krist. – Cryst. Mater.* **1901**, *34*, 449.
[133] J. E. Jaffe, A. C. Hess, *J. Chem. Phys.* **1996**, *105*, 10983.
[134] L. Zhang, Z. Hu, J. Jiang, *J. Phys. Chem. C* **2012**, *116*, 19268.
[135] S. Amirjalayer, M. Tafipolsky, R. Schmid, *J. Phys. Chem. Lett.* **2014**, *5*, 3206.
[136] J. P. Dürholt, R. Galvelis, R. Schmid, *Dalton Trans.* **2016**, *45*, 4370.
[137] M. J. Thompson, C. L. Hobday, I. Senkovska, V. Bon, S. Ehrling, M. Maliuta, S. Kaskel, T. Düren, *J. Mater. Chem. A* **2020**, *8*, 22703.
[138] R. Semino, J. C. Moreton, N. A. Ramsahye, S. M. Cohen, G. Maurin, *Chem. Sci.* **2018**, *9*, 315.
[139] E. B. Doğan, G. Maurin, M. G. Ahunbay, *J. Phys. Chem. C* **2023**, *127*, 20491.
[140] S. Naskar, D. Fan, A. Ghoufi, G. Maurin, *Chem. Sci.* **2023**, *14*, 10435.
[141] R. Luo, H. Lv, Q. Liao, N. Wang, J. Yang, Y. Li, K. Xi, X. Wu, H. Ju, J. Lei, *Nat. Commun.* **2021**, *12*, 6808.
[142] X. Yu, J. Li, M. Du, X. Song, H. Huang, L. Nie, *Cell Rep. Phys. Sci.* **2023**, *4*, 101657.
[143] S. Zhang, Y. He, S. Liu, Z. Zhang, C. Zhong, *J. Chem. Inf. Model.* **2023**, *63*, 7476.
[144] J. Keupp, R. Schmid, *Faraday Discuss.* **2018**, *211*, 79.
[145] S. Bureekaew, V. Balwani, S. Amirjalayer, R. Schmid, *CrystEngComm* **2015**, *17*, 344.
[146] S. Impeng, R. Cedeno, J. P. Dürholt, R. Schmid, S. Bureekaew, *Cryst. Growth Des.* **2018**, *18*, 2699.
[147] H. C. Gulbalkan, G. O. Aksu, G. Ercakir, S. Keskin, *Ind. Eng. Chem. Res.* **2024**, *63*, 37.
[148] C. E. Wilmer, M. Leaf, C. Y. Lee, O. K. Farha, B. G. Hauser, J. T. Hupp, R. Q. Snurr, *Nat. Chem.* **2012**, *4*, 83.
[149] H. Wu, J. M. Simmons, Y. Liu, C. M. Brown, X. Wang, S. Ma, V. K. Peterson, P. D. Southon, C. J. Kepert, H. Zhou, T. Yildirim, W. Zhou, *Chem. – Eur. J.* **2010**, *16*, 5205.
[150] P. G. Boyd, T. K. Woo, *CrystEngComm* **2016**, *18*, 3777.
[151] D. A. Gomez-Gualdron, O. V. Gutov, V. Krungleviciute, B. Borah, J. E. Mondloch, J. T. Hupp, T. Yildirim, O. K. Farha, R. Q. Snurr, *Chem. Mater.* **2014**, *26*, 5632.
[152] J. S. De Vos, S. Borgmans, P. Van Der Voort, S. M. J. Rogge, V. Van Speybroeck, *J. Mater. Chem. A* **2023**, *11*, 7468.
[153] F. L. Oliveira, P. M. Esteves, *J. Chem. Inf. Model.* **2024**, *64*, 3278.
[154] Y. J. Colón, D. A. Gómez-Gualdrón, R. Q. Snurr, *Cryst. Growth Des.* **2017**, *17*, 5801.
[155] F. Cipcigan, J. Booth, R. N. Barros Ferreira, C. Ribeiro Dos Santos, M. Steiner, *Digit. Discov.* **2024**, *3*, 449.
[156] S. Lee, B. Kim, H. Cho, H. Lee, S. Y. Lee, E. S. Cho, J. Kim, *ACS Appl. Mater. Interfaces* **2021**, *13*, 23647.
[157] R. L. Martin, M. Haranczyk, *Cryst. Growth Des.* **2014**, *14*, 2431.
[158] M. A. Addicoat, D. E. Coupry, T. Heine, *J. Phys. Chem. A* **2014**, *118*, 9607.
[159] Advancing Structural Science | CCDC, https://www.ccdc.cam.ac.uk/ (accessed: June 2024).
[160] ToposPro, https://topospro.com/databases/ (accessed: July 2024).
[161] Materials Project, https://next-gen.materialsproject.org/ (accessed: August 2024).
[162] NOMAD, https://nomad-lab.eu/nomad-lab/ (accessed: July 2024).
[163] Y. G. Chung, E. Haldoupis, B. J. Bucior, M. Haranczyk, S. Lee, K. D. Vogiatzis, S. Ling, M. Milisavljevic, H. Zhang, J. S. Camp, B. Slater, J. I. Siepmann, D. S. Sholl, R. Q. Snurr, **2019**, https://doi.org/10.5281/zenodo.3370144.
[164] A. S. Rosen, S. M. Iyer, D. Ray, Z. Yao, A. Aspuru-Guzik, L. Gagliardi, J. M. Notestein, R. Q. Snurr, *Matter* **2021**, *4*, 1578.
[165] A. S. Rosen, V. Fung, P. Huck, C. T. O'Donnell, M. K. Horton, D. G. Truhlar, K. A. Persson, J. M. Notestein, R. Q. Snurr, *Npj Comput. Mater.* **2022**, *8*, 112.
[166] N. T.-A. n8ta.com, MofDB: A database of MOFs/Xeolites, https://mof.tech.northwestern.edu/ (accessed: June 2024).
[167] J. Burner, J. Luo, A. White, A. Mirmiran, O. Kwon, P. G. Boyd, S. Maley, M. Gibaldi, S. Simrod, V. Ogden, T. K. Woo, *Chem. Mater.* **2023**, *35*, 900.
[168] D. Ongari, A. V. Yakutovich, L. Talirz, B. Smit, *ACS Cent. Sci.* **2019**, *5*, 1663.
[169] D. Ongari, L. Talirz, B. Smit, *ACS Cent. Sci.* **2020**, *6*, 1890.
[170] H. Lyu, Z. Ji, S. Wuttke, O. M. Yaghi, *Chem* **2020**, *6*, 2219.
[171] E. O. Pyzer-Knapp, L. Chen, G. M. Day, A. I. Cooper, *Sci. Adv.* **2021**, *7*, eabi4763.
[172] G. Bell, T. Hey, A. Szalay, *Science* **2009**, *323*, 1297.
[173] P. Z. Moghadam, Y. G. Chung, R. Q. Snurr, *Nat. Energy* **2024**, *9*, 121.
[174] H. C. Gulbalkan, A. Uzun, S. Keskin, *Appl. Phys. Lett.* **2024**, *124*, 200501.
[175] F. Zanca, L. T. Glasby, S. Chong, S. Chen, J. Kim, D. Fairen-Jimenez, B. Monserrat, P. Z. Moghadam, *J. Mater. Chem. C* **2021**, *9*, 13584.
[176] K. M. Jablonka, D. Ongari, S. M. Moosavi, B. Smit, *Chem. Rev.* **2020**, *120*, 8066.
[177] P. Reiser, M. Neubert, A. Eberhard, L. Torresi, C. Zhou, C. Shao, H. Metni, C. Van Hoesel, H. Schopmans, T. Sommer, P. Friederich, *Commun. Mater.* **2022**, *3*, 93.
[178] R. Wang, Y. Zou, C. Zhang, X. Wang, M. Yang, D. Xu, *Microporous Mesoporous Mater.* **2022**, *331*, 111666.
[179] Y.-M. Wang, A. Datar, Z.-X. Xu, L.-C. Lin, *J. Phys. Chem. C* **2024**, *128*, 384.
[180] Y. Lim, B. Kim, J. Kim, *Chem. Mater.* **2024**, *36*, 5465.
[181] X. Zhang, K. M. Jablonka, B. Smit, *Digit. Discov.* **2024**.
[182] K. Liu, Z. Chen, T. Islamoglu, S.-J. Lee, H. Chen, T. Yildirim, O. K. Farha, R. Q. Snurr, *J. Phys. Chem. C* **2024**, *128*, 7435.
[183] Z. Yao, B. Sánchez-Lengeling, N. S. Bobbitt, B. J. Bucior, S. G. H. Kumar, S. P. Collins, T. Burns, T. K. Woo, O. K. Farha, R. Q. Snurr, A. Aspuru-Guzik, *Nat. Mach. Intell.* **2021**, *3*, 76.
[184] H. Park, S. Majumdar, X. Zhang, J. Kim, B. Smit, *Digit. Discov.* **2024**, *3*, 728.
[185] X. Fu, T. Xie, A. S. Rosen, T. S. Jaakkola, J. A. Smith, in *Twelfth Int. Conf. Learn. Represent*, **2024**, https://doi.org/10.48550/arXiv.2310.10732.
[186] K. Cui, J. R. Schmidt, *J. Phys. Chem. C* **2020**, *124*, 10550.
[187] Y.-C. Kao, Y.-M. Wang, J.-Y. Yeh, S.-C. Li, K. C.-W. Wu, L.-C. Lin, Y.-P. Li, *Phys. Chem. Chem. Phys.* **2024**, *26*, 20388.
[188] C. Li, Z. Yu, K. Cui, J. R. Schmidt, D. S. Sholl, R. P. Lively, *J. Phys. Chem. C* **2022**, *126*, 21414.
[189] G. Groenhof, in *Biomol. Simul*, (Eds: L. Monticelli, E. Salonen), Humana Press, Totowa, NJ **2013**, pp. 43–66.
[190] F. Noé, A. Tkatchenko, K.-R. Müller, C. Clementi, *Annu. Rev. Phys. Chem.* **2020**, *71*, 361.

[191] K. Ryczko, S. J. Wetzel, R. G. Melko, I. Tamblyn, *J. Chem. Theory Comput.* **2022**, *18*, 1122.
[192] W. Mi, K. Luo, S. B. Trickey, M. Pavanello, *Chem. Rev.* **2023**, *123*, 12039.
[193] H. Zhang, S. Liu, J. You, C. Liu, S. Zheng, Z. Lu, T. Wang, N. Zheng, B. Shao, *Nat. Comput. Sci.* **2024**, *4*, 210.
[194] S. O. Odoh, C. J. Cramer, D. G. Truhlar, L. Gagliardi, *Chem. Rev.* **2015**, *115*, 6051.
[195] J. L. Mancuso, A. M. Mroz, K. N. Le, C. H. Hendon, *Chem. Rev.* **2020**, *120*, 8641.
[196] P. Hohenberg, W. Kohn, *Phys. Rev.* **1964**, *136*, B864.
[197] W. Kohn, L. J. Sham, *Phys. Rev.* **1965**, *140*, A1133.
[198] M. Bursch, J. Mewes, A. Hansen, S. Grimme, *Angew. Chem., Int. Ed.* **2022**, *61*, e202205735.
[199] J. L. Bao, L. Gagliardi, D. G. Truhlar, *J. Phys. Chem. Lett.* **2018**, *9*, 2353.
[200] J. P. Perdew, A. Zunger, *Phys. Rev. B* **1981**, *23*, 5048.
[201] W. Koch, M. C. Holthausen, *A Chemist's Guide to Density Functional Theory*, Wiley-VCH, Weinheim, Germany **2001**.
[202] R. M. Martin, *Electronic Structure: Basic Theory and Practical Methods*, Cambridge University Press, Cambridge, United Kingdom **2004**.
[203] Libxc, https://libxc.gitlab.io/functionals/ (accessed: July 2024).
[204] S. Lehtola, C. Steigemann, M. J. T. Oliveira, M. A. L. Marques, *SoftwareX* **2018**, *7*, 1.
[205] J. P. Perdew, in *AIP Conf. Proc*, AIP, Antwerp, Belgium, **2001**, pp. 1–20.
[206] J. P. Perdew, K. Burke, M. Ernzerhof, *Phys. Rev. Lett.* **1996**, *77*, 3865.
[207] Y. Zhang, W. Yang, *Phys. Rev. Lett.* **1998**, *80*, 890.
[208] B. Hammer, L. B. Hansen, J. K. Nørskov, *Phys. Rev. B* **1999**, *59*, 7413.
[209] J. P. Perdew, A. Ruzsinszky, G. I. Csonka, O. A. Vydrov, G. E. Scuseria, L. A. Constantin, X. Zhou, K. Burke, *Phys. Rev. Lett.* **2008**, *100*, 136406.
[210] M. Dion, H. Rydberg, E. Schröder, D. C. Langreth, B. I. Lundqvist, *Phys. Rev. Lett.* **2004**, *92*, 246401.
[211] K. Lee, É. D. Murray, L. Kong, B. I. Lundqvist, D. C. Langreth, *Phys. Rev. B* **2010**, *82*, 081101.
[212] P. Verma, D. G. Truhlar, *J. Phys. Chem. Lett.* **2017**, *8*, 380.
[213] P. Verma, D. G. Truhlar, *J. Phys. Chem. C* **2017**, *121*, 7144.
[214] L. Donà, J. G. Brandenburg, I. J. Bush, B. Civalleri, *Faraday Discuss.* **2020**, *224*, 292.
[215] S. F. Boys, F. Bernardi, *Mol. Phys.* **1970**, *19*, 553.
[216] Ł. M. Mentel, E. J. Baerends, *J. Chem. Theory Comput.* **2014**, *10*, 252.
[217] D. Vilela Oliveira, J. Laun, M. F. Peintinger, T. Bredow, *J. Comput. Chem.* **2019**, *40*, 2364.
[218] S. Tosoni, C. Tuma, J. Sauer, B. Civalleri, P. Ugliengo, *J. Chem. Phys.* **2007**, *127*, 154102.
[219] F. Formalik, K. Shi, F. Joodaki, X. Wang, R. Q. Snurr, *Adv. Funct. Mater.* **2024**, *34*, 2308130.
[220] M. D'Amore, B. Civalleri, I. J. Bush, E. Albanese, M. Ferrabone, *J. Phys. Chem. C* **2019**, *123*, 28677.
[221] L. Donà, J. G. Brandenburg, B. Civalleri, *J. Chem. Phys.* **2022**, *156*, 094706.
[222] L. Rummel, P. R. Schreiner, *Angew. Chem., Int. Ed.* **2024**, *63*, e202316364.
[223] P. Melix, T. Heine, *J. Phys. Chem. C* **2020**, *124*, 11985.
[224] S. Grimme, A. Hansen, J. G. Brandenburg, C. Bannwarth, *Chem. Rev.* **2016**, *116*, 5105.
[225] S. Grimme, J. Antony, S. Ehrlich, H. Krieg, *J. Chem. Phys.* **2010**, *132*, 154104.
[226] S. Grimme, S. Ehrlich, L. Goerigk, *J. Comput. Chem.* **2011**, *32*, 1456.
[227] E. Caldeweyher, C. Bannwarth, S. Grimme, *J. Chem. Phys.* **2017**, *147*, 034112.
[228] A. Tkatchenko, M. Scheffler, *Phys. Rev. Lett.* **2009**, *102*, 073005.
[229] A. D. Becke, E. R. Johnson, *J. Chem. Phys.* **2006**, *124*, 014104.
[230] A. D. Becke, E. R. Johnson, *J. Chem. Phys.* **2007**, *127*, 154108.
[231] B. M. Axilrod, E. Teller, *J. Chem. Phys.* **1943**, *11*, 299.
[232] Y. Muto, *Proc. Phys.-Math. Soc. Jpn.* **1943**, *17*, 629.
[233] A. Tkatchenko, R. A. DiStasio, R. Car, M. Scheffler, *Phys. Rev. Lett.* **2012**, *108*, 236402.
[234] A. Ambrosetti, A. M. Reilly, R. A. DiStasio, A. Tkatchenko, *J. Chem. Phys.* **2014**, *140*, 18A508.
[235] D. Dubbeldam, K. S. Walton, T. J. H. Vlugt, S. Calero, *Adv. Theory Simul.* **2019**, *2*, 1900135.
[236] H. A. Lorentz, *Ann. Phys.* **1881**, *248*, 127.
[237] D. Berthelot, *Compte Rendus Académie Sci Paris* **1889**, *126*, 1703.
[238] S. L. Mayo, B. D. Olafson, W. A. Goddard, *J. Phys. Chem.* **1990**, *94*, 8897.
[239] A. K. Rappe, C. J. Casewit, K. S. Colwell, W. A. Goddard, W. M. Skiff, *J. Am. Chem. Soc.* **1992**, *114*, 10024.
[240] M. A. Addicoat, N. Vankova, I. F. Akter, T. Heine, *J. Chem. Theory Comput.* **2014**, *10*, 880.
[241] D. E. Coupry, M. A. Addicoat, T. Heine, *J. Chem. Theory Comput.* **2016**, *12*, 5215.
[242] Y. Yang, I. A. Ibikunle, D. F. Sava Gallis, D. S. Sholl, *ACS Appl. Mater. Interfaces* **2022**, *14*, 54101.
[243] S. Bureekaew, S. Amirjalayer, M. Tafipolsky, C. Spickermann, T. K. Roy, R. Schmid, *Phys. Status Solidi B* **2013**, *250*, 1128.
[244] L. Vanduyfhuys, S. Vandenbrande, T. Verstraelen, R. Schmid, M. Waroquier, V. Van Speybroeck, *J. Comput. Chem.* **2015**, *36*, 1015.
[245] L. Vanduyfhuys, S. Vandenbrande, J. Wieme, M. Waroquier, T. Verstraelen, V. Van Speybroeck, *J. Comput. Chem.* **2018**, *39*, 999.
[246] J. K. Bristow, D. Tiana, A. Walsh, *J. Chem. Theory Comput.* **2014**, *10*, 4644.
[247] T. Weng, J. R. Schmidt, *J. Phys. Chem. A* **2019**, *123*, 3000.
[248] J. K. Bristow, J. M. Skelton, K. L. Svane, A. Walsh, J. D. Gale, *Phys. Chem. Chem. Phys.* **2016**, *18*, 29316.
[249] T. M. Becker, J. Heinen, D. Dubbeldam, L.-C. Lin, T. J. H. Vlugt, *J. Phys. Chem. C* **2017**, *121*, 4659.
[250] A. C. T. Van Duin, S. Dasgupta, F. Lorant, W. A. Goddard, *J. Phys. Chem. A* **2001**, *105*, 9396.
[251] A. C. T. Van Duin, B. V. Merinov, S. S. Han, C. O. Dorso, W. A. Goddard, *J. Phys. Chem. A* **2008**, *112*, 11414.
[252] A. C. T. Van Duin, V. S. Bryantsev, M. S. Diallo, W. A. Goddard, O. Rahaman, D. J. Doren, D. Raymand, K. Hermansson, *J. Phys. Chem. A* **2010**, *114*, 9507.
[253] T. P. Senftle, S. Hong, M. M. Islam, S. B. Kylasa, Y. Zheng, Y. K. Shin, C. Junkermeier, R. Engel-Herbert, M. J. Janik, H. M. Aktulga, T. Verstraelen, A. Grama, A. C. T. Van Duin, *Npj Comput. Mater.* **2016**, *2*, 15011.
[254] D. Furman, D. J. Wales, *J. Phys. Chem. Lett.* **2019**, *10*, 7215.
[255] D. Furman, D. J. Wales, *J. Chem. Phys.* **2020**, *153*, 021102.
[256] R. Drautz, *Phys. Rev. B* **2019**, *99*, 014104.
[257] V. L. Deringer, M. A. Caro, G. Csányi, *Adv. Mater.* **2019**, *31*, 1902765.
[258] Y. Zuo, C. Chen, X. Li, Z. Deng, Y. Chen, J. Behler, G. Csányi, A. V. Shapeev, A. P. Thompson, M. A. Wood, S. P. Ong, *J. Phys. Chem. A* **2020**, *124*, 731.
[259] M. Crippa, A. Cardellini, M. Cioni, G. Csányi, G. M. Pavan, *Mach. Learn. Sci. Technol.* **2023**, *4*, 045044.
[260] S. Wieser, E. Zojer, *Npj Comput. Mater.* **2024**, *10*, 18.
[261] T. B. Blank, S. D. Brown, A. W. Calhoun, D. J. Doren, *J. Chem. Phys.* **1995**, *103*, 4129.
[262] J. Behler, M. Parrinello, *Phys. Rev. Lett.* **2007**, *98*, 146401.
[263] J. Behler, G. Csányi, *Eur. Phys. J. B* **2021**, *94*, 142.
[264] O. T. Unke, M. Meuwly, *J. Chem. Theory Comput.* **2019**, *15*, 3678.
[265] R. F. W. Bader, *Atoms in Molecules: A Quantum Theory*, Clarendon Press, New York **1994**.
[266] F. L. Hirshfeld, *Theor. Chim. Acta* **1977**, *44*, 129.

[267] P. Bultinck, C. Van Alsenoy, P. W. Ayers, R. Carbó-Dorca, *J. Chem. Phys.* **2007**, *126*, 144111.
[268] N. G. Limas, T. A. Manz, *RSC Adv.* **2018**, *8*, 2678.
[269] T. Verstraelen, S. Vandenbrande, F. Heidar-Zadeh, L. Vanduyfhuys, V. Van Speybroeck, M. Waroquier, P. W. Ayers, *J. Chem. Theory Comput.* **2016**, *12*, 3894.
[270] N. Marzari, A. A. Mostofi, J. R. Yates, I. Souza, D. Vanderbilt, *Rev. Mod. Phys.* **2012**, *84*, 1419.
[271] A. Gao, R. C. Remsing, *Nat. Commun.* **2022**, *13*, 1572.
[272] J. Gilmer, S. S. Schoenholz, P. F. Riley, O. Vinyals, G. E. Dahl, **2017**, https://doi.org/10.48550/arXiv.1704.01212.
[273] A. Grisafi, M. Ceriotti, *J. Chem. Phys.* **2019**, *151*, 204105.
[274] D. M. Anstine, O. Isayev, *J. Phys. Chem. A* **2023**, *127*, 2417.
[275] D. Anstine, R. Zubatyuk, O. Isayev, **2024**, https://doi.org/10.26434/chemrxiv-2023-296ch-v2.
[276] K. T. Schütt, H. E. Sauceda, P.-J. Kindermans, A. Tkatchenko, K.-R. Müller, *J. Chem. Phys.* **2018**, *148*, 241722.
[277] M. Haghighatlari, J. Li, X. Guan, O. Zhang, A. Das, C. J. Stein, F. Heidar-Zadeh, M. Liu, M. Head-Gordon, L. Bertels, H. Hao, I. Leven, T. Head-Gordon, **2021**, https://doi.org/10.48550/arXiv.2108.02913.
[278] S. Batzner, A. Musaelian, L. Sun, M. Geiger, J. P. Mailoa, M. Kornbluth, N. Molinari, T. E. Smidt, B. Kozinsky, *Nat. Commun.* **2022**, *13*, 2453.
[279] I. Batatia, S. Batzner, D. P. Kovács, A. Musaelian, G. N. C. Simm, R. Drautz, C. Ortner, B. Kozinsky, G. Csányi, **2022**, https://doi.org/10.48550/arXiv.2205.06643.
[280] I. Batatia, D. P. Kovács, G. N. C. Simm, C. Ortner, G. Csányi, **2022**, https://doi.org/10.48550/arXiv.2206.07697.
[281] E. Kocer, T. W. Ko, J. Behler, *Annu. Rev. Phys. Chem.* **2022**, *73*, 163.
[282] I. Batatia, P. Benner, Y. Chiang, A. M. Elena, D. P. Kovács, J. Riebesell, X. R. Advincula, M. Asta, M. Avaylon, W. J. Baldwin, F. Berger, N. Bernstein, A. Bhowmik, S. M. Blau, V. Cărare, J. P. Darby, S. De, F. Della Pia, V. L. Deringer, R. Elijošius, Z. El-Machachi, F. Falcioni, E. Fako, A. C. Ferrari, A. Genreith-Schriever, J. George, R. E. A. Goodall, C. P. Grey, P. Grigorev, S. Han, et al., **2024**, https://doi.org/10.48550/arXiv.2401.00096.
[283] A. Jain, S. P. Ong, G. Hautier, W. Chen, W. D. Richards, S. Dacek, S. Cholia, D. Gunter, D. Skinner, G. Ceder, K. A. Persson, *APL Mater.* **2013**, *1*, 011002.
[284] R. Ramakrishnan, P. O. Dral, M. Rupp, O. A. Von Lilienfeld, *J. Chem. Theory Comput.* **2015**, *11*, 2087.
[285] M. Bogojeski, L. Vogt-Maranto, M. E. Tuckerman, K.-R. Müller, K. Burke, *Nat. Commun.* **2020**, *11*, 5223.
[286] B. Herzog, A. Gallo, F. Hummel, M. Badawi, T. Bučko, S. Lebègue, A. Grüneis, D. Rocca, *Npj Comput. Mater.* **2024**, *10*, 68.
[287] R. Ma, Y. J. Colón, T. Luo, *ACS Appl. Mater. Interfaces* **2020**, *12*, 34041.
[288] S. Vandenhaute, T. Braeckevelt, P. Dobbelaere, M. Bocus, V. Van Speybroeck, **2024**, https://doi.org/10.48550/arXiv.2404.03777.
[289] L. Sarkisov, R. L. Martin, M. Haranczyk, B. Smit, *J. Am. Chem. Soc.* **2014**, *136*, 2228.
[290] S. S.-Y. Chui, S. M.-F. Lo, J. P. H. Charmant, A. G. Orpen, I. D. Williams, *Science* **1999**, *283*, 1148.
[291] R. Semino, J. P. Dürholt, R. Schmid, G. Maurin, *J. Phys. Chem. C* **2017**, *121*, 21491.
[292] S. M. J. Rogge, *Faraday Discuss.* **2021**, *225*, 271.
[293] J. Vandewalle, J. S. De Vos, S. M. J. Rogge, *J. Phys. Chem. C* **2023**, *127*, 6060.
[294] W. G. Noid, J.-W. Chu, G. S. Ayton, V. Krishna, S. Izvekov, G. A. Voth, A. Das, H. C. Andersen, *J. Chem. Phys.* **2008**, *128*, 244114.
[295] J. Wang, S. Olsson, C. Wehmeyer, A. Pérez, N. E. Charron, G. De Fabritiis, F. Noé, C. Clementi, *ACS Cent. Sci.* **2019**, *5*, 755.
[296] J. Gasteiger, M. Shuaibi, A. Sriram, S. Günnemann, Z. Ulissi, C. L. Zitnick, A. Das, **2022**, https://doi.org/10.48550/arXiv.2204.02782.
[297] J. Sohl-Dickstein, E. A. Weiss, N. Maheswaranathan, S. Ganguli, **2015**, https://doi.org/10.48550/arXiv.1503.03585.
[298] M. E. Tuckerman, *Statistical Mechanics: Theory and Molecular Simulation*, Oxford University Press, Oxford **2023**.
[299] K. L. Svane, J. K. Bristow, A. Walsh, *J. Phys. Chem. C* **2017**, *121*, 22010.
[300] S. K. Elsaidi, M. H. Mohamed, D. Banerjee, P. K. Thallapally, *Coord. Chem. Rev.* **2018**, *358*, 125.
[301] T. Kamencek, N. Bedoya-Martínez, E. Zojer, *Phys. Rev. Mater.* **2019**, *3*, 116003.
[302] F. Formalik, M. Fischer, B. Kuchta, *Cryst. Growth Des.* **2023**, *23*, 8962.
[303] A. E. J. Hoffman, I. Senkovska, L. Abylgazina, V. Bon, V. Grzimek, A. M. Dominic, M. Russina, M. A. Kraft, I. Weidinger, W. G. Zeier, V. Van Speybroeck, S. Kaskel, *J. Mater. Chem. A* **2023**, *11*, 15286.
[304] A. E. J. Hoffman, L. Vanduyfhuys, I. Nevjestić, J. Wieme, S. M. J. Rogge, H. Depauw, P. Van Der Voort, H. Vrielinck, V. Van Speybroeck, *J. Phys. Chem. C* **2018**, *122*, 2734.
[305] A. E. J. Hoffman, J. Wieme, S. M. J. Rogge, L. Vanduyfhuys, V. Van Speybroeck, *Z. Für Krist. – Cryst. Mater.* **2019**, *234*, 529.
[306] F. Formalik, M. Fischer, J. Rogacka, L. Firlej, B. Kuchta, *Microporous Mesoporous Mater.* **2020**, *304*, 109132.
[307] T. W. Kim, S. Jun, Y. Ha, R. K. Yadav, A. Kumar, C.-Y. Yoo, I. Oh, H.-K. Lim, J. W. Shin, R. Ryoo, H. Kim, J. Kim, J.-O. Baeg, H. Ihee, *Nat. Commun.* **2019**, *10*, 1873.
[308] A. Fu, G. Yi, Y. Li, *J. Phys. Chem. C* **2022**, *126*, 20127.
[309] R. B. Leighton, *Rev. Mod. Phys.* **1948**, *20*, 165.
[310] A. B. Andreeva, K. N. Le, L. Chen, M. E. Kellman, C. H. Hendon, C. K. Brozek, *J. Am. Chem. Soc.* **2020**, *142*, 19291.
[311] M. T. Dove, *Introduction to Lattice Dynamics*, Cambridge University Press, Cambridge, MA **1993**.
[312] M. R. Ryder, J. Maul, B. Civalleri, A. Erba, *Adv. Theory Simul.* **2019**, *2*, 1900093.
[313] S. Baroni, S. De Gironcoli, A. Dal Corso, P. Giannozzi, *Rev. Mod. Phys.* **2001**, *73*, 515.
[314] A. Beste, *Chem. Phys. Lett.* **2010**, *493*, 200.
[315] J. M. Bowman, *Acc. Chem. Res.* **1986**, *19*, 202.
[316] R. B. Gerber, M. A. Ratner, in *Adv. Chem. Phys*, (Eds: I. Prigogine, S. A. Rice), Wiley, Hoboken, NJ **1988**, pp. 97–132.
[317] C. Møller, M. S. Plesset, *Phys. Rev.* **1934**, *46*, 618.
[318] L. S. Norris, M. A. Ratner, A. E. Roitberg, R. B. Gerber, *J. Chem. Phys.* **1996**, *105*, 11261.
[319] O. Christiansen, *J. Chem. Phys.* **2003**, *119*, 5773.
[320] A. Erba, J. Maul, M. Ferrabone, R. Dovesi, M. Rérat, P. Carbonnière, *J. Chem. Theory Comput.* **2019**, *15*, 3766.
[321] O. Christiansen, *J. Chem. Phys.* **2004**, *120*, 2140.
[322] N. Bedoya-Martínez, A. Giunchi, T. Salzillo, E. Venuti, R. G. Della Valle, E. Zojer, *J. Chem. Theory Comput.* **2018**, *14*, 4380.
[323] B. Kuchta, F. Formalik, J. Rogacka, A. V. Neimark, L. Firlej, *Z. Für Krist. – Cryst. Mater.* **2019**, *234*, 513.
[324] I. Romero-Muñiz, C. Romero-Muñiz, I. Del Castillo-Velilla, C. Marini, S. Calero, F. Zamora, A. E. Platero-Prats, *ACS Appl. Mater. Interfaces* **2022**, *14*, 27040.
[325] A. E. J. Hoffman, W. Temmerman, E. Campbell, A. A. Damin, I. Lezcano-Gonzalez, A. M. Beale, S. Bordiga, J. Hofkens, V. Van Speybroeck, *J. Chem. Theory Comput.* **2024**, *20*, 513.
[326] A. E. J. Hoffman, I. Senkovska, J. Wieme, A. Krylov, S. Kaskel, V. Van Speybroeck, *J. Mater. Chem. A* **2022**, *10*, 17254.
[327] A. Lamaire, J. Wieme, S. M. J. Rogge, M. Waroquier, V. Van Speybroeck, *J. Chem. Phys.* **2019**, *150*, 094503.
[328] M. Ceriotti, M. Parrinello, T. E. Markland, D. E. Manolopoulos, *J. Chem. Phys.* **2010**, *133*, 124104.
[329] S. Habershon, D. E. Manolopoulos, T. E. Markland, T. F. Miller, *Annu. Rev. Phys. Chem.* **2013**, *64*, 387.
[330] J. R. Cendagorta, H. Shen, Z. Bačić, M. E. Tuckerman, *Adv. Theory Simul.* **2021**, *4*, 2000258.

[331] M. Rossi, *J. Chem. Phys.* **2021**, *154*, 170902.
[332] A. Lamaire, M. Cools-Ceuppens, M. Bocus, T. Verstraelen, V. Van Speybroeck, *J. Chem. Theory Comput.* **2023**, *19*, 18.
[333] M. Bocus, R. Goeminne, A. Lamaire, M. Cools-Ceuppens, T. Verstraelen, V. Van Speybroeck, *Nat. Commun.* **2023**, *14*, 1008.
[334] F.-X. Coudert, M. Jeffroy, A. H. Fuchs, A. Boutin, C. Mellot-Draznieks, *J. Am. Chem. Soc.* **2008**, *130*, 14294.
[335] A. Hardiagon, F.-X. Coudert, *Acc. Chem. Res.* **2024**, *57*, 1620.
[336] M. Witman, S. Ling, S. Jawahery, P. G. Boyd, M. Haranczyk, B. Slater, B. Smit, Elsevier, Amsterdam, Netherlands, *J. Am. Chem. Soc* **2017**, *139*, 5547.
[337] M. Witman, N. A. Mahynski, B. Smit, *J. Chem. Theory Comput.* **2018**, *14*, 6149.
[338] A. Datar, M. Witman, L.-C. Lin, *J. Phys. Chem. C* **2021**, *125*, 4253.
[339] M. Mehta, D. A. Kofke, *Chem. Eng. Sci.* **1994**, *49*, 2633.
[340] B. J. Banaszak, R. Faller, J. J. De Pablo, *J. Chem. Phys.* **2004**, *120*, 11304.
[341] A. Ghoufi, G. Maurin, *J. Phys. Chem. C* **2010**, *114*, 6496.
[342] S. M. J. Rogge, R. Goeminne, R. Demuynck, J. J. Gutiérrez-Sevillano, S. Vandenbrande, L. Vanduyfhuys, M. Waroquier, T. Verstraelen, V. Van Speybroeck, *Adv. Theory Simul.* **2019**, *2*, 1800177.
[343] R. Goeminne, S. Krause, S. Kaskel, T. Verstraelen, J. D. Evans, *J. Am. Chem. Soc.* **2021**, *143*, 4143.
[344] A. P. J. Jansen, *An Introduction to Kinetic Monte Carlo Simulations of Surface Reactions*, Springer Berlin Heidelberg, Berlin, Heidelberg **2012**.
[345] M. Andersen, C. Panosetti, K. Reuter, *Front. Chem.* **2019**, *7*, 202.
[346] T.-H. T. Le, D. Ferro-Costas, A. Fernández-Ramos, M. A. Ortuño, *J. Phys. Chem. C* **2024**, *128*, 1049.
[347] J.-H. Guo, X.-D. Li, H.-Y. Liu, S.-J. Li, G. Chen, *J. Phys. Chem. C* **2019**, *123*, 15935.
[348] H. Li, A. D. Chavez, H. Li, H. Li, W. R. Dichtel, J.-L. Bredas, *J. Am. Chem. Soc.* **2017**, *139*, 16310.
[349] I. Castano, A. M. Evans, H. Li, E. Vitaku, M. J. Strauss, J.-L. Brédas, N. C. Gianneschi, W. R. Dichtel, *ACS Cent. Sci.* **2019**, *5*, 1892.
[350] B. T. Koo, P. G. Berard, P. Clancy, *J. Chem. Theory Comput.* **2015**, *11*, 1172.
[351] J. Guo, X.-L. Cheng, S.-J. Li, G. Chen, *J. Phys. Chem. C* **2016**, *120*, 17153.
[352] V. Van Speybroeck, M. Bocus, P. Cnudde, L. Vanduyfhuys, *ACS Catal.* **2023**, *13*, 11455.
[353] L. Bonati, E. Trizio, A. Rizzi, M. Parrinello, *J. Chem. Phys.* **2023**, *159*, 014801.
[354] G. M. Torrie, J. P. Valleau, *Chem. Phys. Lett.* **1974**, *28*, 578.
[355] G. M. Torrie, J. P. Valleau, *J. Comput. Phys.* **1977**, *23*, 187.
[356] A. Laio, M. Parrinello, *Proc. Natl. Acad. Sci.* **2002**, *99*, 12562.
[357] W. K. Den Otter, *J. Chem. Phys.* **2000**, *112*, 7283.
[358] O. Valsson, M. Parrinello, *Phys. Rev. Lett.* **2014**, *113*, 090601.
[359] R. Demuynck, S. M. J. Rogge, L. Vanduyfhuys, J. Wieme, M. Waroquier, V. Van Speybroeck, *J. Chem. Theory Comput.* **2017**, *13*, 5861.
[360] N. Leventis, S. B. Hanna, C. Sotiriou-Leventis, *J. Chem. Educ.* **1997**, *74*, 813.
[361] R. Demuynck, J. Wieme, S. M. J. Rogge, K. D. Dedecker, L. Vanduyfhuys, M. Waroquier, V. Van Speybroeck, *J. Chem. Theory Comput.* **2018**, *14*, 5511.
[362] C. J. Geyer, E. A. Thompson, *J. R. Stat. Soc. Ser. B Stat. Methodol.* **1992**, *54*, 657.
[363] R. H. Swendsen, J.-S. Wang, *Phys. Rev. Lett.* **1986**, *57*, 2607.
[364] E. Marinari, G. Parisi, *Europhys. Lett. EPL* **1992**, *19*, 451.
[365] A. P. Lyubartsev, A. A. Martsinovski, S. V. Shevkunov, P. N. Vorontsov-Velyaminov, *J. Chem. Phys.* **1992**, *96*, 1776.
[366] Q. Liao, in *Prog. Mol. Biol. Transl. Sci*, Elsevier, Amsterdam, Netherlands **2020**, pp. 177–213.
[367] J. Hénin, T. Lelièvre, M. R. Shirts, O. Valsson, L. Delemotte, *Living J. Comput. Mol. Sci.* **2022**, *4*, 1583.
[368] G. Piccini, M.-S. Lee, S. F. Yuk, D. Zhang, G. Collinge, L. Kollias, M.-T. Nguyen, V.-A. Glezakou, R. Rousseau, *Catal. Sci. Technol.* **2022**, *12*, 12.
[369] K. Stracke, J. D. Evans, *Nanoscale* **2024**, *16*, 9186.
[370] WHAM – Grossfield Lab, (accessed: May 2024).
[371] J. Kästner, W. Thiel, *J. Chem. Phys.* **2006**, *124*, 234106.
[372] S. Borgmans, S. M. J. Rogge, L. Vanduyfhuys, V. Van Speybroeck, *J. Chem. Theory Comput.* **2023**, *19*, 9032.
[373] S. Borgmans, SanderBorgmans/OGRe, https://github.com/SanderBorgmans/OGRe (accessed: July 2024).
[374] ThermoLIB | Center for Molecular Modeling, https://molmod.ugent.be/software/thermolib (accessed: August 2024).
[375] J. Maul, M. R. Ryder, M. T. Ruggiero, A. Erba, *Phys. Rev. B* **2019**, *99*, 014102.
[376] P. Iacomi, G. Maurin, *ACS Appl. Mater. Interfaces* **2021**, *13*, 50602.
[377] P. Vervoorts, J. Stebani, A. S. J. Méndez, G. Kieslich, *ACS Mater. Lett.* **2021**, *3*, 1635.
[378] B. Wang, P. Ying, J. Zhang, *J. Phys. Chem. C* **2023**, *127*, 2533.
[379] J. W. Jaeken, S. Cottenier, *Comput. Phys. Commun.* **2016**, *207*, 445.
[380] S. M. J. Rogge, M. Waroquier, V. Van Speybroeck, *Acc. Chem. Res.* **2018**.
[381] P. Z. Moghadam, S. M. J. Rogge, A. Li, C.-M. Chow, J. Wieme, N. Moharrami, M. Aragones-Anglada, G. Conduit, D. A. Gomez-Gualdron, V. Van Speybroeck, D. Fairen-Jimenez, *Matter* **2019**, *1*, 219.
[382] J. Wieme, L. Vanduyfhuys, S. M. J. Rogge, M. Waroquier, V. Van Speybroeck, *J. Phys. Chem. C* **2016**, *120*, 14934.
[383] J. F. Nye, *Physical Properties of Crystals: Their Representation by Tensors and Matrices*, Clarendon Press, Oxford **1990**.
[384] S. M. J. Rogge, in *Mech. Behav. Met. – Org. Framew. Mater* (Ed: J.-C. Tan), The Royal Society of Chemistry, London, United Kingdom **2023**, pp. 113–204.
[385] F. Colmenero, *Phys. Chem. Chem. Phys.* **2021**, *23*, 8508.
[386] D. Fan, S. Naskar, G. Maurin, *Nat. Commun.* **2024**, *15*, 3251.
[387] M. R. Ryder, B. Civalleri, G. Cinque, J.-C. Tan, *CrystEngComm* **2016**, *18*, 4303.
[388] P. Serra-Crespo, A. Dikhtiarenko, E. Stavitski, J. Juan-Alcañiz, F. Kapteijn, F.-X. Coudert, J. Gascon, *CrystEngComm* **2015**, *17*, 276.
[389] M. R. Ryder, B. Civalleri, J.-C. Tan, *Phys. Chem. Chem. Phys.* **2016**, *18*, 9079.
[390] M. R. Ryder, J.-C. Tan, *Dalton Trans.* **2016**, *45*, 4154.
[391] J.-C. Tan, B. Civalleri, A. Erba, E. Albanese, *CrystEngComm* **2015**, *17*, 375.
[392] F. Colmenero, V. Timón, *Appl. Sci.* **2022**, *12*, 10413.
[393] E. Jin, I. S. Lee, D. Kim, H. Lee, W.-D. Jang, M. S. Lah, S. K. Min, W. Choe, *Sci. Adv.* **2019**, *5*, eaav4119.
[394] F.-X. Coudert, J. D. Evans, *Coord. Chem. Rev.* **2019**, *388*, 48.
[395] B. Garai, V. Bon, A. Efimova, M. Gerlach, I. Senkovska, S. Kaskel, *J. Mater. Chem. A* **2020**, *8*, 20420.
[396] A. Giri, A. M. Evans, M. A. Rahman, A. J. H. McGaughey, P. E. Hopkins, *ACS Nano* **2022**, *16*, 2843.
[397] S. Thakur, A. Giri, *Mater. Horiz.* **2023**, *10*, 5484.
[398] S. Krause, N. Hosono, S. Kitagawa, *Angew. Chem., Int. Ed.* **2020**, *59*, 15325.
[399] Z. Chen, C.-H. Ho, X. Wang, S. M. Vornholt, T. M. Rayder, T. Islamoglu, O. K. Farha, F. Paesani, K. W. Chapman, *ACS Mater. Lett.* **2023**, *5*, 2942.
[400] S. Krause, J. D. Evans, V. Bon, I. Senkovska, P. Iacomi, F. Kolbe, S. Ehrling, E. Troschke, J. Getzschmann, D. M. Többens, A. Franz, D. Wallacher, P. G. Yot, G. Maurin, E. Brunner, P. L. Llewellyn, F.-X. Coudert, S. Kaskel, *Nat. Commun.* **2019**, *10*, 3632.
[401] J. D. Evans, F.-X. Coudert, *Acc. Mater. Res.* **2024**, *5*, 640.

[402] R. Goeminne, L. Vanduyfhuys, V. Van Speybroeck, T. Verstraelen, *J. Chem. Theory Comput.* **2023**, *19*, 6313.
[403] F. Auras, L. Ascherl, V. Bon, S. M. Vornholt, S. Krause, M. Döblinger, D. Bessinger, S. Reuter, K. W. Chapman, S. Kaskel, R. H. Friend, T. Bein, *Nat. Chem.* **2024**, *16*, 1373.
[404] C. Zhao, C. S. Diercks, C. Zhu, N. Hanikel, X. Pei, O. M. Yaghi, *J. Am. Chem. Soc.* **2018**, *140*, 16438.
[405] G. O. Aksu, H. Daglar, C. Altintas, S. Keskin, *J. Phys. Chem. C* **2020**, *124*, 22577.
[406] C. Zhao, L. Sun, Y. Ai, W. Liu, *J. Clean. Prod.* **2022**, *338*, 130566.
[407] D. Dubbeldam, K. S. Walton, D. E. Ellis, R. Q. Snurr, *Angew. Chem., Int. Ed.* **2007**, *46*, 4496.
[408] N. Lock, Y. Wu, M. Christensen, L. J. Cameron, V. K. Peterson, A. J. Bridgeman, C. J. Kepert, B. B. Iversen, *J. Phys. Chem. C* **2010**, *114*, 16181.
[409] J. D. Evans, J. P. Dürholt, S. Kaskel, R. Schmid, *J. Mater. Chem. A* **2019**, *7*, 24019.
[410] M. J. Cliffe, J. A. Hill, C. A. Murray, F.-X. Coudert, A. L. Goodwin, *Phys. Chem. Chem. Phys.* **2015**, *17*, 11586.
[411] R. Mittal, M. K. Gupta, S. L. Chaplot, *Prog. Mater. Sci.* **2018**, *92*, 360.
[412] C. S. Coates, A. L. Goodwin, *Mater. Horiz.* **2019**, *6*, 211.
[413] J. Lee, M. Kim, D. Lee, H. Ahn, M. Kim, C. Lee, *AIChE J.* **2008**, *54*, 2054.
[414] J. Wieme, S. Vandenbrande, A. Lamaire, V. Kapil, L. Vanduyfhuys, V. Van Speybroeck, *ACS Appl. Mater. Interfaces* **2019**, *11*, 38697.
[415] P. K. Schelling, S. R. Phillpot, P. Keblinski, *Phys. Rev. B* **2002**, *65*, 144306.
[416] A. J. H. McGaughey, M. Kaviany, in *Adv. Heat Transf*, Elsevier, Amsterdam, Netherlands **2006**, pp. 169–255.
[417] S. Wieser, T. Kamencek, J. P. Dürholt, R. Schmid, N. Bedoya-Martínez, E. Zojer, *Adv. Theory Simul.* **2021**, *4*, 2000211.
[418] H. Babaei, M. E. DeCoster, M. Jeong, Z. M. Hassan, T. Islamoglu, H. Baumgart, A. J. H. McGaughey, E. Redel, O. K. Farha, P. E. Hopkins, J. A. Malen, C. E. Wilmer, *Nat. Commun.* **2020**, *11*, 4010.
[419] M. S. Green, *J. Chem. Phys.* **1954**, *22*, 398.
[420] R. Kubo, *J. Phys. Soc. Jpn.* **1957**, *12*, 570.
[421] S. Yamaguchi, I. Tsunekawa, M. Furuta, C. Anilkumar, Y. Liao, T. Shiga, T. Kodama, J. Shiomi, *J. Phys. Chem. Lett.* **2024**, *15*, 6628.
[422] F. Müller-Plathe, *J. Chem. Phys.* **1997**, *106*, 6082.
[423] K. B. Sezginel, S. Lee, H. Babaei, C. E. Wilmer, *J. Phys. Chem. C* **2020**, *124*, 18604.
[424] R. Cheng, W. Wei, J. Zhang, S. Li, *J. Phys. Chem. B* **2023**, *127*, 9390.
[425] J. Kwon, H. Ma, A. Giri, P. E. Hopkins, N. B. Shustova, Z. Tian, *ACS Nano* **2023**, *17*, 15222.
[426] M. A. Rahman, S. Thakur, P. E. Hopkins, A. Giri, *J. Phys. Chem. C* **2023**, *127*, 11157.
[427] J.-L. Bredas, *Mater. Horiz.* **2014**, *1*, 17.
[428] M. R. Ryder, L. Donà, J. G. Vitillo, B. Civalleri, *ChemPlusChem* **2018**, *83*, 308.
[429] F. Liu, Y. He, X. Liu, Z. Wang, H.-L. Liu, X. Zhu, C.-C. Hou, Y. Weng, Q. Zhang, Y. Chen, *ACS Catal.* **2022**, *12*, 9494.
[430] K. Fabrizio, K. N. Le, A. B. Andreeva, C. H. Hendon, C. K. Brozek, *ACS Mater. Lett.* **2022**, *4*, 457.
[431] J. Tauc, *Mater. Res. Bull.* **1968**, *3*, 37.
[432] T. M. Mok, S. K. O'Leary, *J. Appl. Phys.* **2007**, *102*, 113525.
[433] J. Heyd, G. E. Scuseria, M. Ernzerhof, *J. Chem. Phys.* **2003**, *118*, 8207.
[434] H. Yu, D. Wang, *JACS Au* **2022**, *2*, 1848.
[435] M. R. Slot, T. S. Gardenier, P. H. Jacobse, G. C. P. Van Miert, S. N. Kempkes, S. J. M. Zevenhuizen, C. M. Smith, D. Vanmaekelbergh, I. Swart, *Nat. Phys.* **2017**, *13*, 672.
[436] B. Cui, X. Zheng, J. Wang, D. Liu, S. Xie, B. Huang, *Nat. Commun.* **2020**, *11*, 66.
[437] M. S. Hybertsen, S. G. Louie, *Phys. Rev. B* **1986**, *34*, 5390.
[438] S. Albrecht, L. Reining, R. Del Sole, G. Onida, *Phys. Rev. Lett.* **1998**, *80*, 4510.
[439] S. Latini, T. Olsen, K. S. Thygesen, *Phys. Rev. B* **2015**, *92*, 245123.
[440] A. R. Kshirsagar, X. Blase, C. Attaccalite, R. Poloni, *J. Phys. Chem. Lett.* **2021**, *12*, 4045.
[441] S. Ling, B. Slater, *J. Phys. Chem. C* **2015**, *119*, 16667.
[442] R. Aniruddha, I. Sreedhar, B. M. Reddy, *J. CO2 Util.* **2020**, *42*, 101297.
[443] S. Mahajan, M. Lahtinen, *J. Environ. Chem. Eng.* **2022**, *10*, 108930.
[444] A. Boretti, L. Rosa, *Npj Clean Water* **2019**, *2*, 15.
[445] W. Xu, O. M. Yaghi, *ACS Cent. Sci.* **2020**, *6*, 1348.
[446] K. C. Christoforidis, P. Fornasiero, *ChemCatChem* **2017**, *9*, 1523.
[447] H. Gröger, A. Allahverdiyev, J. Yang, J. Stiehm, *Adv. Funct. Mater.* **2024**, *34*, 2304794.
[448] J. Liang, K. Liang, *Adv. Funct. Mater.* **2020**, *30*, 2001648.
[449] B. Li, M. Ashrafizadeh, T. Jiao, *Int. J. Biol. Macromol.* **2024**, *260*, 129391.
[450] J. Liang, K. Liang, *Coord. Chem. Rev.* **2024**, *501*, 215572.
[451] M. Kotzabasaki, G. E. Froudakis, *Inorg. Chem. Front.* **2018**, *5*, 1255.
[452] A. Bieniek, A. P. Terzyk, M. Wiśniewski, K. Roszek, P. Kowalczyk, L. Sarkisov, S. Keskin, K. Kaneko, *Prog. Mater. Sci.* **2021**, *117*, 100743.
[453] H. Demir, H. Daglar, H. C. Gulbalkan, G. O. Aksu, S. Keskin, *Coord. Chem. Rev.* **2023**, *484*, 215112.
[454] M. Ding, R. W. Flaig, H. L. Jiang, O. M. Yaghi, *Chem. Soc. Rev.* **2019**, *48*, 2783.
[455] Y. Liu, Z. U. Wang, H. C. Zhou, *Greenh. Gases Sci. Technol.* **2012**, *2*, 239.
[456] R. Sabouni, H. Kazemian, S. Rohani, *Environ. Sci. Pollut. Res.* **2014**, *21*, 5427.
[457] A. C. Kizzie, A. G. Wong-Foy, A. J. Matzger, *Langmuir* **2011**, *27*, 6368.
[458] N. C. Burtch, H. Jasuja, K. S. Walton, *Chem. Rev.* **2014**, *114*, 10575.
[459] J. Yu, L. H. Xie, J. R. Li, Y. Ma, J. M. Seminario, P. B. Balbuena, *Chem. Rev.* **2017**, *117*, 9674.
[460] J. H. Choe, H. Kim, C. S. Hong, *Mater. Chem. Front.* **2021**, *5*, 5172.
[461] J. Yu, P. B. Balbuena, *J. Phys. Chem. C* **2013**, *117*, 3383.
[462] P. G. Boyd, A. Chidambaram, E. García-Díez, C. P. Ireland, T. D. Daff, R. Bounds, A. Gładysiak, P. Schouwink, S. M. Moosavi, M. M. Maroto-Valer, J. A. Reimer, J. A. R. Navarro, T. K. Woo, S. Garcia, K. C. Stylianou, B. Smit, *Nature* **2019**, *576*, 253.
[463] G. Shimizu, R. Vaidhyanathan, S. Iremonger, K. Deakin, J.-B. Lin, K. W. Dawson, *Metal Organic Framework, Production and Use Thereof*, **2014**, WO2014138878A1.
[464] J.-B. Lin, T. T. T. Nguyen, R. Vaidhyanathan, J. Burner, J. M. Taylor, H. Durekova, F. Akhtar, R. K. Mah, O. Ghaffari-Nik, S. Marx, N. Fylstra, S. S. Iremonger, K. W. Dawson, P. Sarkar, P. Hovington, A. Rajendran, T. K. Woo, G. K. H. Shimizu, *Science* **2021**, *374*, 1464.
[465] Y. Higuchi, M. Sugita, S. Moriya, T. Takewaki, S. Tanaka, *Microporous Mesoporous Mater.* **2024**, *374*, 113137.
[466] Y. Magnin, E. Dirand, G. Maurin, P. L. Llewellyn, *ACS Appl. Nano Mater.* **2023**, *6*, 19963.
[467] R. Oktavian, R. Goeminne, L. T. Glasby, P. Song, R. Huynh, O. T. Qazvini, O. Ghaffari-Nik, N. Masoumifard, J. L. Cordiner, P. Hovington, V. Van Speybroeck, P. Z. Moghadam, *Nat. Commun.* **2024**, *15*, 3898.
[468] C. H. Ho, F. Paesani, *ACS Appl. Mater. Interfaces* **2023**, *15*, 48287.
[469] K. Gopalsamy, D. Fan, S. Naskar, Y. Magnin, G. Maurin, *ACS Appl. Eng. Mater.* **2024**, *2*, 96.
[470] W. L. Jorgensen, J. Chandrasekhar, J. D. Madura, R. W. Impey, M. L. Klein, *J. Chem. Phys.* **1983**, *79*, 926.
[471] H. J. C. Berendsen, J. R. Grigera, T. P. Straatsma, *J. Phys. Chem.* **1987**, *91*, 6269.
[472] J. L. F. Abascal, C. Vega, *J. Chem. Phys.* **2005**, *123*, 234505.
[473] P. Ghosh, Y. J. Colón, R. Q. Snurr, *Chem. Commun.* **2014**, *50*, 11329.

[474] S. Chheda, W. Jeong, N. Hanikel, L. Gagliardi, J. I. Siepmann, *J. Phys. Chem. C* **2023**, *127*, 7837.
[475] S. Ravichandran, M. Najafi, R. Goeminne, J. F. M. Denayer, V. Van Speybroeck, L. Vanduyfhuys, *J. Chem. Theory Comput.* **2024**, *20*, 5225.
[476] R. Goeminne, V. Van Speybroeck, **2024**, https://doi.org/10.26434/chemrxiv-2024-lpm8c.
[477] A. Datar, M. Witman, L. C. Lin, *AIChE J.* **2021**, *67*, e17447.
[478] H. Zhang, R. Q. Snurr, *J. Phys. Chem. C* **2017**, *121*, 24000.
[479] J. Choi, L.-C. Lin, J. C. Grossman, *J. Phys. Chem. C* **2018**, *122*, 5545.
[480] C. Mellot-Draznieks, C. Serre, S. Surblé, N. Audebrand, G. Férey, *J. Am. Chem. Soc.* **2005**, *127*, 16273.
[481] H. Furukawa, F. Gándara, Y. B. Zhang, J. Jiang, W. L. Queen, M. R. Hudson, O. M. Yaghi, *J. Am. Chem. Soc.* **2014**, *136*, 4369.
[482] H. Kim, S. Yang, S. R. Rao, S. Narayanan, E. A. Kapustin, H. Furukawa, A. S. Umans, O. M. Yaghi, E. N. Wang, *Science* **2017**, *356*, 430.
[483] F. Fathieh, M. J. Kalmutzki, E. A. Kapustin, P. J. Waller, J. Yang, O. M. Yaghi, *Sci. Adv.* **2018**, *4*.
[484] N. Hanikel, M. S. Prévot, F. Fathieh, E. A. Kapustin, H. Lyu, H. Wang, N. J. Diercks, T. G. Glover, O. M. Yaghi, *ACS Cent. Sci.* **2019**, *5*, 1699.
[485] N. Hanikel, X. Pei, S. Chheda, H. Lyu, W. Jeong, J. Sauer, L. Gagliardi, O. M. Yaghi, *Science* **2021**, *374*, 454.
[486] F. Fathieh, M. J. Kalmutzki, E. A. Kapustin, P. J. Waller, J. Yang, O. M. Yaghi, *Sci. Adv.* **2018**, *4*, eaat3198.
[487] X. Liu, X. Wang, F. Kapteijn, *Chem. Rev.* **2020**, *120*, 8303.
[488] M. J. Kalmutzki, C. S. Diercks, O. M. Yaghi, M. J. Kalmutzki, C. S. Diercks, O. M. Yaghi, *Adv. Mater.* **2018**, *30*, 1704304.
[489] B. Mazur, L. Firlej, B. Kuchta, *ACS Appl. Mater. Interfaces* **2024**, *16*, 25559.
[490] N. Hanikel, D. Kurandina, S. Chheda, Z. Zheng, Z. Rong, S. E. Neumann, J. Sauer, J. I. Siepmann, L. Gagliardi, O. M. Yaghi, *ACS Cent. Sci.* **2023**, *9*, 551.
[491] C. Krishnaraj, H. Sekhar Jena, L. Bourda, A. Laemont, P. Pachfule, J. Roeser, C. V. Chandran, S. Borgmans, S. M. J. Rogge, K. Leus, C. V. Stevens, J. A. Martens, V. Van Speybroeck, E. Breynaert, A. Thomas, P. Van Der Voort, *J. Am. Chem. Soc.* **2020**, *142*, 20107.
[492] J. Sun, H. Sekhar Jena, C. Krishnaraj, K. Singh Rawat, S. Abednatanzi, J. Chakraborty, A. Laemont, W. Liu, H. Chen, Y.-Y. Liu, K. Leus, H. Vrielinck, V. Van Speybroeck, P. Van Der Voort, *Angew. Chem., Int. Ed.* **2023**, *62*, e202216719.
[493] M. Debruyne, S. Borgmans, S. Radhakrishnan, E. Breynaert, H. Vrielinck, K. Leus, A. Laemont, J. De Vos, K. S. Rawat, S. Vanlommel, H. Rijckaert, H. Salemi, J. Everaert, F. Vanden Bussche, D. Poelman, R. Morent, N. De Geyter, P. Van Der Voort, V. Van Speybroeck, C. V. Stevens, *ACS Appl. Mater. Interfaces* **2023**, *15*, 35092.
[494] Y. Yang, X. Chu, H.-Y. Zhang, R. Zhang, Y.-H. Liu, F.-M. Zhang, M. Lu, Z.-D. Yang, Y.-Q. Lan, *Nat. Commun.* **2023**, *14*, 593.
[495] E. Jin, Z. Lan, Q. Jiang, K. Geng, G. Li, X. Wang, D. Jiang, *Chem* **2019**, *5*, 1632.
[496] Y. Fu, X. Zhu, L. Huang, X. Zhang, F. Zhang, W. Zhu, *Appl. Catal. B Environ.* **2018**, *239*, 46.
[497] C. Wang, H. Zhang, W. Luo, T. Sun, Y. Xu, *Angew. Chem., Int. Ed.* **2021**, *60*, 25381.
[498] L. Guo, Y. Niu, H. Xu, Q. Li, S. Razzaque, Q. Huang, S. Jin, B. Tan, *J. Mater. Chem. A* **2018**, *6*, 19775.
[499] L. Wang, R. Wang, X. Zhang, J. Mu, Z. Zhou, Z. Su, *ChemSusChem* **2020**, *13*, 2973.
[500] W.-K. Han, W. Yuan, Z.-G. Gu, Y. Zhao, *ACS Mater. Lett.* **2024**, *6*, 2276.
[501] Y. Wan, P. Sun, L. Shi, X. Yan, X. Zhang, *J. Phys. Chem. Lett.* **2023**, *14*, 7411.
[502] F.-D. Wang, W. Liu, J. Wang, C.-X. Zhang, *Processes* **2023**, *11*, 347.
[503] M. Xu, S. Yu, W. Li, C. Li, Y. Peng, F. Yu, *Polym. Chem.* **2023**, *14*, 5133.
[504] L. Sun, M. G. Campbell, M. Dincă, *Angew. Chem., Int. Ed.* **2016**, *55*, 3566.
[505] L. S. Xie, G. Skorupskii, M. Dincă, *Chem. Rev.* **2020**, *120*, 8536.
[506] A. Walsh, K. T. Butler, C. H. Hendon, *MRS Bull.* **2016**, *41*, 870.
[507] P. Thanasekaran, C.-H. Su, Y.-H. Liu, K.-L. Lu, *Coord. Chem. Rev.* **2021**, *442*, 213987.
[508] A. D. Vos, Ph.D. Thesis, Ghent University, **2020**.
[509] A. De Vos, K. Hendrickx, P. Van Der Voort, V. Van Speybroeck, K. Lejaeghere, *Chem. Mater.* **2017**, *29*, 3006.
[510] M. Taddei, G. M. Schukraft, M. E. A. Warwick, D. Tiana, M. J. McPherson, D. R. Jones, C. Petit, *J. Mater. Chem. A* **2019**, *7*, 23781.
[511] X. Guo, L. Liu, Y. Xiao, Y. Qi, C. Duan, F. Zhang, *Coord. Chem. Rev.* **2021**, *435*, 213785.
[512] A. De Vos, K. Lejaeghere, F. Muniz Miranda, C. V. Stevens, P. Van Der Voort, V. Van Speybroeck, *J. Mater. Chem. A* **2019**, *7*, 8433.
[513] Z.-A. Lan, Y. Fang, Y. Zhang, X. Wang, *Angew. Chem., Int. Ed.* **2018**, *57*, 470.
[514] L. Liao, M. Li, Y. Yin, J. Chen, Q. Zhong, R. Du, S. Liu, Y. He, W. Fu, F. Zeng, *ACS Omega* **2023**, *8*, 4527.
[515] P. Yang, R. Wang, M. Zhou, X. Wang, *Angew. Chem., Int. Ed.* **2018**, *57*, 8674.
[516] M. Liu, K. Yang, Z. Li, E. Fan, H. Fu, L. Zhang, Y. Zhang, Z. Zheng, *Chem. Commun.* **2022**, *58*, 92.
[517] S. Pakhira, K. P. Lucht, J. L. Mendoza-Cortes, *J. Phys. Chem. C* **2017**, *121*, 21160.
[518] Y. Wan, L. Wang, H. Xu, X. Wu, J. Yang, *J. Am. Chem. Soc.* **2020**, *142*, 4508.
[519] Y. Zheng, Y. Jiao, Y. Zhu, L. H. Li, Y. Han, Y. Chen, A. Du, M. Jaroniec, S. Z. Qiao, *Nat. Commun.* **2014**, *5*, 3783.
[520] L. Wang, Y. Wan, Y. Ding, S. Wu, Y. Zhang, X. Zhang, G. Zhang, Y. Xiong, X. Wu, J. Yang, H. Xu, *Adv. Mater.* **2017**, *29*, 1702428.
[521] K. S. Rawat, S. Borgmans, T. Braeckevelt, C. V. Stevens, P. Van Der Voort, V. Van Speybroeck, *ACS Appl. Nano Mater.* **2022**, *5*, 14377.
[522] H. Sajid, *Phys. Chem. Chem. Phys.* **2024**, *26*, 8577.
[523] C. Winkler, T. Kamencek, E. Zojer, *Nanoscale* **2021**, *13*, 9339.
[524] Y. Liu, H. Wu, Q. Wang, *J. Mater. Chem. A* **2023**, *11*, 21470.
[525] Z.-A. Lan, X. Chi, M. Wu, X. Zhang, X. Chen, G. Zhang, X. Wang, *Small* **2022**, *18*, 2200129.
[526] Y. Qian, Y. Han, X. Zhang, G. Yang, G. Zhang, H.-L. Jiang, *Nat. Commun.* **2023**, *14*, 3083.
[527] C. A. Ullrich, *Time-Dependent Density-Functional Theory: Concepts and Applications*, Oxford University Press, Oxford, UK **2011**.
[528] C. Li, J. Liu, H. Li, K. Wu, J. Wang, Q. Yang, *Nat. Commun.* **2022**, *13*, 2357.
[529] H. Wang, S. Jin, X. Zhang, Y. Xie, *Angew. Chem., Int. Ed.* **2020**, *59*, 22828.
[530] Z.-A. Lan, M. Wu, Z. Fang, X. Chi, X. Chen, Y. Zhang, X. Wang, *Angew. Chem., Int. Ed.* **2021**, *60*, 16355.
[531] X. Wang, L. Chen, S. Y. Chong, M. A. Little, Y. Wu, W.-H. Zhu, R. Clowes, Y. Yan, M. A. Zwijnenburg, R. S. Sprick, A. I. Cooper, *Nat. Chem.* **2018**, *10*, 1180.
[532] T. Ma, Y. Zhou, C. S. Diercks, J. Kwon, F. Gándara, H. Lyu, N. Hanikel, P. Pena-Sánchez, Y. Liu, N. J. Diercks, R. O. Ritchie, D. M. Proserpio, O. Terasaki, O. M. Yaghi, *Nat. Synth.* **2023**, *2*, 286.
[533] S. Borgmans, S. M. J. Rogge, J. S. De Vos, P. Van Der Voort, V. Van Speybroeck, *Commun. Chem.* **2023**, *6*, 5.
[534] C. Bustamante, D. Keller, G. Oster, *Acc. Chem. Res.* **2001**, *34*, 412.
[535] R. Iino, K. Kinbara, Z. Bryant, *Chem. Rev.* **2020**, *120*, 1.
[536] W. Meng, S. Kondo, T. Ito, K. Komatsu, J. Pirillo, Y. Hijikata, Y. Ikuhara, T. Aida, H. Sato, *Nature* **2021**, *598*, 298.
[537] L. Liu, Z. Chen, J. Wang, D. Zhang, Y. Zhu, S. Ling, K.-W. Huang, Y. Belmabkhout, K. Adil, Y. Zhang, B. Slater, M. Eddaoudi, Y. Han, *Nat. Chem.* **2019**, *11*, 622.

[538] D. N. Johnstone, F. C. N. Firth, C. P. Grey, P. A. Midgley, M. J. Cliffe, S. M. Collins, *J. Am. Chem. Soc.* **2020**, *142*, 13081.
[539] M. J. Cliffe, W. Wan, X. Zou, P. A. Chater, A. K. Kleppe, M. G. Tucker, H. Wilhelm, N. P. Funnell, F.-X. Coudert, A. L. Goodwin, *Nat. Commun.* **2014**, *5*, 4176.
[540] T. Yang, T. Willhammar, H. Xu, X. Zou, Z. Huang, *Nat. Protoc.* **2022**, *17*, 2389.
[541] V. Bon, N. Busov, I. Senkovska, N. Bönisch, L. Abylgazina, A. Khadiev, D. Novikov, S. Kaskel, *Chem. Commun.* **2022**, *58*, 10492.
[542] M. Šípka, A. Erlebach, L. Grajciar, *J. Chem. Theory Comput.* **2023**, *19*, 887.
[543] S. Mehdi, Z. Smith, L. Herron, Z. Zou, P. Tiwary, *Annu. Rev. Phys. Chem.* **2024**, *75*, 347.
[544] T. S. Van Erp, D. Moroni, P. G. Bolhuis, *J. Chem. Phys.* **2003**, *118*, 7762.
[545] D. Moroni, P. G. Bolhuis, T. S. Van Erp, *J. Chem. Phys.* **2004**, *120*, 4055.
[546] T. S. Van Erp, P. G. Bolhuis, *J. Comput. Phys.* **2005**, *205*, 157.
[547] R. Cabriolu, K. M. Skjelbred Refsnes, P. G. Bolhuis, T. S. Van Erp, *J. Chem. Phys.* **2017**, *147*, 152722.
[548] T. Loiseau, C. Serre, C. Huguenard, G. Fink, F. Taulelle, M. Henry, T. Bataille, G. Férey, *Chem. – Eur. J.* **2004**, *10*, 1373.
[549] M. Vougo-Zanda, J. Huang, E. Anokhina, X. Wang, A. J. Jacobson, *Inorg. Chem.* **2008**, *47*, 11535.
[550] C. Volkringer, T. Loiseau, N. Guillou, G. Férey, E. Elkaïm, A. Vimont, *Dalton Trans.* **2009**, 2241.
[551] E. V. Anokhina, M. Vougo-Zanda, X. Wang, A. J. Jacobson, *J. Am. Chem. Soc.* **2005**, *127*, 15000.
[552] J. P. S. Mowat, S. R. Miller, A. M. Z. Slawin, V. R. Seymour, S. E. Ashbrook, P. A. Wright, *Microporous Mesoporous Mater.* **2011**, *142*, 322.
[553] C. Serre, F. Millange, C. Thouvenot, M. Noguès, G. Marsolier, D. Louër, G. Férey, *J. Am. Chem. Soc.* **2002**, *124*, 13519.
[554] D. Cunha, M. Ben Yahia, S. Hall, S. R. Miller, H. Chevreau, E. Elkaïm, G. Maurin, P. Horcajada, C. Serre, *Chem. Mater.* **2013**, *25*, 2767.
[555] L. J. Sham, M. Schlüter, *Phys. Rev. Lett.* **1983**, *51*, 1888.
[556] I. E. Castelli, F. Hüser, M. Pandey, H. Li, K. S. Thygesen, B. Seger, A. Jain, K. A. Persson, G. Ceder, K. W. Jacobsen, *Adv. Energy Mater.* **2015**, *5*, 1400915.
[557] J. P. Perdew, *Int. J. Quantum Chem.* **2009**, *28*, 497.
[558] J. Wieme, K. Lejaeghere, G. Kresse, V. Van Speybroeck, *Nat. Commun.* **2018**, *9*, 4899.
[559] H. Eshuis, J. E. Bates, F. Furche, *Theor. Chem. Acc.* **2012**, *131*, 1084.
[560] J. Harl, G. Kresse, *Phys. Rev. Lett.* **2009**, *103*, 056401.
[561] X. Ren, P. Rinke, C. Joas, M. Scheffler, *J. Mater. Sci.* **2012**, *47*, 7447.
[562] F. Aryasetiawan, M. Imada, A. Georges, G. Kotliar, S. Biermann, A. I. Lichtenstein, *Phys. Rev. B* **2004**, *70*, 195104.
[563] M. Shishkin, M. Marsman, G. Kresse, *Phys. Rev. Lett.* **2007**, *99*, 246403.
[564] L. Hedin, *Phys. Rev.* **1965**, *139*, A796.
[565] A. Georges, G. Kotliar, W. Krauth, M. J. Rozenberg, *Rev. Mod. Phys.* **1996**, *68*, 13.
[566] T. Maier, M. Jarrell, T. Pruschke, M. H. Hettler, *Rev. Mod. Phys.* **2005**, *77*, 1027.
[567] M. Wallerberger, A. Hausoel, P. Gunacker, A. Kowalski, N. Parragh, F. Goth, K. Held, G. Sangiovanni, *Comput. Phys. Commun.* **2019**, *235*, 388.
[568] G. Knizia, G. K.-L. Chan, *J. Chem. Theory Comput.* **2013**, *9*, 1428.
[569] S. Wouters, C. A. Jiménez-Hoyos, Q. Sun, G. K.-L. Chan, *J. Chem. Theory Comput.* **2016**, *12*, 2706.
[570] Z.-H. Cui, T. Zhu, G. K.-L. Chan, *J. Chem. Theory Comput.* **2020**, *16*, 119.
[571] A. Mitra, M. R. Hermes, L. Gagliardi, *J. Chem. Theory Comput.* **2023**, *19*, 3498.
[572] I. Syozi, *Prog. Theor. Phys.* **1951**, *6*, 306.
[573] M. Fuchs, P. Liu, T. Schwemmer, G. Sangiovanni, R. Thomale, C. Franchini, D. Di Sante, *J. Phys. Mater.* **2020**, *3*, 025001.
[574] D. Kumar, J. Hellerstedt, B. Field, B. Lowe, Y. Yin, N. V. Medhekar, A. Schiffrin, *Adv. Funct. Mater.* **2021**, *31*, 2106474.
[575] B. Field, A. Schiffrin, N. V. Medhekar, *Npj Comput. Mater.* **2022**, *8*, 227.
[576] A. Aldossary, J. A. Campos-Gonzalez-Angulo, S. Pablo-García, S. X. Leong, E. M. Rajaonson, L. Thiede, G. Tom, A. Wang, D. Avagliano, A. Aspuru-Guzik, *Adv. Mater.* **2024**, *36*, 2402369.
[577] J. Behler, *Chem. Rev.* **2021**, *121*, 10037.
[578] S. Vandenhaute, M. Cools-Ceuppens, S. DeKeyser, T. Verstraelen, V. Van Speybroeck, *Npj Comput. Mater.* **2023**, *9*, 19.
[579] A. Musaelian, S. Batzner, A. Johansson, L. Sun, C. J. Owen, M. Kornbluth, B. Kozinsky, *Nat. Commun.* **2023**, *14*, 579.
[580] J. T. Frank, O. T. Unke, K.-R. Müller, **2023**, https://doi.org/10.48550/arXiv.2205.14276.
[581] P. G. Vekilov, in *ACS Symp. Ser*, (Ed: X. Zhang), American Chemical Society, Washington, DC, **2020**, pp. 19–46.
[582] H. Fu, X. Gao, X. Zhang, L. Ling, *Cryst. Growth Des.* **2022**, *22*, 1476.
[583] M. Filez, C. Caratelli, M. Rivera-Torrente, F. Muniz-Miranda, M. Hoek, M. Altelaar, A. J. R. Heck, V. Van Speybroeck, B. M. Weckhuysen, *Cell Rep. Phys. Sci.* **2021**, *2*, 100680.
[584] S. R. G. Balestra, R. Semino, *J. Chem. Phys.* **2022**, *157*, 184502.
[585] Y. Zhu, J. Ciston, B. Zheng, X. Miao, C. Czarnik, Y. Pan, R. Sougrat, Z. Lai, C.-E. Hsiung, K. Yao, I. Pinnau, M. Pan, Y. Han, *Nat. Mater.* **2017**, *16*, 532.
[586] J. Xing, L. Schweighauser, S. Okada, K. Harano, E. Nakamura, *Nat. Commun.* **2019**, *10*, 3608.
[587] C. Feriante, A. M. Evans, S. Jhulki, I. Castano, M. J. Strauss, S. Barlow, W. R. Dichtel, S. R. Marder, *J. Am. Chem. Soc.* **2020**, *142*, 18637.
[588] J. S. Du, Y. Bae, J. J. De Yoreo, *Nat. Rev. Mater.* **2024**, *9*, 229.
[589] D. Biswal, P. G. Kusalik, *ACS Nano* **2017**, *11*, 258.
[590] D. Biswal, P. G. Kusalik, *J. Chem. Phys.* **2017**, *147*, 044702.
[591] S. A. Wells, N. F. Cessford, N. A. Seaton, T. Düren, *RSC Adv.* **2019**, *9*, 14382.
[592] L. Kollias, R. Rousseau, V.-A. Glezakou, M. Salvalaglio, *J. Am. Chem. Soc.* **2022**, *144*, 11099.
[593] S. R. G. Balestra, B. Martínez-Haya, N. Cruz-Hernández, D. W. Lewis, S. M. Woodley, R. Semino, G. Maurin, A. R. Ruiz-Salvador, S. Hamad, *Nanoscale* **2023**, *15*, 3504.
[594] B. P. Carpenter, A. R. Talosig, B. Rose, G. Di Palma, J. P. Patterson, *Chem. Soc. Rev.* **2023**, *52*, 6918.
[595] W. Ostwald, *Z. Für Phys. Chem.* **1897**, *22U*, 289.
[596] P. T. Cardew, *Cryst. Growth Des.* **2023**, *23*, 3958.
[597] J. Jiang, Y. Zhao, O. M. Yaghi, *J. Am. Chem. Soc.* **2016**, *138*, 3255.
[598] F. Haase, B. V. Lotsch, *Chem. Soc. Rev.* **2020**, *49*, 8469.
[599] R. A. Dodson, A. P. Kalenak, A. J. Matzger, *J. Am. Chem. Soc.* **2020**, *142*, 20806.
[600] A. Lewis, F. S. Butt, X. Wei, N. A. Mazlan, Z. Chen, Y. Yang, S. Yang, N. Radacsi, X. Chen, Y. Huang, *Results Eng* **2023**, *17*, 100751.
[601] C. G. Gruber, L. Frey, R. Guntermann, D. D. Medina, E. Cortés, *Nature* **2024**, *630*, 872.
[602] J. Zhang, H. Zhang, T. Wu, Q. Wang, D. Van Der Spoel, *J. Chem. Theory Comput.* **2017**, *13*, 1034.
[603] Y. Wang, C. Teng, E. Begin, M. Bussiere, J. L. Bao, *J. Chem. Theory Comput.* **2024**, *20*, 6826.

Wim Temmerman received a B.Sc. and M.Sc. in chemical engineering from Ghent University and started a Ph.D. in chemical engineering under the guidance of Prof. Veronique Van Speybroeck at the Center for Molecular Modeling in Ghent, Belgium. His primary research interests include computational chemistry, vibrational analysis, and the development of nanoporous materials with applications in the separation, storage, and valorization of CO_2.

Ruben Goeminne received a B.Sc. and M.Sc. in engineering physics from Ghent University and started a Ph.D. in physics under the guidance of Prof. Toon Verstraelen at the Center for Molecular Modeling in Ghent, Belgium. Currently, he is a postdoctoral fellow working with Prof. Veronique Van Speybroeck. His primary research interests lie at the intersection of machine learning and molecular simulations, focusing on modeling adsorption in nanoporous materials with quantum mechanical accuracy.

Kuber Singh Rawat obtained his M.Sc. in Chemistry from Devi Ahilya Vishwavidyalaya, Indore, and his Ph.D. in Chemistry from the Indian Institute of Technology Indore, India. He is currently a postdoctoral researcher at the Center for Molecular Modeling (CMM), Ghent University, Belgium, working with Prof. Veronique Van Speybroeck. His current research focuses on employing computational modeling to understand the reaction mechanisms governing photo-electrocatalytic processes for clean energy production, particularly water splitting and CO_2 reduction.

Veronique Van Speybroeck is full professor at Ghent University and head of the Center for Molecular Modeling. She obtained her Ph.D. in 2001 from Ghent University and is an expert in modeling nanoporous materials, e.g. zeolites, Metal-Organic, Covalent Organic Frameworks for catalysis, adsorption, separations. She developed various methods to model as close as possible realistic materials/processes at operating conditions. She is recipient of two ERC grants and various prizes, e.g. the Dr. Karl Wamsler Innovation Award (2023), the Francqui prize in exact sciences (2024), and an elected member of the Royal (Flemish) Academy for Science and the Arts of Belgium.